

https://dspace.org/

Neutron activation analysis for the determination of gold and the platinum group elements in large samples

Lycoudi, Maria

1994
https://hdl.handle.net/10539/31189

Downloaded from a DSpace repository. https://dspace.org/

NEUTRON ACTIVATION ANALYSIS FOR THE DETERMINATION OF GOLD AND THE PLATINUM GROUP ELEMENTS IN LARGE SAMPLES

Maria Lycoudi

A Dissertation Submitted to the Faculty of Science
University of the Witwatersrand, Johannesburg,
for the Degree of Master of Science.

Johannesburg 1994

4134?


301063098

WITS UNIVERSITY LIBRARY

BD179593



DECLARATION

I declare that this dissertation is my own, unaided work. It is being submitted for the degree of Master of Science in the University of the Witwatersrand, Johannesburg. It has not been submitted before for any degree or examination in any other University.

MLycoudi

Maria Lycoudi

19th day of April, 1995

ABSTRACT

The method of activation analysis is extended to the analysis of very large samples (up to 1 kg) of ores and minerals.

The use of such large samples has two advantages : first the sensitivity of the method is greatly increased and secondly inhomogeneity of distribution and hence sampling problems are greatly reduced. Samples are used without any kind of treatment and the method is non - destructive.

There are also disadvantages associated with the use of large samples. Absorption effects (both of neutron and γ - rays) become important and as a result the calibration curves are influenced by the bulk density and composition of the samples. In certain cases, the calibration curves may also be non - linear.

These effects have been studied in detail for the determination of gold, through the reaction $^{198}Au(n,\gamma)^{198}Au$. After irradiating various samples of known concentrations of gold, calibration curves for gold in gold ore and carbon samples have been established. The effect of γ -ray and neutron absorption has been studied in carbon samples using either thermal or epithermal neutrons and the optimum sample thickness has been established. In addition, the curve for the optimum decay time has been obtained for gold in ore samples.

Based on the experimental results, a theoretical model has been applied to study the variation of the statistical error with the various factors involved, i.e. irradiation, decay, counting times, source strength and sample size. It has been also used to analyse theoretically the results for the optimum thickness and the variation of the background under the 411.8 keV peak of Au-198.

Further work has been undertaken to investigate whether the method can be used to determine elements from the platinum group which are much less active than the gold. Gamma ray peaks from Ir - 192, Au - 199, Pt - 199 Rh - 104m and Os-193 could be identified and possibly from Pd-109. Further work is necessary to study each element separately.

In the case of gold, very satisfactory results were obtained. It is too early to state that it provides a replacement for the fire - essay method for gold, but the potential definitely exists.

ACKNOWLEDGEMENTS

I would like to express my sincere thanks to the following people who helped make this work possible. Dr. J.I.W. Watterson my supervisor, for his constant encouragement and infinite patience, his constructive critisism and helpful suggestions during the research programme and the preparation of this dissertation.

The Council for Mineral Technology for the support of this project, their financial assistance and for the provision of all these expensive samples.

Many. thanks to the most stimulating and helpful colleagues and friends in the Neutron Source Lab, D.R. Lala, R. Kala and J. Ramahlo for their precious assistance and help of any kind.

To H.A. Andeweg and his group from the electronics workshop, for his clever suggestions and for making everything work.

To the technical staff of the workshop, L. Verga, I. McKowen and I. McQueen, for constructing so succesfully all those numerous apparatus for the experiments and to all the members of the staff of the Schonland Centre for their advices, helpful discussions and encouragement. I concider myself lucky for having met these people.

Finally, I would like to thank Prof J.P.F. Sellschop for the help and trust he has shown me, giving me the opportunity to study at the University of the Witwatersrand and for making possible for me the use of all the facilities at the S.R.C. I thank him for giving me the chance to introduce myself to experimental physics, an experiance which will last a lifetime.

TABLE OF CONTENTS

page

ABSTRACT ii

ACKNOWLEDGEMENTS iii

LIST OF TABLES vii

LIST OF FIGURES viii

chapter

1. INTRODUCTION 1

1.1 General 1
1.2 Instrumental techniques and the analysis of large samples 2
1.3 Scope and objectives of the study 3

2. THEORETICAL BACKGROUND 4

2.1 Properties of neutrons 4
2.2 Production of isotopes and radioactivity 4
2.3 Activation analysis 5
2.4 Interaction of neutrons with matter 10
a. Cross-sections 10
b. Variation of the cross-section with energy 13
2.5 The slowing down of fast neutrons 15
a. Number of collisions made by a neutron in a slowing down process 15
b. The mean cosine of the scattering angle for a single neutron collision 17
2.6 Moderators 17
2.7 Neutron sources 20
a. Introduction 20
b. Radioactive (α,n) sources. Ra-Be or Am-Be source 20
c. Radioactive (γ,n) sources 20
d. Fission neutron sources 21
e. Accelerator neutron sources 22

3. APPARATUS 23

3.1 Californium-252 irradiation facility 23
3.2 Detection equipment 25
a. Ge(Li) detectors 25
b. NaI(Tl) detectors 26
3.3 Multichannel analysers and data reduction 27

4. NEUTRON FLUX MEASUREMENTS 29

4.1 Introduction 29
4.2 Experimental 30
4.3 Results 32
4.4 Discussion 32

5. GAMMA - RAY SPECTROSCOPY OF THE GOLD ORE AND CARBON SAMPLES 33

5.1 Introduction 33
5.2 Experimental 33
5.3 Results 35
a. Gold ore samples 35
b. Activated carbon samples 40
5.4 Discussion 42

6. GAMMA - RAY SPECTROSCOPY OF THE PLATINUM GROUP ELEMENTS 43

6.1 Introduction 43
6.2 Experimental 45
6.3 Results - general 46
6.4 Results - individual elements 51
6.5 Discussion 56

7. QUANTITATIVE DETERMINATION OF GOLD IN ORES AND ACTIVATED CHARCOAL 59

7.1 Introduction 59
7.2 Experimental 59
a. Experimental for the ores 59
b. Experimental for the activated charcoal 61
7.3 Results 62
a. Results for the ores 62
b. Results for the activated charcoal 63
7.4 Discussion 63

8. OPTIMISATION OF THE IRRADIATION, DECAY AND COUNTING TIMES 65

8.1 Introduction 65
8.2 Theory - development of a model 65
a. Formula for peak area and statistical error 66
b. Variation of standard deviation with the irradiation, decay and counting time 67
8.3 Experimental results 68
8.4 Measured components of the background 69
a. General 69
b. Room background and natural activity of the ore 69
c. Background contributions from other elements 70
8.5 Application of the model 72
a. Optimum decay time for the determination of the 411 keV photopeak 72
b. Variation of the statistical error with the irradiation and counting times 74
c. Variation of the statistical error with source strength 76

9. NEUTRON AND GAMMA-RAY ABSORPTION 77

9.1 Introduction 77
9.2 Theory - neutron and gamma-ray absorption coefficients 77
9.3 Experimental 78
(a) Experimental investigation of γ–ray absorption 78
(b) Experimental investigation of neutron absorption 79
(c) Combined neutron and gamma-ray absorption - - optimum thickness 81
9.4 Results 83
(a) Results for γ–ray absorption 83
(b) Results for neutron absorption 83
(c) Combined neutron and gamma-ray absorption - - optimum thickness 84
9.5 Discussion 86

10. CONCLUSIONS 89

APPENDIX A 94

APPENDIX B 96

LIST OF REFERENCES 99

LIST OF TABLES

Table		page
1	Terms describing neutron energies	11
2	Moderators	19
3	Spontaneus fission neutron sources	21
4	Comparison between accelerator and isotopic source neutrons	22
5	Nuclear properties of ^{252}Cf neutron source	23
6	Foil data for neutron flux calculations	32
7	Results for neutron flux determination	32
8	Gamma-ray lines identified in spectra from gold ore NIM 62/69	38
9	Gamma-ray peaks identified in spectra from Carbon 1/78	41
10	Nuclear data for the P.G.E.'s	44
11	Experimental conditions for the P.G.E.'s	46
12	Gamma-ray lines identified in spectra from platinum concentrate NIM 26/78	48
13	Gamma-ray lines identified in spectra from platinum ore SARM 7	49
14	Experimental results for the P.G.E.'s	58
15	Contributions to the background under the 411 keV peak in gold ore	72

LIST OF FIGURES

Figure		page
2.1	Production and decay of Au-197	7
2.2	Absorption cross-section of Au-197 for epithermal neutrons	12
2.3	Elastic collision in the laboratory system (L.S.)	14
2.4	Elastic collision in the centre of mass system (C.M.S.)	14
2.5	Velocities of a neutron after collision in the C.M.S. and L.S	15
2.6	Maxwell distribution of thermal neutron flux and density	18
3.1	Schematic diagram of the irradiation facility and the source transfer system	24
3.2	Variation of absolute efficiency of a NaI(Tl) detector with distance from sample, for the 412 keV line	27
4.1	Variation in thermal flux with distance from source	29
4.2	Variation in epithermal flux with distance from source	30
4.3	Irradiation and counting geometry for the determination of the neutron flux	31
5.1	Marinelli type perspex sample holders	34
5.2	Irradiation and counting geometry	35
5.3	Spectrum from gold ore sample NIM 23/81 (0.5ppm Au) after Ti=69h, Td=1d, Tc=10h	36
5.4	Spectrum from gold ore sample NIM 62/69 (11.5ppm Au) after Ti=18.5h, Td=5h, Tc=5h	36
5.5	Spectrum from carbon activated sample 1/78 (1015-1081ppm Au) after Ti=64h, Td=2.3d, Tc=15h	40

6.1	Irradiation and counting geometry for platinum group element samples	45
6.2	Spectrum from platinum mattes sample 5/76 after Ti=3d, Td=4d, Tc=10h	47
6.3	Spectrum from platinum ore sample SARM 7 (for Pt) after Ti=94.5h, Td=3d, Tc=24h	47
6.4	Spectrum of platinum cup after Ti=2.5h, Td=10m, Tc=15m	50
6.5	Spectrum from platinum concentrate sample 16/76 (for Pt) after Ti=2.5h, Td=10m, Tc=15m	50
6.6.a	Spectrum from platinum mattes sample 5/76 (for Rh) after Ti=5m, Td=1m, Tc=5m	52
6.6.b	Spectrum from platinum mattes sample 5/76 (for Rh) after Ti=5m, Td=22m, Tc=5m	52
6.7	Spectrum from platinum matte sample 5/76 (for Pd) after Ti=13.5h, Td=10m, Tc=10h	53
6.8	Spectrum from platinum matte sample 5/76 (for Ir) after Ti=12h, Td=3 weeks, Tc=15h	54
6.9	Spectrum from platinum mattes sample 5/76 (for Pt) after Ti=2.5h, Td=10m, Tc=15m	56
7.1	Sample holders for the experiments in series B	60
7.2	Irradiation and counting geometry for series B	60
7.3	Irradiation and counting geometry for the calibration of the activated carbon samples	61
7.4	Calibration curves for the gold ores	62
7.5	Calibration curve for the activated carbon samples	63

8.1 Measured statistical error vs decay time 68
8.2 Spectrum from room background, Tc=10h 71
8.3 Spectrum from unirradiated ore, sample NIM 62/69, 11.5 ppm of gold, Tc=10h 71
8.4 Spectrum from irradiated ore, sample NIM 62/69, 11.5 ppm of gold, Ti=14.5h, Td=10h, Tc=10h 71
8.5 Calculated statistical error vs decay time 73
8.6 Statistical error vs irradiation time 75
8.7 Statistical error vs counting time 75
8.8 Statistical error vs Ti/T, considering the constant background 75
8.9 Statistical error vs source strength 76

9.1 Irradiation and counting geometry for the gamma-ray mass absorption coefficient of activated carbon 79
9.2 Irradiation and counting geometry for the neutron mass absorption measurement for activated carbon 80
9.3 Irradiation geometry for the determination of the optimum thickness 81
9.4.a Counting geometry with the detector facing the irradiated surface of the sample 81
9.4.b Counting geometry with the detector facing the opposite surface of the sample 82
9.5 Gamma-ray mass absorption for activated carbon 83
9.6 Variation of the neutron flux inside the activated carbon sample 84
9.7 Graph of measured counts against sample thickness after Ti=2.25h, Td=5d, Tc=15m 85
9.8 Graph of measured statistical error against sample thickness after Ti=2.25h, Td=5d, Tc=15m 85
9.9 (a) Variation of the activity inside the sample after thermal irradiation 87
(b) Variation of the thermal neutron flux 87
9.10 (a) Variation of the activity inside the sample after epithermal irradiation 87
(b) Variation of the epithermal neutron flux 87

1. INTRODUCTION

1.1 General

Neutron Activation Analysis (N.A.A.) is a nuclear technique whose usefulness as a multi-element analytical tool has been clearly demonstrated over the past forty years. Many publications have described successful applications in the trace analysis of samples for geology, biology, archaeology, chemistry and metallurgy[1,2,3,4]. Significant advances have been made in the measurement of spectroscopic decay data and in the determination of decay schemes for most isotopes. Because of improvements in the efficiency and resolution of detectors and specially Ge(Li) detectors and associated electronics, determinations can be carried out instrumentally rather than chemically, as was done in the early years when the elements were separated by chemical methods and radiochemical purity had to be established before counting.

The sensitivity and multi - element capability of reactor neutron activation analysis has made it a highly desirable technique for many applications, but reactors are not always a convenient source of neutrons for activation. Isotopic sources offer a simple and economical way to use neutron activation analysis in industrial applications. Potential applications have been discussed and feasibility studies have been described in several papers[1-11], but the routine use of sources remains limited. Today, various neutron sources are available. Some of them, are described in Chapter 2.

Neutron activation analysis, utilises the fact that neutrons are absorbed by nuclei to produce radioactive isotopes. The gamma-radiation from these isotopes can be detected and used to identify and quantify the elemental composition. Since both neutrons and gamma-rays are highly penetrating radiations, this method can be used in principle to analyse samples in bulk. The use of large samples has two major advantages. First the large sample size overcomes inhomogeneity and sampling problems and second it improves the sensitivity of the method. These characteristics are of particular interest where inhomogeneity of distribution and hence sampling and sample preparation are of importance.

1.2 Instrumental techniques and the analysis of large samples

A number of instrumental techniques are used for analysis. Many of these, for example atomic absorption spectroscopy, require the dissolution of the sample and are therefore unsuitable for the analysis of large samples.

X - ray fluorescence spectrometry[12] can be used non-destructively, but because of the limited range of the X - Rays, only very small samples can be analysed and the detectors are highly susceptible to damage due to their thin window.

A number of nuclear techniques such as ion beam analysis (I.B.A.), 14 MeV N.A.A., reactor N.A.A. and isotope source N.A.A., are widely used for analysis. All of these are non - destructive but I.B.A. in general and specifically particle induced X - ray emission (P.I.X.E.), are only capable of analysing small samples.

In a review in 1969, Rhodes[5] pointed out that because of neutron and γ - ray penetration, a sample several inches thick can be analysed by neutron activation analysis. Thus, errors due to heterogeneity and variable particle size would be reduced as compared to other analytical methods, X - ray fluorescence for instance. In spite of these advantages, large sample sizes have not been widely used, undoubtedly because of the difficulty arising from neutron and γ - ray absorption in the sample, as well as the decrease of the neutron flux with the distance from the source, as a result of both the inverse square law and neutron absorption.

More recently, research concerning isotope source N.A.A. of large samples, has taken place using the neutron capture γ - ray method, that is by measuring the emitted prompt gamma rays that immediately follow the capture of a neutron, i.e. during irradiation. This method, according to D. Duffey et al.[6], has two potential advantages : a) irradiation and counting times are not controlled by the decay constants and b) elements can be determined whether or not they go to stable nuclides or to β emitting radionuclides after neutron capture.

This method nevertheless has some serious disadvantages. Firstly, capture γ - ray spectra are more complicated than delayed γ - ray spectra and secondly the background is very high because of the neutrons. To obtain the required resolution, it is usually necessary to

use Ge detectors, which have a lower efficiency than NaI(Tl) detectors. Neutron damage to the detectors, must also be taken into consideration and this damage can be costly.

The analysis of large samples is of particular relevance in the mining industry where the accurate sampling of inhomogeneous materials is a problem. The isotope californium - 252, offers a neutron source with a large output but yet of a size that can be easily housed in any analytical laboratory. At the Savannah River Laboratory[11], a 100-mg ^{252}Cf N.A.A. facility has been used routinely for multielement analysis of small solid and liquid samples. With the totally automated pneumatic sample transfer system, cyclic irradiation - decay - counting regimes can be preselected for up to 40 samples and samples can be analysed with this facility unattended. Over 40 elements can be detected at the sub-ppm level. Precisions and accuracies of 10% for most elements were demonstrated in the extensive multielement analysis of standards.

In the present work a nominal one mg ^{252}Cf source was used for the activation analysis of large samples using the delayed gamma-ray technique. The method has no constraints regarding detector damage or very high background. Furthermore, a radioactive source needs no maintenance as does an X - ray tube.

1.3 Scope and objectives of the study

The aim of this project is to investigate the use of isotope - source neutron activation analysis, using a one mg Cf - 252 neutron source and the delayed γ - ray technique, for the determination of elements of particular interest to the minerals industry. The specific aim is to investigate the use of large sample sizes, in particular to study the limitations of sample size and the effects of neutron and gamma-ray absorption in determining this limitation. The use of different types and shapes of sample holder in extending this range are of particular interest.

This work could provide the base for a new method for the assay of gold and the platinum group elements in sample sizes ranging up to several hundred grams, using a non - destructive technique that would require an absolute minimum of sample preparation and treatment.

2. THEORETICAL BACKGROUND

2.1 Properties of neutrons

The neutron is a neutral particle (electric charge less than 10^{-18} e) of mass 1.674663×10^{-24} g, or 1.008665 u, spin $\frac{1}{2}$ and magnetic moment -1.913148 NM^2. It is not a stable particle except if it is bound in a nucleus. Because the neutron is 0.840×10^{-3} u heavier than the hydrogen atom, it is possible for a neutron to undergo a β-decay into a proton and an electron with a maximum energy of 782 keV. The half - life of the neutron against this β-decay is 11.7 min. This instability of the free neutrons is of no importance for nuclear reactors, because from the moment of their production up to the moment of their absorption inside the reactor, they remain free only for times of the order of milli-seconds.

2.2 Production of isotopes and radioactivity

A neutron can be captured by a nucleus to form a compound nucleus with a mass number one unit greater than the target and usually with an excitation energy of several MeV. This nucleus reverts to its ground state generally by emitting one or more γ - rays.

$$ {}_{Z}X^{A} + n \rightarrow {}_{Z}X^{A+1} + \gamma \qquad \text{or} \qquad {}_{Z}X^{A}(n,\gamma){}_{Z}X^{A+1} $$

We will see later that this is the most probable reaction that occurs with slow neutrons, i.e. with energies up to a few eV. At higher neutron energies the compound nucleus can emit particles and (n,p) as well as (n,α) and (n,2n) reactions are also useful in neutron activation analysis. In general the product nucleus has too high a mass / charge ratio for stability and decays by emitting a β-particle. The resulting decay is written :

$$ {}_{Z}X^{A+1} \rightarrow {}_{Z+1}X^{A+1} + \beta^{-} $$

Generally excited nuclei can emit γ-rays and possibly nucleons, in a short time of the order of 10^{-14} sec and decay into a ground state of a new nucleus which can be unstable against β^- or β^+ emission. This latter process of decay is a relatively slower process and is known as radioactivity. The probability of decay is constant for any particular isotope. This constant is denoted by λ and it is known as the decay constant.

If there are N atoms of a radioactive isotope at a time t, the number decaying in a time dt is given by :

$$dN = -\lambda N dt$$

with solution : $N = N_o e^{-\lambda t}$ where N_o = the number of atoms at $t = 0$.

The number of atoms initially present, is reduced to one half after a time T1/2 given by :

$$T_{1/2} = \frac{0.693}{\lambda} = \frac{\ln 2}{\lambda}$$

and T1/2 is usually known as the half - life of the isotope.

2.3 Activation analysis

In general, the procedure of activation analysis involves the bombardment of a sample with a flux of particles which, upon interaction, converts the elements in the sample to various radionuclides. These nuclides decay with the emission of characteristic radiation at a rate that is well defined for each nuclide. These two parameters, namely the energy emission spectrum and half-life, permit the identification of the elements originally present in the sample.

When a radioisotope is produced at a constant rate, the rate of accumulation of the isotope is given by the difference between the rate of production and the rate of decay of the isotope. The rate of production is characterised by the factor $\Phi\sigma$ which is the probability per unit time that a nucleus with cross-section σ in a flux Φ will undergo a transformation.

Say that nuclide A has an absorption cross-section σ_{abs} and an activation cross-section σ_{act} leading to the production of isotope B.

Generally excited nuclei can emit γ-rays and possibly nucleons, in a short time of the order of 10^{-14} sec and decay into a ground state of a new nucleus which can be unstable against β^- or β^+ emission. This latter process of decay is a relatively slower process and is known as radioactivity. The probability of decay is constant for any particular isotope. This constant is denoted by λ and it is known as the decay constant.

If there are N atoms of a radioactive isotope at a time t, the number decaying in a time dt is given by :

$$dN = -\lambda N dt$$

with solution : $N = N_O e^{-\lambda t}$ where N_O = the number of atoms at $t = 0$.

The number of atoms initially present, is reduced to one half after a time T1/2 given by :

$$T_{1/2} = \frac{0.693}{\lambda} = \frac{\ln 2}{\lambda}$$

and T1/2 is usually known as the half - life of the isotope.

2.3 Activation analysis

In general, the procedure of activation analysis involves the bombardment of a sample with a flux of particles which, upon interaction, converts the elements in the sample to various radionuclides. These nuclides decay with the emission of characteristic radiation at a rate that is well defined for each nuclide. These two parameters, namely the energy emission spectrum and half-life, permit the identification of the elements originally present in the sample.

When a radioisotope is produced at a constant rate, the rate of accumulation of the isotope is given by the difference between the rate of production and the rate of decay of the isotope. The rate of production is characterised by the factor $\Phi\sigma$ which is the probability per unit time that a nucleus with cross-section σ in a flux Φ will undergo a transformation.

Say that nuclide A has an absorption cross-section σ_{abs} and an activation cross-section σ_{act} leading to the production of isotope B.

i.e. $A + n \rightarrow B \xrightarrow[(\beta^-)]{} B'$

where σ_{act} is the cross-section for the production of B whose activity is to be measured. B decays to B′ with the decay constant λ.

The rate of production of B is

$$\frac{dN_B}{dt} = \sigma_{act}\Phi N_A - \lambda N_B,$$

where in general N_A and N_B are both functions of time, while

$$\frac{dN_A}{dt} = \sigma_{abs}\Phi N_A .$$

If N_A^0 is the number of nuclides of A at t=0, then the two above equations can be solved to give:

$$N_B = \frac{\sigma_{act}\Phi N_A^0}{\lambda - \sigma_{abs}\Phi} (e^{-\sigma_{abs}\Phi t} - e^{-\lambda t})$$

If, as is usual, the assumptions are made that $\sigma\Phi << \lambda$ and $e^{-\sigma\Phi t} = 1$, then this equation reduces to:

$$N_B = \frac{\sigma_{act}\Phi N_A^o}{\lambda} (1 - e^{-\lambda t})$$

The rate of disintegration of these radioactive atoms at any time is given by:

$$\frac{dN_B}{dt} = \lambda N_B = \sigma_{act}\Phi N_A^0 (1 - e^{-\lambda t_i})$$

The number of activated atoms will approach a saturation value asymptotically.

Figure 2.1, shows a typical growth curve for ^{197}Au. The activity after seven half-lives is about 99.2% of saturation. Irradiation of a material over a period of seven half-lives, will

only produce twice as much activity than if it was irradiated for only one half-life. It is also worth noting that for irradiation times shorter than one half-life, the relationship between induced activity and irradiation time is approximately linear.

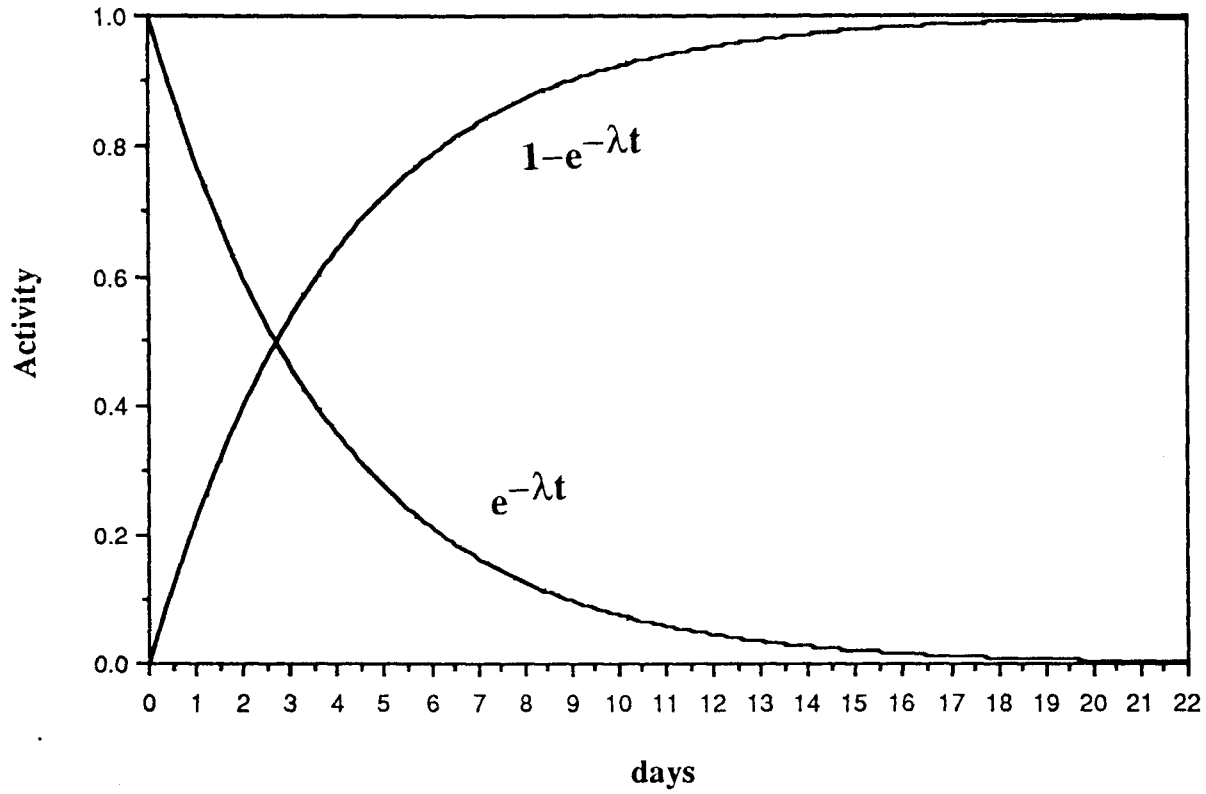


Figure 2.1 Production and decay of Au-197

In general, the activity will not be determined until a time t_d after the irradiation has ended, so that the radioactive atoms produced will have decayed by a factor $e^{-\lambda t_d}$. The time of counting t_c, will also affect the activity, since during counting the sample will have decayed by a factor $e^{-\lambda t_c}$. Hence the number of decays during the counting time is given by:

$$n = \sigma_{act}\Phi N_A^{o} (1 - e^{-\lambda t_i}) e^{-\lambda t_d} (1 - e^{-\lambda t_c})$$

In neutron activation, the radiation detected is directly proportional to the activity of the radionuclide produced in a neutron flux, which in turn is directly proportional to the amount of the parent isotope. Factors which affect the determination of original quantities include the irradiation, decay and counting time, the reaction cross-section, neutron flux, isotopic abundance, radionuclide half-life, atomic mass, decay scheme and detection efficiency. In terms of all these quantities the neutron activation equation is:

$$n = \frac{N_o mf\Phi\sigma\varepsilon\gamma}{A\lambda}(1 - e^{-\lambda t_i})e^{-\lambda t_d}(1 - e^{-\lambda t_c}) \qquad (2\text{-}1)$$

In this equation the symbols are defined as follows:

n : the area of a particular gamma - ray peak, i.e. the number of counts that is detected

N_O : Avogadro's number = 6.02486×10^{23} atoms / mole

m : mass of the particular element in the sample

A : atomic mass of the particular nucleus

f : isotopic abundance of the isotope

N $= \frac{N_O mf}{A}$: the total number of atoms (or nuclei) of a particular species present in the sample

Φ : the neutron flux, measured as n cm^{-2} s^{-1}

σ : the cross section

γ : the branching ratio, i.e. the proportion of beta decays that produce the γ - ray that is detected

λ : the decay constant of the beta decaying isotope produced by the neutron reaction,

λ : $\frac{\ln 2}{T_{1/2}}$, where $T_{1/2}$ is the half-life of the isotope

ε : the detector efficiency

t_i : the irradiation time, the time that the sample is exposed to the neutron flux

t_d : the decay time, the time that elapses between the irradiation and the measurement

t_c : the counting time

2.4 Interaction of neutrons with matter

2.4.a Cross-sections

Since the neutron is uncharged there is no nuclear coulomb barrier nor is there any interaction with the planetary electrons. The interactions between neutrons and nuclei depend on nuclear reactions through the strong nuclear force and their detail depends on the neutron energy and the element involved. In Table 1 there is a description of the different neutron energy regimes. It is possible to consider various energy ranges where one type of mechanism tends to be more probable than the others. It is important to have some measure of this probability in numbers so that we can compare it for different materials. The "cross - section" for a given reaction gives a quantitative measure of the probability of a particular reaction.

If I_0 is the intensity of a neutron beam falling on to a target of thickness x, and I is the intensity of the beam as it comes out of the target, then :

$$I = I_0 e^{-\sigma \rho N_0 x} = I_0 e^{-\sigma N}$$

where N is the number of atoms / cm^2 in the target
N_0 is the number of atoms per unit mass of the material which has a density ρ (g/cm^3)
σ is a constant of proportionality, known as the nuclear cross - section for the reaction that leads to the loss of the neutron.
σ is measured in barns. 1 barn = 10^{-24} cm^2.

Usually we use a suffix to denote the mechanism concerned, e.g.
σ_c = capture cross-section
σ_f = fission cross-section
σ_s = scattering cross-section
$\sigma_a = \sigma_f + \sigma_c$ = absorption cross-section

Total cross-section $\sigma_{tot} = \sigma_c + \sigma_f + \sigma_s + ...$

The average penetration of the neutron beam into the sample x_{av}, is given by :

$$x_{av} = \frac{\int_0^\infty x e^{-\Sigma x} dx}{\int_0^\infty e^{-\Sigma x} dx} = \frac{1}{\Delta N_0 \sigma_{tot}} = t$$

t = the mean free path of the neutron in the material.

$$I = I_o e^{-x/t} = I_o e^{-\Sigma x}$$

where $\Sigma = 1 / t = \Delta N_o \sigma_{tot}$ the macroscopic cross-section of the material.

$\Sigma_a = 1 / t_a = \Delta N_o \sigma_a$: macroscopic absorption cross-section.
$\Sigma_s = 1 / t_s = \Delta N_o \sigma_s$: macroscopic scattering cross-section.

$\tau = t / v$ = mean free time between two collisions.
$1/\tau = v/t = v\Sigma$: the number of collisions per sec.

TABLE 1

TERMS DESCRIBING NEUTRON ENERGIES

TERM	DESCRIPTION	ENERGY REGIONS	
Thermal	Neutrons in thermal equilibrium with surroundings	Most probable energy at 20°C Maxwellian distribution at 20°C, extends to about	0.025eV 0.1 eV
Epithermal	Neutrons of energy just greater than thermal	Energies above about	0.2 eV
Cadmium	Neutrons which are strongly absorbed by cadmium	Energies below about	0.4 eV
Epicadmium	Neutrons which are not strongly absorbed by cadmium	Energies above about	0.6 eV
Slow		Usually means less than Occasionally less than	1-10 eV 1 keV
Resonance	In pile neutron physics usually refers to neutrons which are strongly captured in the resonances of ^{238}U, or of a few commonly used detectors, e.g. In, Au.	A broad band of energies extending from about to about	1 eV 300 eV
Intermediate	Neutrons of energies between slow and fast	From to	a few 100eV 0.5 MeV
Fast		Neutrons of energy greater than	0.5 MeV
Ultra-fast		Neutrons of energy greater than	20 MeV
Pile	Neutrons of all energies present in a nuclear reactor		0.001eV to 15 MeV
Fission	Neutrons formed directly in fission	From 100 KeV to 15 MeV Most probable energy Average energy	 0.8 MeV 2 MeV

2.4.b Variation of the cross-section with energy

A knowledge of the variation of the partial cross-section with energy enables one to decide which is the most probable reaction that occurs at a given neutron energy. In Figure 2.2 the absorption cross-section of ^{197}Au for epithermal neutrons is illustrated. At approximately 5 eV there is a very large resonance and neutrons in this energy region are strongly absorbed by the gold nuclei.

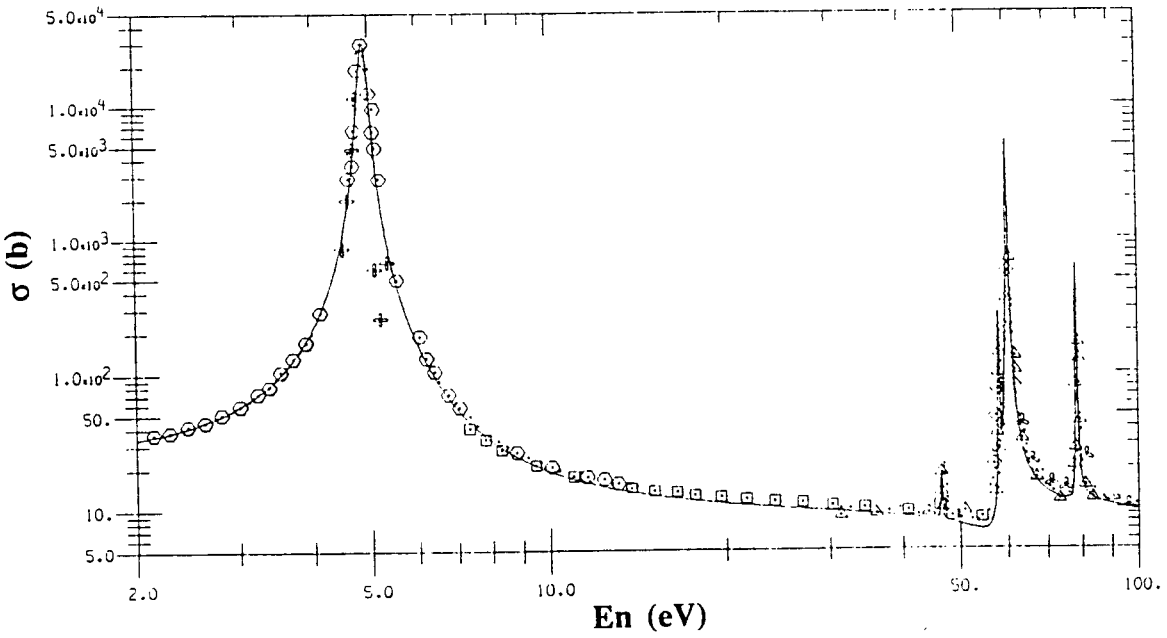


Figure 2.2 Absorption cross-section of Au-197 for epithermal neutrons

The following sections describe the general characteristics of the various neutron reactions.

a) Reactions without formation of a compound nucleus (direct reactions), e.g. potential scattering.

In this case, kinetic energy and momentum between the two nuclei is conserved. Energy lost by neutrons appears as kinetic energy of the target nucleus. This is the most probable

reaction at high energies (greater than 1 MeV), because of the short time the neutron takes to pass the target nucleus.

b) Reactions involving the formation of a compound nucleus.

When the neutron energy is lower, the interaction time is longer and the probability of compound nucleus formation increases. Since the compound nucleus is formed with an excitation energy equal to the neutron binding energy plus its kinetic energy, the probability of resonance reactions will depend on the distribution of energy levels in the compound nucleus at approximately 8 MeV above the ground state.

The compound nucleus is relatively long lived (more than 10^{-17} sec) and its decay can occur in various ways.

(i) A neutron with the same energy as the originally captured neutron can be emitted. This process is called compound elastic scattering, or resonance scattering.

(ii) The excitation energy of the compound nucleus can be given up by emission of one or several γ-rays. This phenomenon is called radiative capture, or the (n, γ) process. The resulting nucleus is frequently unstable against β^- decay. An example of a radiative capture is the reaction ^{197}Au (n, γ) ^{198}Au. The resultant nucleus ^{198}Au β^- decays to ^{198}Hg.

(iii) For sufficiently high excitation energies, the compound nucleus can emit charged particles or two neutrons; for example (n,α), (n,p), (n,np) and (n,2n) reactions.

(iv) A neutron with a kinetic energy smaller than that of the incident neutron can also be emitted and the residual nucleus remains in an excited state which decays by γ-ray emission (inelastic scattering). Finally fission can occur in the heaviest nuclei.

2.5 The Slowing down of fast neutrons

The most important mechanism for slowing down fast neutrons in the MeV region is elastic scattering.

2.5.a Number of collisions made by a neutron in a slowing down process

Consider the elastic collision between a fast neutron with initial velocity $\bar{v}_N$ and a free target nucleus of mass number A, initially at rest. Suppose the centre of mass of the two particles is at a distance x from A and that the neutron is at distance y from A, as shown in Figure 2.3. Because the elastic scattering of neutrons is isotropic in the C.M. system for the energy region we are intrested here, we consider the C.M. at rest (Figure 2.4) and we subtract a velocity of $\frac{\bar{v}_N}{A+1}$ from both of the particles. Hence,

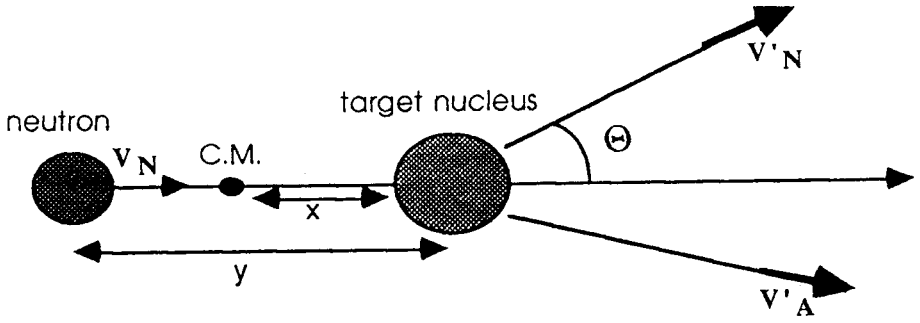


Figure 2.3 Elastic collision in the Laboratory System.

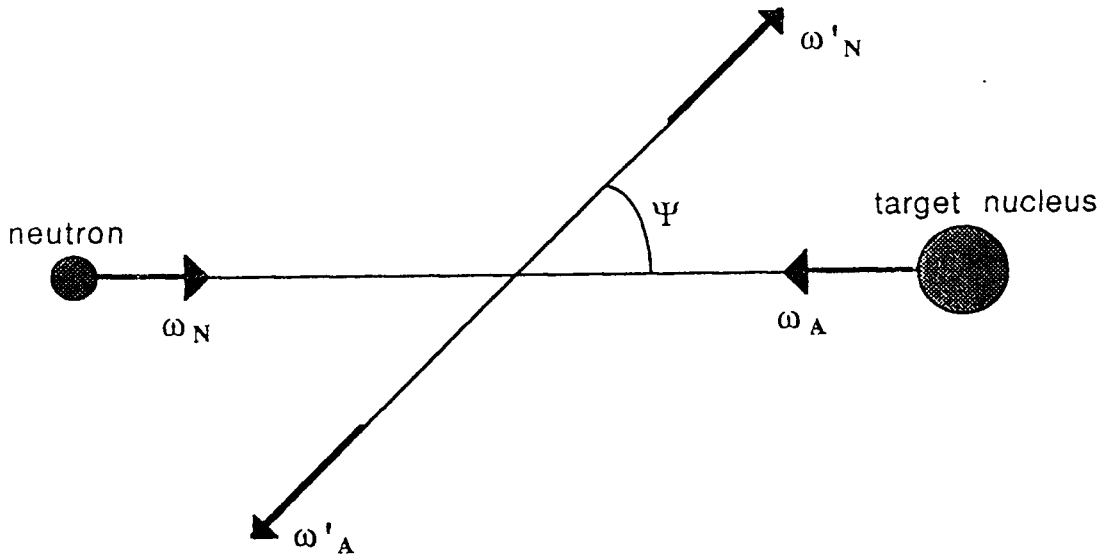


Figure 2.4 Elastic collision in the Centre of Mass System.

$$\vec{\omega}_N = \vec{v}_N - \frac{\vec{v}_N}{A+1}$$

$$\vec{\omega}_A = -\frac{\vec{v}_N}{A+1}$$

where $\vec{\omega}_N$ and $\vec{\omega}_A$ the velocities of the neutron and the nucleus in the C.M. system.

In the C.M. system the speeds are unchanged by the collision; it is the direction of the velocities which is altered. In the laboratory system, the neutron velocity is $\vec{v}'_N = \vec{\omega}'_N + \frac{\vec{v}_N}{A+1}$ after collision, and it makes an angle θ with its original direction (Figure 2.5). Then :

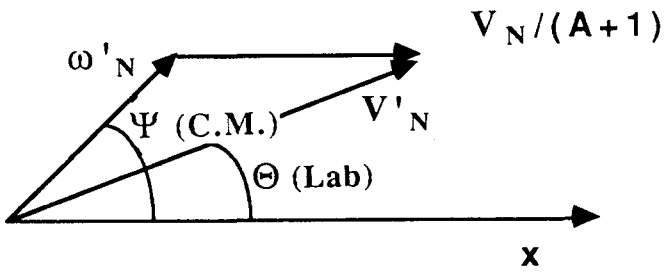


Figure 2.5 Velocities of a neutron after collision in the C.M. and Lab. System.

$$\frac{(v'_N)^2}{(v_N)^2} = \frac{E_2}{E_1} = \frac{A^2 + 2A\cos\Psi + 1}{(A+1)^2}$$

where E_2 is the energy of the neutron after collision and E_1 its energy before. The maximum value of E_2 (Ψ=0) is E_1 and the minimum (Ψ=π) is $E_1\frac{(A-1)^2}{(A+1)^2} = \alpha E_1$, after collision. The probability that a neutron will be scattered at an angle between Ψ and $\Psi + d\Psi$ will be given by

$$\frac{2\pi\sin\Psi d\Psi}{4\pi} = \frac{-d(\cos\Psi)}{2}$$

For each scattering angle Ψ we have a particular value of the final energy E_2 and the probability $F(E)dE$ of having a final energy between E and E + dE is given by

$$F(E)dE = \frac{-d(\cos\Psi)}{2} = \frac{-dE}{(1-\alpha)E_1}$$

Thus the neutron may have any energy between E_1 and αE_1 after the collision, as we have seen before. The average energy after the collision will be given by

$$E_{av} = \frac{(1+\alpha)E_1}{2}$$

thus $$(\frac{E_1}{E_2})_{av} = \frac{2}{(1+\alpha)}$$

and after N collisions $$\frac{E_i}{E_f} = [(\frac{E_1}{E_2})_{av}]^N$$

where N is the number of collisions made by a fast neutron in slowing down from some initial energy E_i to some final energy E_f, therefore

$$N = \frac{\ln\frac{E_i}{E_f}}{[\ln\frac{E_1}{E_2}]_{av}}$$

The quantity $[\ln\frac{E_1}{E_2}]_{av} = \xi$, is the logarithmic energy decrement, i.e. the average logarithmic energy loss per collision and it can be calculated that

$$\xi = 1 - \frac{(A-1)^2}{2A}\ln\frac{A+1}{A-1}$$

Thus $$N = \frac{1}{\xi}\ln\frac{E_i}{E_f}$$

is the average number of collisions for the neutrons to have passed the energy mark Ef. If E_i = 2 MeV which is the mean energy of fission neutrons and E_f = 0.025 eV the energy corresponding to the most probable velocity at 20°C, then $\ln\frac{E_i}{E_f} = 18.2$.

2.5.b The mean cosine of the scattering angle for a single neutron collision.

From Figures 2.3, 2.4 and 2.5, it can be calculated that :

$$\cos\theta = \frac{A+1}{2}\sqrt{\frac{E_2}{E_1}} - \frac{A-1}{2}\sqrt{\frac{E_1}{E_2}}$$

As above mentioned, the scattering of neutrons is isotropic in the centre of mass system, therefore anisotropic in the laboratory system. Hence the mean cosine of the scattering angle in the lab system is important. It is essential therefore, to weigh the values of cos θ with the probabilities of their occurrence and take the average. If the mean cosine of the scattering angle for a single collision is b, then the well known relation holds:

$$b = \frac{2}{3}A$$

2.6 Moderators

Consider a source in a scattering medium that emits neutrons with an energy distribution S(E). These neutrons exchange kinetic energy with the atoms of the scattering substance through elastic and frequently also inelastic collisions. If the neutrons are emitted with energies higher than the kinetic energy of the thermal motion of the scattering atoms, they lose energy in successive collisions until they are in equilibrium with the thermal motion of their surroundings. Their energies then approximate a Maxwell distribution with the temperature of the scattering medium (Figure 2.6). Neutrons with such energy distribution are called "thermal neutrons".

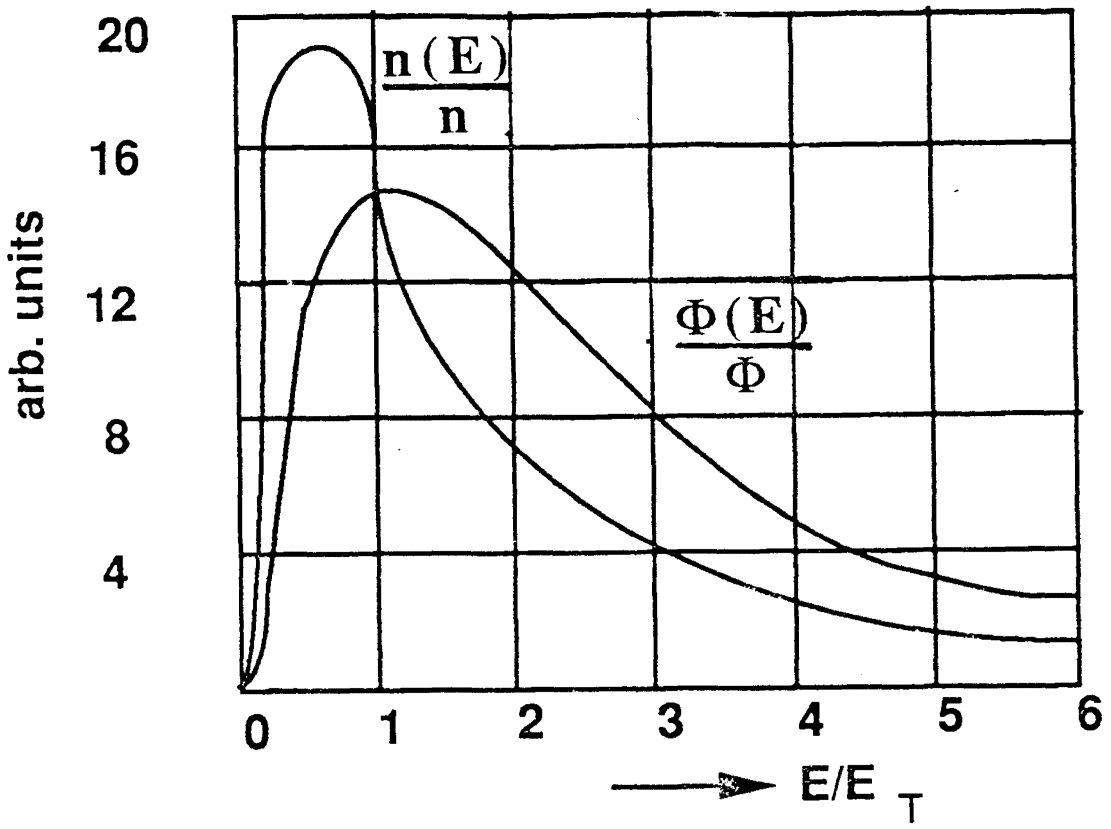


Figure 2.6 Maxwell distribution of neutron flux and density.

In practice in a good moderator, the neutron energy distribution at the end of the slowing down process approximates an equilibrium distribution. From Boltzmann's distribution and equation of state, it follows that :

$$E_{av} = \frac{3}{2} kT \quad \text{average energy}$$

$$v_T = \sqrt{\frac{2kT}{m}} \quad \text{most probable velocity,}$$

furthermore $\frac{1}{2} m v_T^2 = kT = E_T$ the most probable energy.

If T = 293.6 K (20.4 ^{o}C), kT = E_T = 0.0253 eV, v_T = 2200 m/sec = v_O while the average velocity v_{av} is generally :

$$v_{av} = \frac{2v_T}{\sqrt{\pi}}$$

For moderation, great importance is attached to substances which :

(i) have large scattering cross-sections,
(ii) have low atomic weight (i.e. moderate neutrons strongly), hence have large slowing down power,
(iii) absorb neutrons weakly, i.e. have small absorption cross-sections (σ_a much smaller than σ_s).

Such substances are good moderators to slow down neutrons. In Table 2 data are given for the most commonly used moderators.

TABLE 2

Moderators[14]

Moderator	Density	Slowing down power $\xi\Sigma_s$	Moderating ratio $\xi\Sigma_s/\Sigma_a$
H_2O	1.0	1.35 cm^{-1}	71
D_2O	1.1	0.176 cm^{-1}	5670
graphite	1.6	0.060 cm^{-1}	192
beryllium	1.85	0.158 cm^{-1}	143

were ξ is the logarithmic energy decrement described above.

2.7 Neutron sources

2.7.a Introduction

Because of their short lifetime, free neutrons do not exist in nature and must be artificially produced. There are a variety of nuclear reactions which lead to neutron production. In such reactions compound nuclei excited to the sum of the binding energy and kinetic energy (in the centre of mass system) of the projectiles are formed by bombardment of target nuclei with α - particles, protons, deuterons, or γ - rays. If the excitation energy is larger than the binding energy of the "last neutron" in the compound nucleus, then a neutron is very likely to be emitted. The remaining excitation energy is distributed as kinetic energy between the neutron and the residual nucleus, which can later return to the ground state by γ - emission.

For neutron production, light nuclei are most important. In many cases they can be thought of as being composed of α - particles and in this configuration their binding energies are particularly large. The majority of these nuclei are very stable and an excess neutron added to such a nucleus is very loosely bound.

2.7.b Radioactive (α,n) sources. Ra - Be or Am - Be source

A strong isotopic neutron source which is nearly constant in time can be produced with the $^{9}Be\ (\alpha,n)^{12}C$ reaction if one uses the strong α - activity of natural radium or ^{241}Am for example. These neutron sources are frequently found in laboratories working with low neutron intensities and often serve as standard neutron sources. A disadvantage of the Ra - Be source is the strong γ - radiation accompanying the neutrons. The Am - Be source emits low energy gamma - rays, a characteristic that makes it more favorable for use than the Ra - Be source.

2.7.c Radioactive (γ,n) sources

In contrast with the radioactive (α,n) sources which emit a continuous spectrum of neutrons, nearly monoenergetic neutrons can be produced in photoneutron sources by use of monochromatic γ - rays. Since the γ - energy of radioactive substances rarely exceeds 3 MeV, only the (γ ,n) reactions in beryllium (Q = –1.665 MeV) and deuterium (Q = –2.225 MeV) come into consideration. Disadvantages of photoneutron sources are their small yield and the

usually short half-life of the γ - emitters. Because of their strong penetrating γ - radiation, work with large photoneutron sources requires special protective measures.

2.7.d Fission neutron sources

Some heavy nuclei decay by spontaneus fission. Since in fission several neutrons are produced, these heavy nuclei can be used as neutron sources. Table 3 contains useful data concerning some of the transuranic isotopes that undergo spontaneus fission. With the exception of Cf - 252, all of the nuclei are strong α - emitters. In practice the Cf - 252 source is particularly widely used.

TABLE 3

Spontaneous fission neutron sources[14]

Nucleus	Half-life	α particles ($mg^{-1}sec^{-1}$)	n per fission	neutrons ($mg^{-1}sec^{-1}$)
Pu^{236}	2.85y	$1.3x10^{9}$	1.9	26
Pu^{238}	89.4y	$5.5x10^{8}$	2.0	2.2
Pu^{240}	6600y	$1.9x10^{7}$	2.1	1.1
Pu^{242}	$3.79x10^{5}$y	$1.9x10^{5}$	2.3	1.7
Cm^{242}	162.5d	$1.6x10^{7}$	2.3	$1.7x10^{4}$
Cm^{244}	18.4y	$7.6x10^{5}$	2.6	$9x10^{3}$
Cf^{252}	2.7y	$2.4x10^{10}$	3.5	$2.7x10^{9}$

The nuclide ^{252}Cf emits neutrons through spontaneous fission decay.

Although the neutron flux from radioactive sources is comparatively small, they are quite useful for specific purposes, due to their extreme simplicity, reliability and small size. The gamma-radiation which is also present is however a disadvantage. From this point of view, ^{252}Cf is a very convenient neutron source, but it has a relatively short half-life compared with some of the other sources.

2.7.e Accelerator neutron sources

Another way of obtaining neutron fluxes is through accelerator - induced reactions. The most common reactions are the deuteron reactions $T(d,n)^4He$ and $D(d,n)^3He$. The reaction $^9Be\ (d,n)^{10}B$ is often used with medium energy accelerators. The proton reactions $^7Li\ (p,n)^7Be$ and $^9Be\ (p,n)^9B$ are also used. Generally the neutron yield increases with increasing beam energy up to some maximum value of the latter after which competition from other reaction channels reduces the yield. The reaction $^7Li\ (p,n)\ ^7Be$ is used for the production of monoenergetic neutrons. Higher neutron yields can be obtained by the reaction $^9Be\ (d,n)\ ^{10}B$.

TABLE 4

COMPARISON BETWEEN ACCELERATOR AND ISOTOPIC SOURCE NEUTRONS

ACCELERATOR NEUTRONS	ISOTOPIC SOURCE NEUTRONS
Neutron energy depends on the energy of the accelerated particle and can therefore be controlled to some degree.	There is a wide distribution of neutron energies. Suitable absorbers can be used to modify this distribution.
Neutron output depends on the beam current.	Neutron flux varies according to activity and half-life of the source.
Neutron output depends on the beam energy.	Restricted in intensity.
The neutron beam can be switched off or pulsed.	Cannot be switched off.
Samples have to be transported to central irradiation sites.	Portable and convenient for transporting to different sample sites, at least in the case of smaller sources.

3. APPARATUS

3.1 Californium - 252 irradiation facility

The source used in this work consisted of a nominal one mg ^{252}Cf that emitted neutrons with a typical fission spectrum. The unmoderated fission spectrum is centered at about 2.3 MeV. The emitted γ - rays have energies up to 5 MeV. Characteristic nuclear properties of the source are detailed in Table 5.

TABLE 5

NUCLEAR PROPERTIES OF ^{252}Cf NEUTRON SOURCE[14]

Effective half-life	2.646 + 0.004 years
Alpha decay half-life	2.731 + 0.007 years
Spontaneus fission half-life	85.5 + 0.5 years
Average neutron energy	2.348 MeV
Average alpha particle energy	6.117 MeV
Gamma emission rate	1.3×10^{13} photons per sec per gram
Decay heat (57.1 % from fission, 48.9 % from alpha decay)	38.5 watts per gram
Neutrons per spontaneous fission	3.5 neutrons
Specific neutron activity	4.4×10^{9} neutrons per sec per curie
Neutron emission rate	2.7×10^{12} neutrons per sec per gram

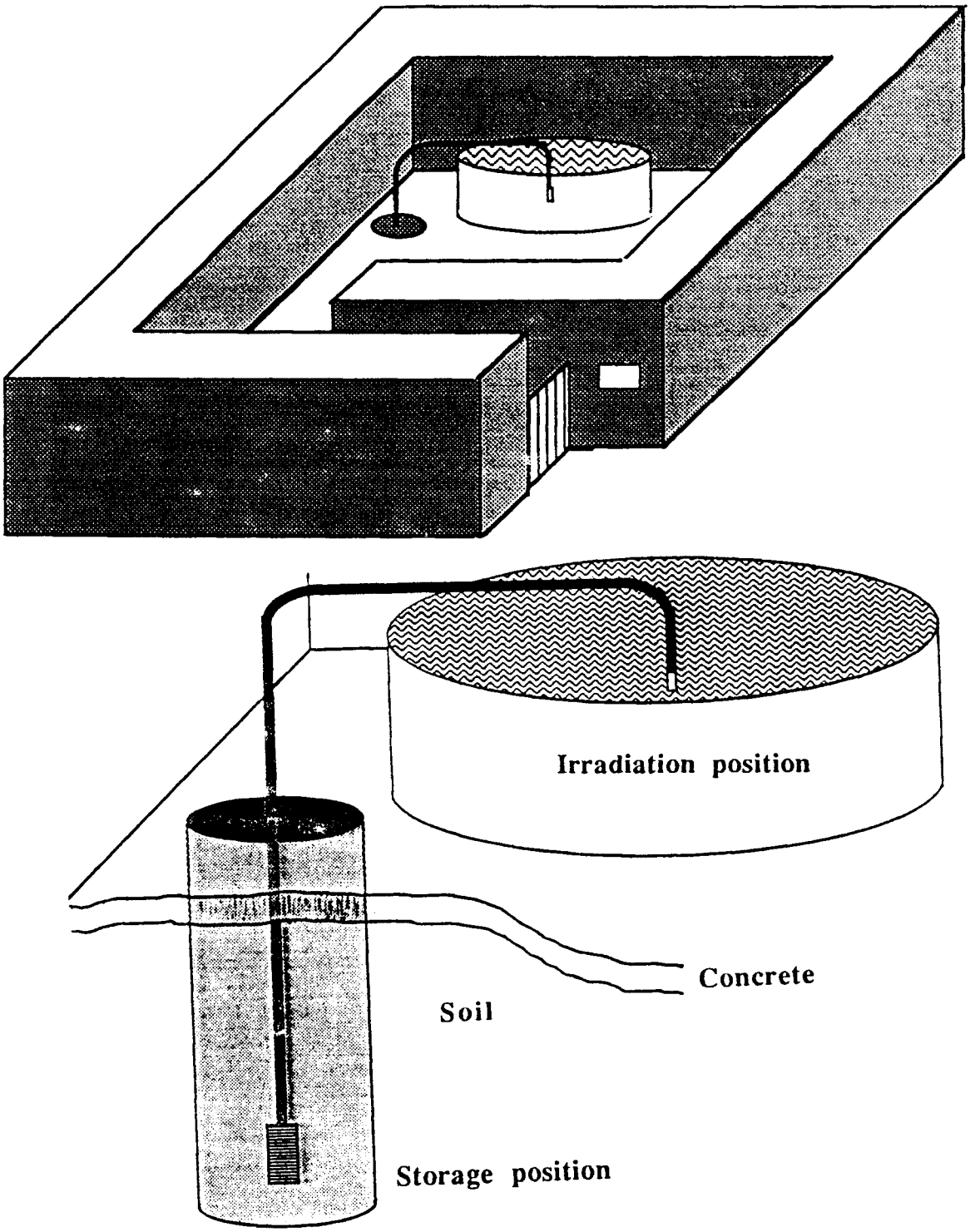


Figure 3.1 Schematic diagram of the irradiation room and the source transfer system.

The irradiation facility is shown schematically in Figure 3.1 which illustrates the arrangement in the irradiation room and the source transfer system. In order to protect the users from irradiation, the storage position of the source was 2.5m beneath the ground. An electronically controlled device activated compressed air to shoot the source up to the irradiation position, through a long steel pipe. This pipe was embedded in a column of polythene beads. The source was returned pneumatically at the end of the irradiation[15].

The steel pipe ended up in the middle of a cylindrical tank, where the irradiation site was. The source tank was filled with water, to take advantage of its rapid slowing-down power and its low cost, for moderation and also for radiation shielding. The energies of the moderated neutrons, (see Chapter 2) follow a Maxwellian distribution, centered at 0.0253 eV at 293 K. The water was circulated through a filtration system. Samples inside polyethylene, perspex or aluminium containers, were introduced to the irradiation site manually. The tank was surrounded for additional shielding, by a wall of 1 m thickness, made from a special high density concrete. For safety, an alarm was activated when the source was transferred to the irradiation position. There was also an interlock on the access gate.

Different irradiation geometries were used for the various experiments and are described in the relevant sections.

3.2 Detection equipment

Most activation products are γ - ray emitters, therefore emphasis is placed on detecting these γ - rays as efficiently as possible and with the best resolution. Two practical detector types currently available commercially are NaI(Tl) and Ge(Li). NaI detectors have higher efficiency and lower resolution than Ge(Li) detectors. NaI(Tl) detectors are normally used when the γ - ray energy is high (greater than 2 MeV, say) or when the gamma-ray spectrum is simple.

a) Ge(Li) detectors

Two germanium coaxial photon detectors have been used.

i) The first detector is a lithium-drifted germanium detector manufactured by ORTEC, mod. GEM-381805. It has a large active volume with a crystal diam. of 57.7 mm and a length of 72.5 mm with an absorbing layer of 1 mm aluminium. The distance from the endcap to the crystal is 6 mm, and the efficiency is 36.5 % at 1332.5 keV relative to a 75 mm x 75 mm NaI(Tl) detector at 10 cm, the resolution was 1.72 keV FWHM (full width at half - maximum) resolution at the same energy. This detector was used in the initial phase of this research, for the qualitative analysis of the composition of all the samples.

ii) In later work, a second detector was used, also manufactured by ORTEC, mod. GMX-20200. This is a hyper pure co-axial detector constructed of n-type germanium. This type of detector is much less susceptible to neutron damage than the normal p-type detector. The dimensions of the crystal are 52.3 mm diam. by 54.0 mm length. The absorbing layer is 0.5 mm beryllium and the distance between window and detector is 3.0 mm. The resolution (FWHM) at 1332.5 keV (^{60}Co) is 1.86 keV and the relative efficiency at 1332.5 keV is 25.8%. The active volume of this detector is thus appreciably less than that of the first detector, but it has the advantage of being portable and thus flexible in use.

b) NaI(Tl) detectors

A 75 mm x 75 mm NaI(Tl) detector manufactured by BICRON, with 6.5% resolution at 662 keV was also used for detection. Normally for analyses where only one element is activated and the product emits only one γ - ray, the NaI detector provides maximum γ - ray detection sensitivity and the lowest possible detection limit. This detector was used in the case of the gold in activated carbon samples because of their high concentration in gold. In this case high resolution was not important, because the 411 keV peak from the ^{198}Au was dominant. The same detector was also used for the measurements of the neutron flux by activation of metal foils.

Figure 3.2, illustrates the variation of the detectors absolute efficiency with the distance for the 411.8 keV line of the isotope Au-198, as was calculated from data in the literature[13].

During the counting of the irradiated samples, the detectors were surrounded by a lead shield of thickness 5 cm.

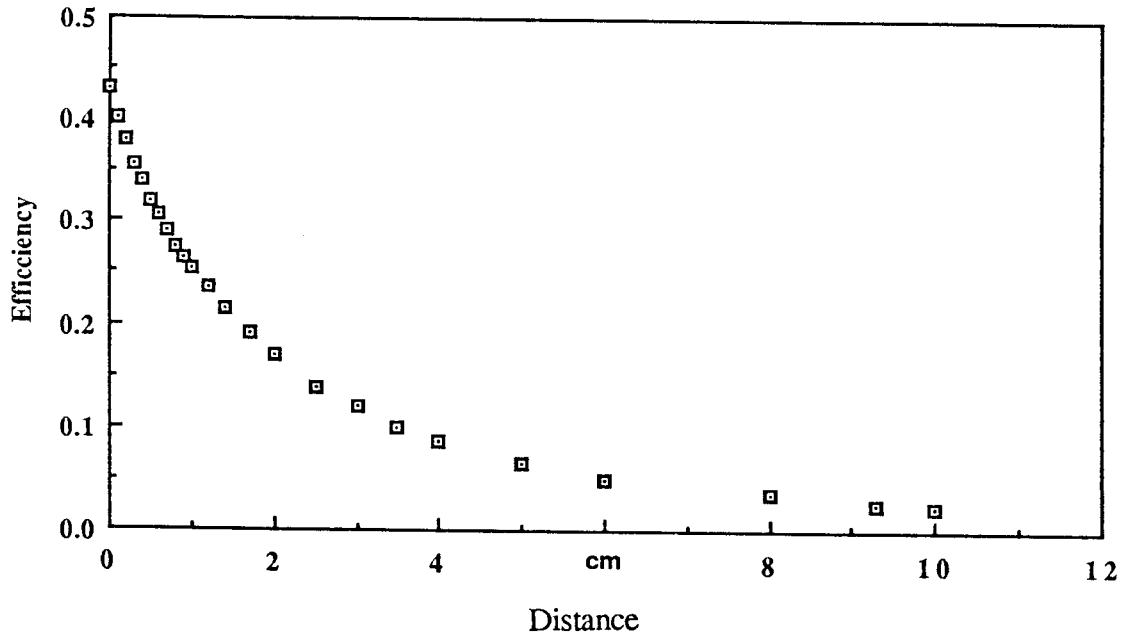


Figure 3.2 Variation of absolute efficiency of the NaI(Tl) detector with distance from sample, for the 412 keV line.

3.3 Multichannel analysers and data reduction

Three multichannel analysers (MCA's) have been used:

a) a Tracor Northern model TN-7200,
b) a CANBERRA series 20 and
c) a CANBERRA series 90.

The Canberra series 90 was used extensively because it is a very sophisticated multichannel analyser, with 16384 channel memory and a variety of time saving functions, i.e. energy calibration, smoothing (3 & 5 point), peak and background integration,

differentiation, counting errors, group transfers, spectrum stripping, peak search, FWHM, etc. This MCA was interfaced to a micro-PDP11 computer linked to a HP plotter and printer.

The gamma - ray spectra from the irradiated samples, were transferred either to a magnetic tape or a floppy disc. In the first case, the programme Yule[29] was used to locate, identify and integrate the peaks in the gamma-ray spectra. A list of significant photopeak energies, integrated areas and their associated statistical errors was produced. The appropriate neutron activation product(s) were assigned to each photopeak by comparing peak energies with tabulated gamma - ray energies. In the second case, the spectra from the floppy discs were processed with the aid of either an Olivetti P.C. or a Macintosh microcomputer using computer programmes.

4. NEUTRON FLUX MEASUREMENTS

4.1 Introduction

At the time of the source's purchase in August 1983, the emission rate was 2.3×10^9 neutrons per second into 4π. When these measurements were made the emission rate was 10^8 neutrons per second. In this work, water was used as moderator and the flux of thermal neutrons was measured. Figures 4.1 and 4.2, illustrate the results obtained at Savannah River[11] for the neutron flux distribution around a 17 mg Cf - 252 source with an output of 3.51×10^{10} $n.s^{-1}$ into 4π.

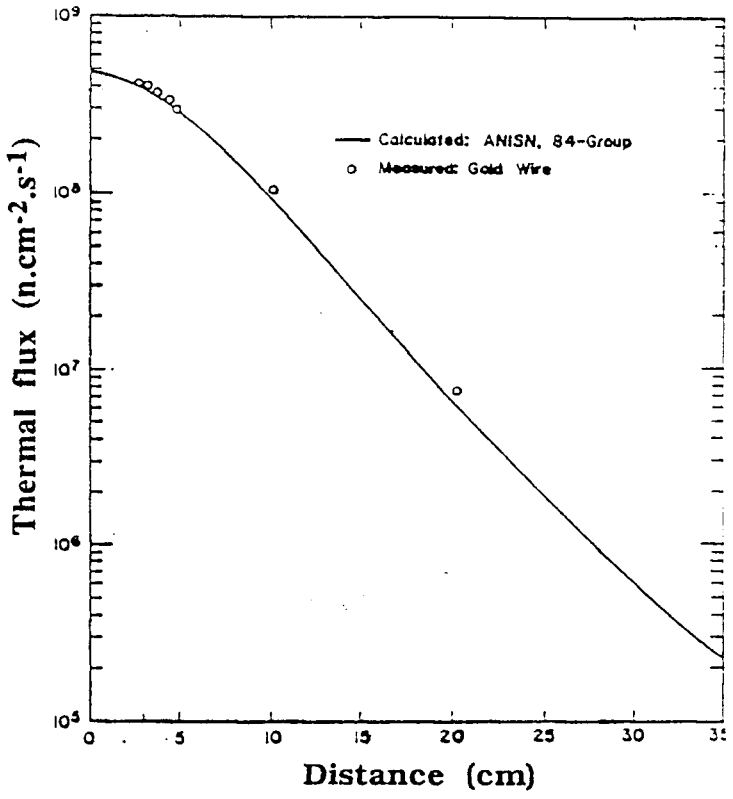


Figure 4.1 Change in thermal flux with distance from source.

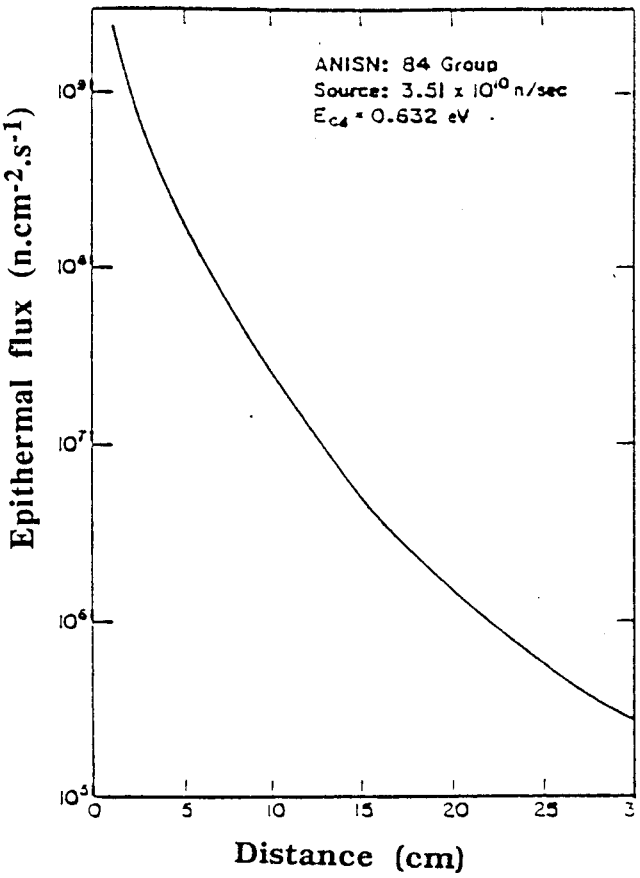


Figure 4.2 Change in epithermal flux with distance from source.

4.2 Experimental

The flux from the neutron source was measured on several occasions. The measurements were performed using standard foils (N.B.S.)[17]. Manganese and cobalt foils were used.

The foils were irradiated for a set time against the irradiation head of the source transfer system. After irradiation, they were transferred manually to a 75 mm diameter by 75 mm long NaI(Tl) detector (see Figure 4.3). The signal from the detector was transferred to a Canberra (model 20) MCA. The irradiation and counting geometries are shown schematically in Figure 4.3. The characteristic data for the above foils are given in Table 6.

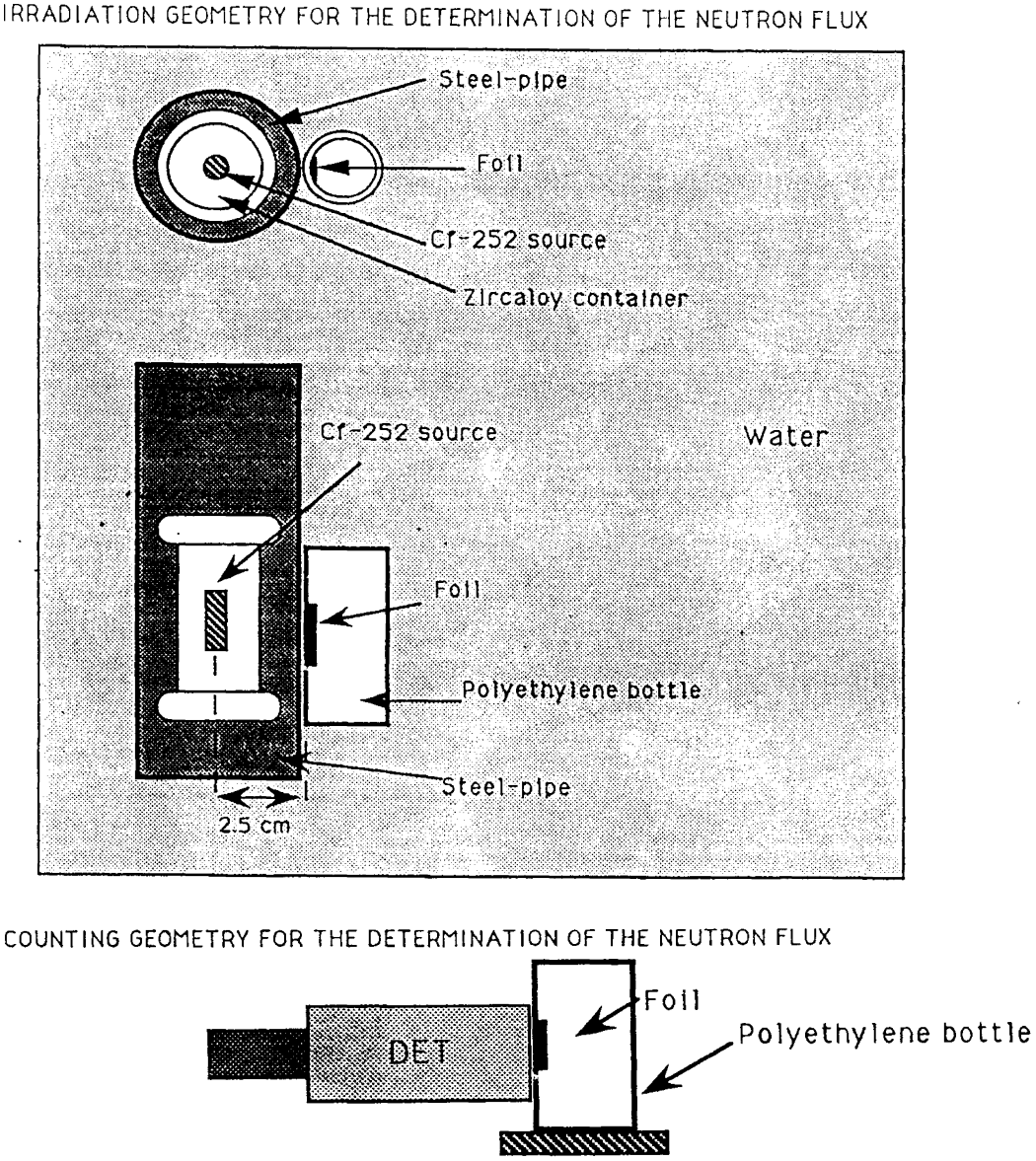


Figure 4.3 Irradiation and counting geometry for the determination of the neutron flux.

TABLE 6

Foil data for neutron flux calculations

Reaction	m (g)	Conc. %	f %	σ barns	E_γ (keV)	γ	ε	T1/2	A
$^{55}Mn(n,\gamma)^{56}Mn$	.0501	81.3	100	13.3	847	1.00	.1564	154.56m	55
$^{59}Co(n,\gamma)^{60}Co$	.0634	99.89	100	20	1333	.25	.105	10.5m	59

The symbols in the headings of Table 6 are defined as in page 8.

4.3 Results

Equation (2-1) was used for the manganese foil calculations and equation (2-2) for the cobalt due to its short half-life in comparison with the irradiation and counting times. Table 7, shows typical results from the neutron flux measurements.

TABLE 7

Results for neutron flux determination

Reaction	T_i (min)	T_d (min)	T_c (sec)	counts	Φ (n cm)
$^{55}Mn(n,\gamma)^{56}Mn$	1114	135	300	398299	1.22×10^6
$^{59}Co(n,\gamma)^{60}Co$	256	2	3600	9128	0.89×10^6

The symbols in the headings of Table 7 are defined as in page 8.

4.4 Discussion

On the basis of the results of Bowman and Mac Murdo[11], the thermal flux at 2.5 cm from a Cf-252 source emitting 3.5×10^{10} n s^{-1} was 4×10^8 n $cm^{-2}s^{-1}$ at a distance of 2.5 cm in water. This gives a thermalisation constant of 87.5.

On the basis of these results the expected flux would have been $\frac{10^8}{87.5} = 1.1\times10^6$ n $cm^{-2}s^{-1}$.

The results from the measurements of the flux are in good accord with the predicted value as can be seen from Table 7.

5. GAMMA-RAY SPECTROSCOPY OF THE GOLD ORE AND CARBON SAMPLES

5.1 Introduction

The samples investigated included a Witwatersrand gold ore containing a range of concentrations of gold as well as activated carbon samples. Details of the samples used, are given in the Table in Appendix A. The same Table also gives the descriptions of the samples and the known concentrations of the elements.

The Table in Appendix B, gives the energies in keV of the gamma - ray lines (and their intensities), which were used to identify the respective isotopes of interest. It also shows their half-lives and the nuclear reactions that produced these isotopes. The symbol f, stands for the isotopic abundance and σ for the cross-section for thermal neutron capture.

5.2 Experimental

In this research one of the most important factors is the geometry of the sample holder. This should be such as to make the optimum use of the neutrons during irradiation, to allow a good geometrical efficiency during counting and to minimise the effect of neutron and gamma-ray self-absorption. This was achieved by the use of annular sample holders in the form of "Marinelli beakers"[19], i.e. cylindrical perspex containers of three different thicknesses (i.e. 1, 1.5 and 2 cm), having a cylindrical hole on the axis with a diameter of 82 mm. The geometry of these holders is shown in Figure 5.1.

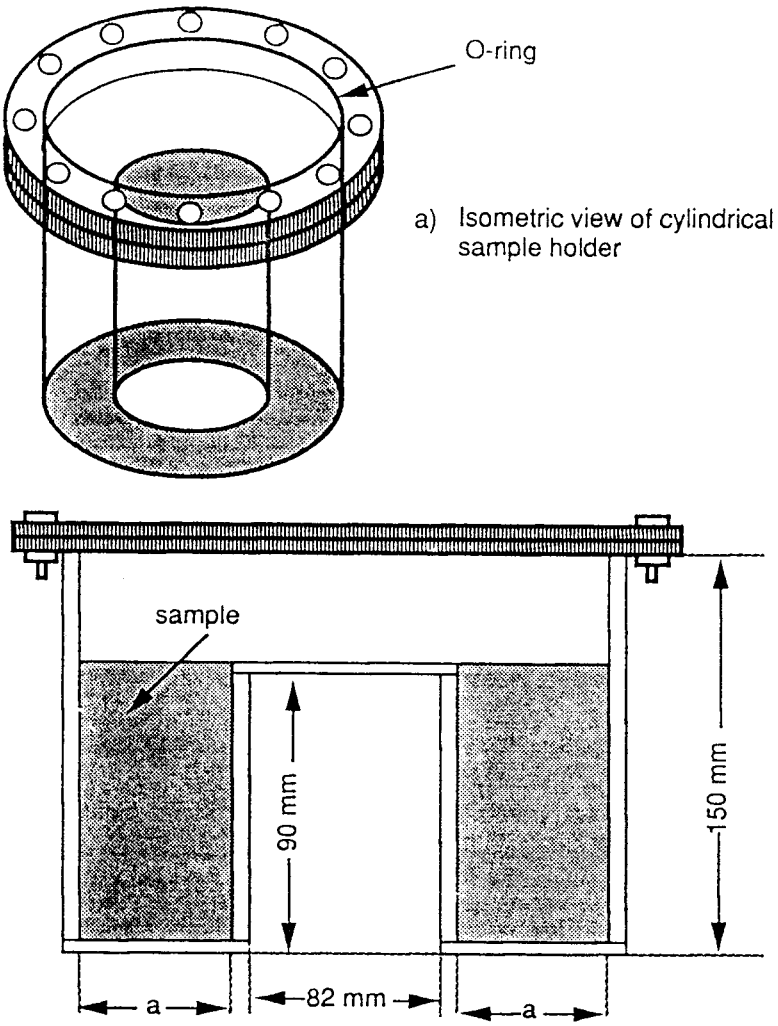


Figure 5.1 Marinelli - type perspex sample holders.

The mass of the samples was between 150g and 1200g (large samples). The holders were filled up as shown in Figure 5.1, then an O-ring and twelve bolts around the lid, made the sample - holder water - proof. Figure 5.2, illustrates schematically the irradiation and counting geometry. The samples were attached to a rotator and were placed inside the pool near the end of the source transfer pipe, fully submerged in the water. During irradiation, the sample was rotated around its axis as close to the source as possible. All the different samples from each group were irradiated for sixteen hours at least, each one separately. After irradiation, they were transferred manually from the irradiation site to the counting room, where they were counted with different decay and counting regimes with

the Ge(Li) γ - ray detector. An MCA received the signals and the spectra were transferred automatically to the computer which analysed the spectra. After the end of each count, a print - out was available with the necessary information concerning the gamma-ray spectrum.

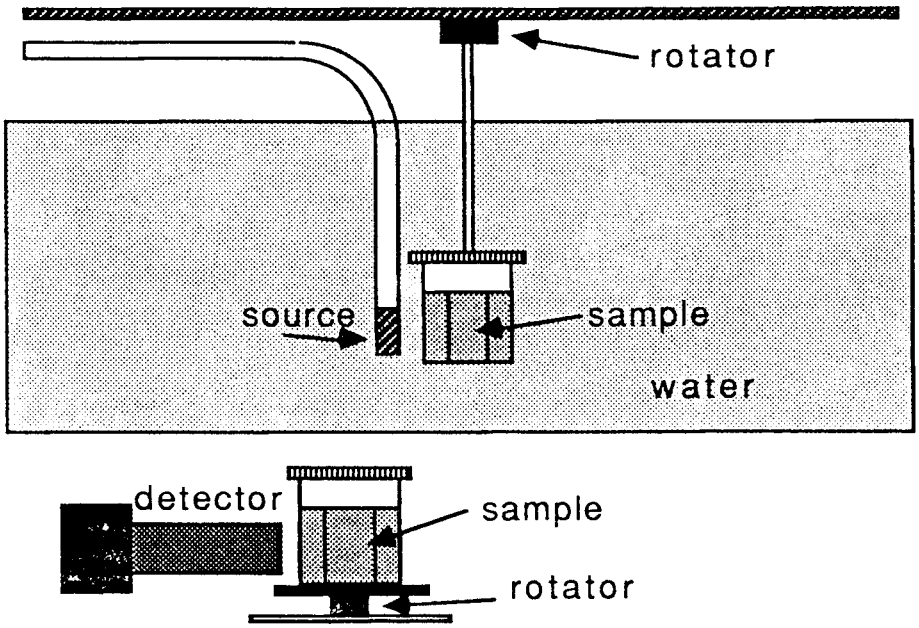


Figure 5.2 Irradiation and counting geometry.

5.3 Results

5.3.a. Gold ore samples

The gold peak at 411.8 keV could be clearly seen even in the sample NIM 23/81 with the smallest concentration (0.5 ppm Au) of gold as shown in Figure 5.3. Under these circumstances, the L.O.D. for gold was 0.0169 ppm of Au. The spectrum was taken after an irradiation time of 69h, a decay time of one day and a counting time of 10h.

The composition of all the gold ore samples was similar, except for their gold concentration. For that reason we shall refer only to the spectrum from NIM 62/69 (11.5 ppm Au), as representative of all the other cases. The spectrum is shown in Figure 5.4.

It covers an energy region from 0 to 2000 keV. It was obtained with an 18.5h irradiation time, a 5h decay

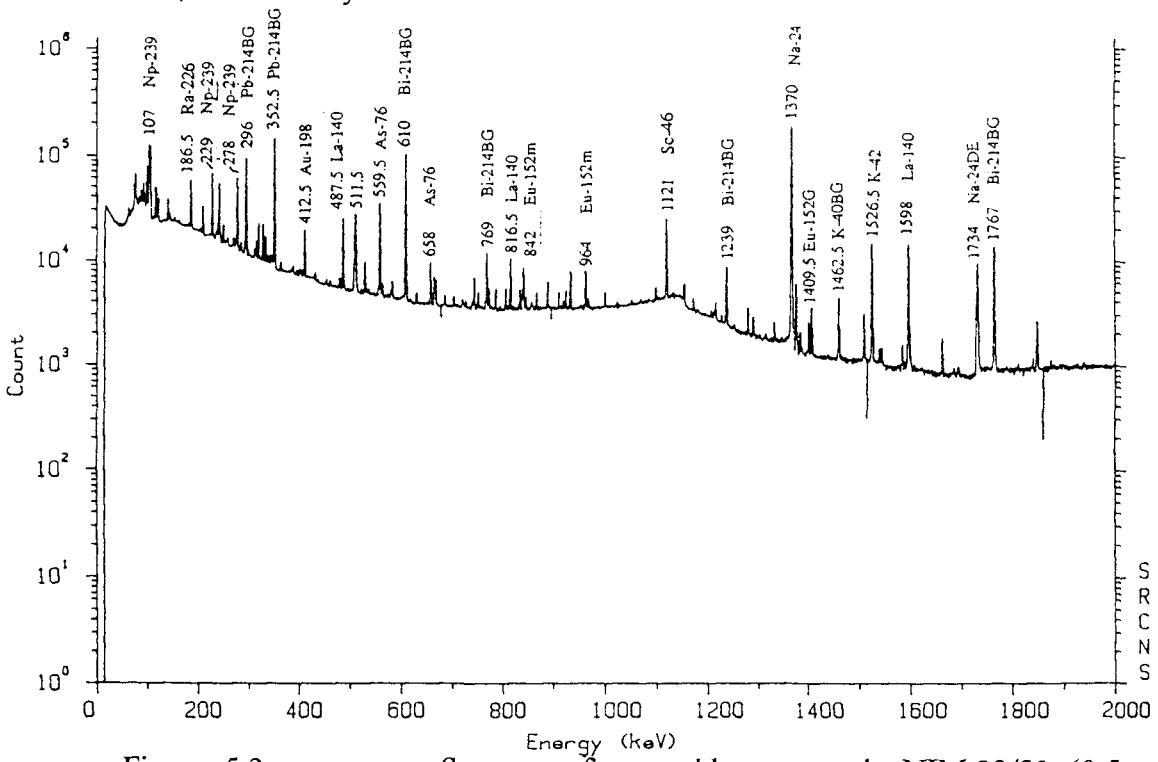


Figure 5.3 Spectrum from gold ore sample NIM 23/81 (0.5ppm Au) after T_i =69h, T_d =1d, T_c =10h.

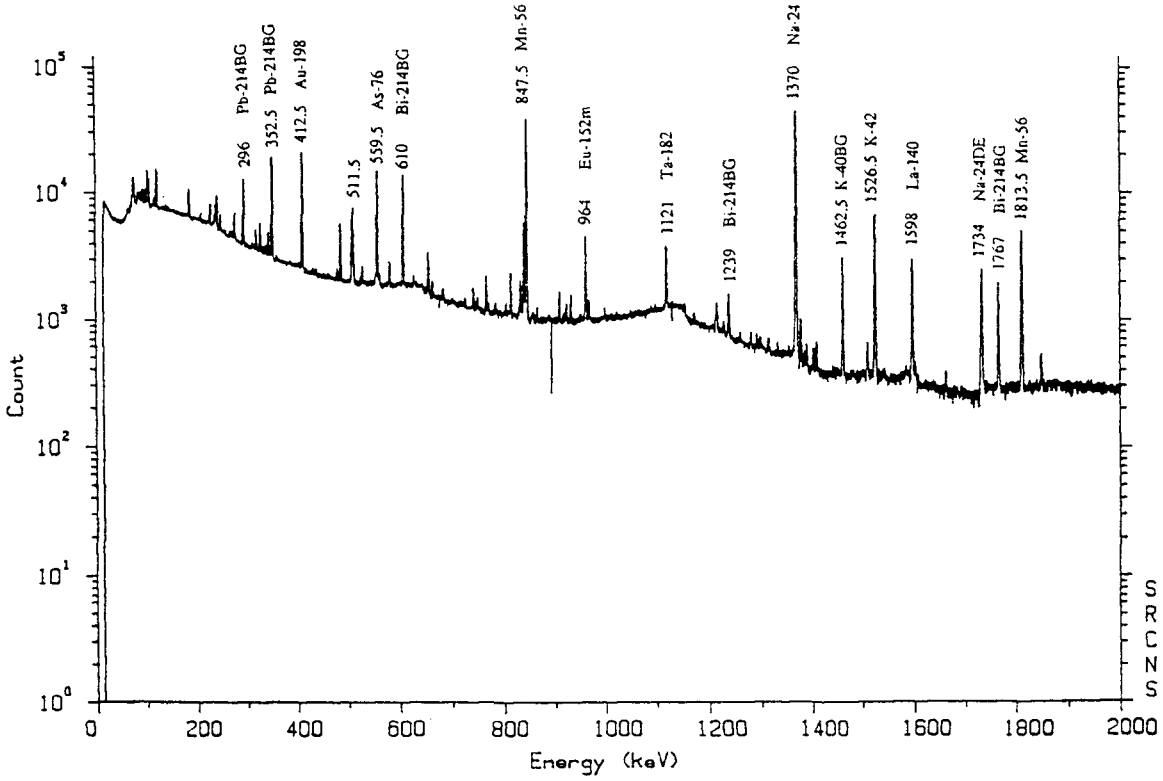


Figure 5.4 Spectrum from gold ore sample NIM 62/69 (11.5ppm Au) after T_i =18.5h, T_d =5h, T_c =5h.

time and a 5h count time. All the main peaks from this spectrum, with their statistical errors and the identified isotopes are tabulated in Table 8. The nuclear reactions which occur during irradiation are also shown in the table as well as the original elements in the ore. The peaks due to the background are also identified.

There are several strong peaks, but most of them are due to the background. Of all these peaks, only a few are of interest. At 1368 keV and 1734 keV, there are strong peaks from Na-24. Sodium, is a major constituent of the ore, as well as potassium, which is identified from the peak at 1526.5 keV from the isotope K-42. Peaks from La-140, Mn-56 and As-76 can also be identified. Peaks from europium, samarium, tantalum and uranium, were also observed in the spectrum. The peak of interest for the determination of gold at 411.8 keV is strong but of the same order of magnitude as the 352 keV peak from the natural uranium activity.

TABLE 8

GAMMA-RAY PEAKS IDENTIFIED IN SPECTRA FROM

GOLD ORE 62/69 (11.5ppm Au)

Ti = 18.59h Td = 4h:59m:49s Tc = 5h

Peak Energy (keV) (%)	Counting Statistics	Isotope	Reaction	Element
104	3.38	Sm-153	$^{152}Sm(n,\gamma)^{153}Sm$	Sm
107	5.52	Np-239	$^{238}U(n,\gamma)^{239}U(\beta^-)$	U
117.5	12.82	Ta-182	$^{181}Ta(n,\gamma)^{182}Ta$	Ta
186.5	5.46	Ra-226	Background	
229	7.09	Np-239	$^{238}U(n,\gamma)^{239}U(\beta^-)$	U
239.5	5.49	Pb-212BG	Background	
242.5	4.19	Pb214BG	Background	
250.5	10.04			
278	7.79	Np-239	$^{238}U(n,\gamma)^{239}U(\beta^-)$	U
296	1.80	Pb-214BG	Background	
329.5	6.45	La-140	$^{139}La(n,\gamma)^{140}La$	La
335	22.67	Np-239	$^{238}U(n,\gamma)^{239}U(\beta^-)$	U
339	17.64			
345	7.85	Eu-152	$^{151}Eu(n,\gamma)^{152}Eu$	Eu
352.5	1.31	Pb-214BG	Background	
412.5	0.90	Au-198	$^{197}Au(n,\gamma)^{198}Au$	Au
487.5	3.33	La-140	$^{139}La(n,\gamma)^{140}La$	La
511.5	1.99		Annihilation	
559.5	0.84	As-76	$^{75}As(n,\gamma)^{76}As$	As
583.5	11.18	Tl-208BG	Background	
609.5	1.18	Bi-214BG	Background	
658	4.50	As-76	$^{75}As(n,\gamma)^{76}As$	As
676.5	27.25	Au-198	$^{197}Au(n,\gamma)^{198}Au$	Au
744	14.26			
752	21.68	La-140	$^{139}La(n,\gamma)^{140}La$	La
769	6.38	Bi-214BG	Background	
786.5	32.41	Mn-56DE		

TABLE 8 CONT.

Peak Energy keV	Counting Statistics %	Isotope	Reaction	Element
816.5	5.74	La-140	$^{139}La(n,\gamma)^{140}La$	La
834.5	8.64	Mn-54	$^{54}Fe(n,p)^{54}Mn$	Mn
842	1.67	Eu-152m	$^{151}Eu(n,\gamma)^{152m}Eu$	Eu
847.5	0.32	Mn-56	$^{55}Mn(n,\gamma)^{56}Mn$	Mn
889	13.11	Sc-46		
912	11.85	Ac-228BG	Background	
926	17.85	La-140	$^{139}La(n,\gamma)^{140}La$	La
964	2.48	Eu-152m	$^{151}Eu(n,\gamma)^{152m}Eu$	Eu
970	13.76	Ac-228BG	Background	
1217	10.13	As-76	$^{75}As(n,\gamma)^{76}As$	As
1239	6.40	Bi-214BG	Background	
1370	0.27	Na-24	$^{23}Na(n,\gamma)^{24}Na$	Na
1379	7.12	Bi-214BG	Background	
1409.5	12.58	Eu-152G	$^{151}Eu(n,\gamma)^{152}Eu$	Eu
14.62.5	1.95	K-40BG	Background	
1511	13.37			
1526.5	1.00	K-42	$^{41}K(n,\gamma)^{42}K$	K
1598	1.95	La-140	$^{139}La(n,\gamma)^{140}La$	La
1734	1.95	Na-24DE		
1767	2.86	Bi-214BG	Background	
1813.5	1.23	Mn-56	$^{55}Mn(n,\gamma)^{56}Mn$	Mn
1850	14.33			

5.3.b Activated Carbon samples

The second group of samples are activated carbon loaded with gold. In order to study the gamma-ray spectrum, sample Carbon 1/78 containing approx. 1020 ppm of Au was taken as representative. Figure 5.5 shows the spectrum from this sample after a 64h irradiation, 2.3 days decay time and a 15h counting time. The data obtained from this spectrum, in the same way as in the case of the gold ores are tabulated in Table 9.

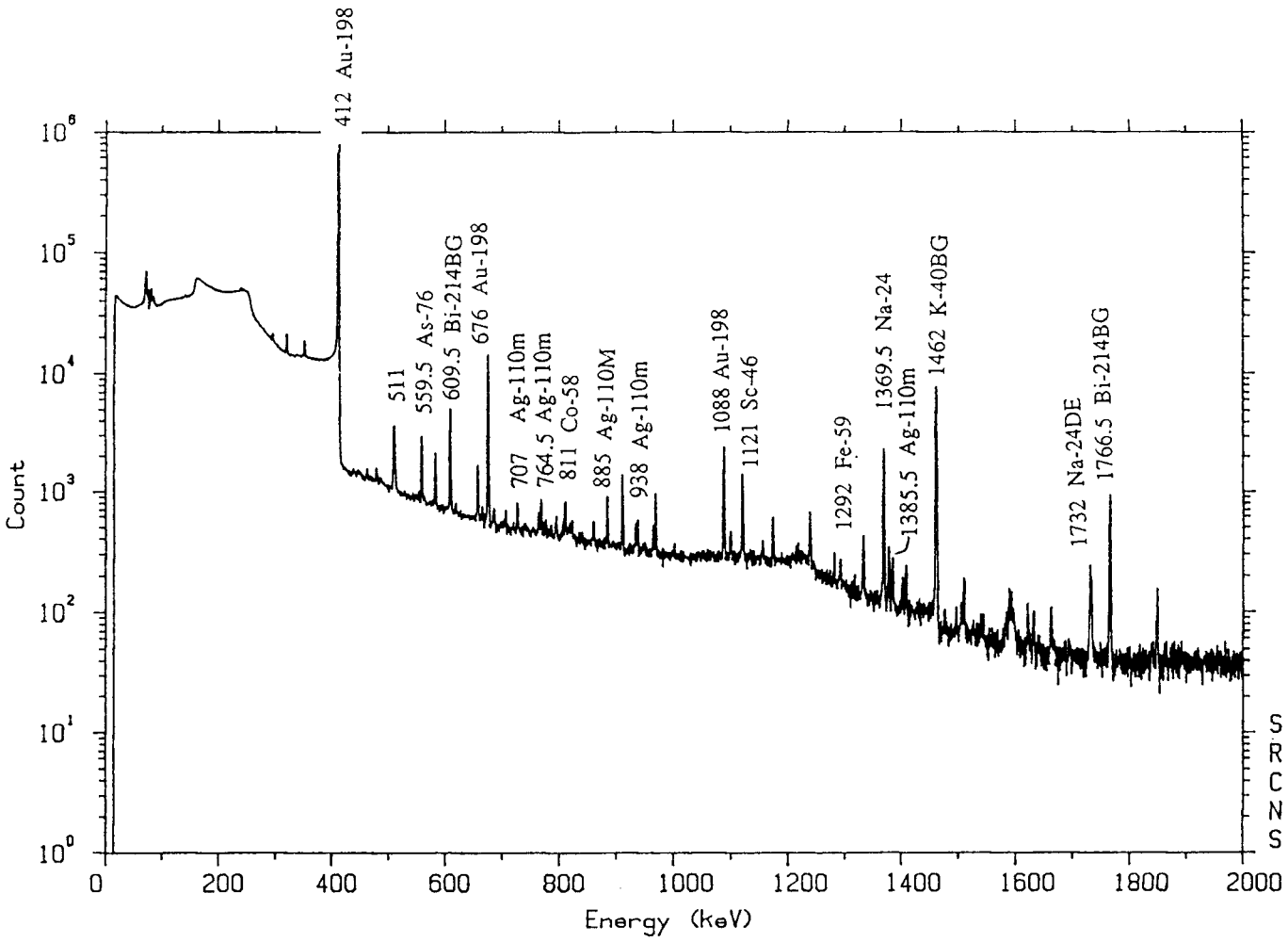


Figure 5.5 Spectrum from carbon activated sample 1/78 (1015-1081ppm Au) after Ti=64h, Td=2.3d, Tc=15h.

TABLE 9

GAMMA-RAY PEAKS IDENTIFIED IN SPECTRA FROM

CARBON 1/78

Ti = 64h Td = 2d:8h:4m Tc = 15h

Peak Energy (keV) (%)	Counting Statistics	Isotope	Reaction	Element
239.5	18.94	Pb-212BG	Background	
246	6.11	Eu-152G	$^{151}Eu(n,\gamma)^{152}Eu$	Eu
296	10.16	Pb-214BG	Background	
352.5	7.41	Pb-214BG	Background	
413	0.07	Au-198	$^{197}Au(n,\gamma)^{198}Au$	Au
511.5	3.07		Annihilation	
559.5	2.68	As-76	$^{75}As(n,\gamma)^{76}As$	As
583.5	4.24	Tl-208BG	Background	
609.5	2.30	Bi-214BG	Background	
658	4.51	As-76	$^{75}As(n,\gamma)^{76}As$	As
676	0.61	Au-198	$^{197}Au(n,\gamma)^{198}Au$	Au
707	20.22	Ag-110m	$^{109}Ag(n,\gamma)^{110m}Ag$	Ag
764.5	18.71	Ag-110m	$^{109}Ag(n,\gamma)^{110m}Ag$	Ag
885	6.97	Ag-110m	$^{109}Ag(n,\gamma)^{110m}Ag$	Ag
911.5	3.65	Ac-228BG	Background	
938	14.86	Ag-110m	$^{109}Ag(n,\gamma)^{110m}Ag$	Ag
965	15.33	Eu-152G	$^{151}Eu(n,\gamma)^{152}Eu$	Eu
969.5	5.48	Ac-228BG	Background	
1088.5	1.90	Eu-152G	$^{151}Eu(n,\gamma)^{152}Eu$	Eu
1100	18.10	Fe-59	$^{58}Fe(n,\gamma)^{59}Fe$	Fe
1174	9.03	Co-60	$^{59}Co(n,\gamma)^{60}Co$	Co
1217	24.22	As-76	$^{75}As(n,\gamma)^{76}As$	As
1239	6.73	Bi-214BG	Background	
1293	22.59	Fe-59	$^{58}Fe(n,\gamma)^{59}Fe$	Fe
1333.5	11.16	Co-60	$^{59}Co(n,\gamma)^{60}Co$	Co
1369.5	1.87	Na-24	$^{23}Na(n,\gamma)^{24}Na$	Na
1378.5	8.62	Bi-214BG	Background	
1385.5	11.35	Ag-110m	$^{109}Ag(n,\gamma)^{110m}Ag$	Ag
1409	12.09	Eu-152G	$^{151}Eu(n,\gamma)^{152}Eu$	Eu
1462	0.62	K-40BG	Background	
1731.5	7.87	Na-24DE		
1766.5	2.30	Bi-214BG	Background	

There is a high concentration of gold (1015-1081 ppm) in this sample, and the peak at 411.8 keV, due to Au-198 is dominant. In this spectrum, peaks at 676 and 1088 keV from the same isotope can be seen, with a statistical error of 0.61% and 1.9% respectively. The intensities of these two peaks are extremely low in comparison with the 95.5% intensity of the main peak of Au-198, at 411.8 keV (see Table 8). This is the reason why they were not seen in the gold ore samples. As in the case of the ore, the 411.8 keV line was used as the analytical peak.

It is interesting to note the main peaks from Ag-110m, at 707, 764.5, 885, 938 and 1385.5 keV shown in Figure 5.5, which indicate that the sample contains silver. There are also peaks from sodium, arsenic, nickel, scandium and iron. Three of the lines, come from the background (see Table 8). The only additional isotope present at short decay times is Mn-56. Isotopes with very short decay times (of the order of minutes or less) could not be investigated because of the distance between the irradiation and counting facilities.

5.4 Discussion

In the spectra from the gold ores, peaks from uranium, samarium, lanthanum, europium, gold, arsenic, manganese, potassium, and sodium were identified. In the case of carbon samples, peaks from gold, arsenic, silver, europium, iron, and cobalt were seen.

Very long irradiation and counting times are necessary to obtain peaks that are comparable with the natural uranium activity in the ores. In the case of the ore most of the activity originates in the ore itself (not in the room background).

If a vertically mounted detector is available then the sample could surround the detector during the count, greatly improving the counting efficiency (see Chapter 7).

6. GAMMA-RAY SPECTROSCOPY OF THE PLATINUM GROUP ELEMENTS

6.1 Introduction

The platinum group consists of six elements, the three lighter elements: ruthenium, rhodium and palladium and the three heavier elements: osmium, iridium and platinum.

There are seven different neutron capture reactions with the six platinum group elements that can be used for neutron activation analysis. These are shown in Table 10. The objective of this section was to determine experimentally the best reactions and gamma-ray peaks to use for the present project, i.e. neutron activation analysis with a ^{252}Cf source and a large sample, using different irradiation and counting conditions.

The details of the best conditions and the best reactions depend on the composition of the sample. In the present case, three different types of sample were used, namely ores, concentrates and mattes. These are described in detail and their compositions are given in Appendix A.

Irradiation and counting were performed several times for each sample. In what follows, we shall refer only to the cases were it was most likely to identify a γ-ray peak from the element under consideration. For convenience, Table 10 gives a summary of the nuclear data of the most important analytical reactions for platinum group elements.

TABLE 10

Nuclear data for the P.G.E.'s

Element	I* %	σ** barn	Reaction	Reac. No	$T_{1/2}$	Main peak (keV)	Intensity %
Ru	31.6	2.56	$^{102}Ru(n,\gamma)^{103}Ru$	1	39.25d	497.1	89.5
Rh	100	150	$^{103}Rh(n,\gamma)^{104}Rh$	2	42s	555.8	1.99
Rh	100	11	$^{103}Rh(n,\gamma)^{104m}Rh$	3	4.34m	51.4	48.2
Pd	26.7	12	$^{108}Pd(n,\gamma)^{109}Pd$	4	13.46h	88.0	3.61
Os	41	1.6	$^{192}Os(n,\gamma)^{193}Os$	5	30.5h	138.9	4.27
Ir	37.3	300	$^{191}Ir(n,\gamma)^{192}Ir$	6	73.8d	316.5	82.9
Pt	7.2	4	$^{198}Pt(n,\gamma)^{199}Pt$	7	30.8m	543	14.8
Pt			$^{199}Pt(\beta^-)^{199}Au$	8	3.14d	158.4	36.9

* I = the isotopic abundance.

** σ = the thermal neutron capture cross - section.

6.2 Experimental

The samples were irradiated using Marinelli type sample containers as before. The estimated average neutron flux was of the order of 10^6 n.cm^{-2}s^{-1} (see Chapter 4). During irradiation, the samples surrounded the source and during counting they surrounded the detector (see Chapter 3), in both cases without rotating. The irradiation and counting geometry is illustrated in Figure 6.1.

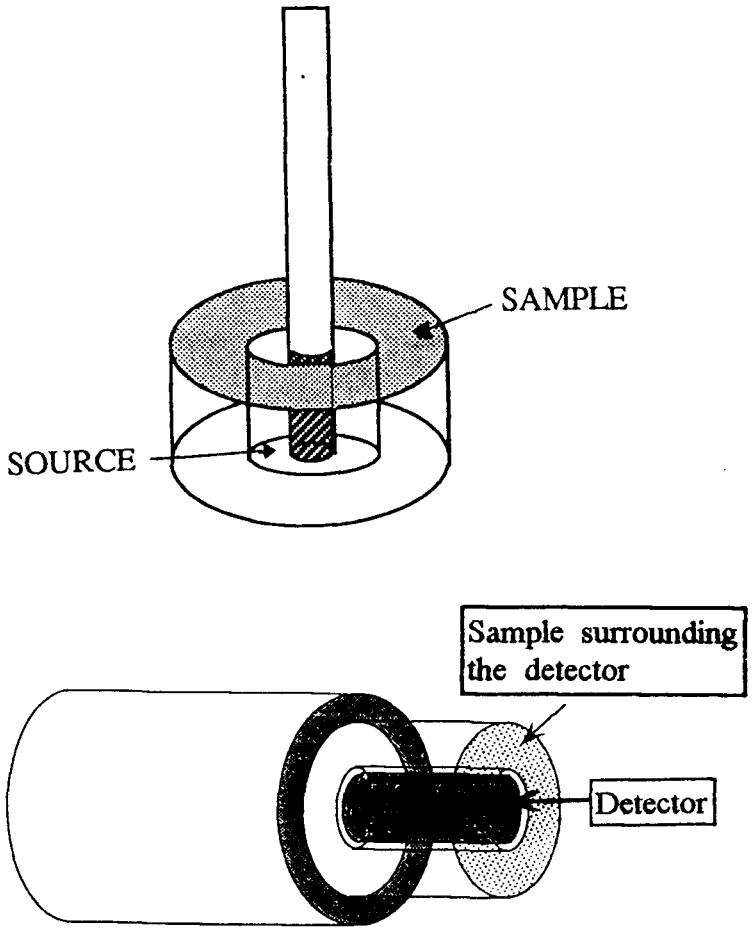


Figure 6.1 Irradiation and counting geometry for P.G.E. samples

Different irradiation, decay and counting times were used for the different elements in the various samples and the different conditions are given in Table 11.

TABLE 11

Experimental conditions for the P.G.E.'s

Sample description	mass (g)	Experimental conditions			Elements observed		
		T_i	T_d	T_c	Element	Concen. ppm	Reaction
Platinum concentrate 16/76	911.45	19h 5min 2.5h	1month 1min 10min	10-15h 5min 15min	Ru Rh Pt	18.6 9 135	1 3 7
Platinum concentrate 26/78	817.31	3d 3d	4d 4d	10h 10h	Os Ir	unkn. unkn.	5 6
Platinum mattes 5/76	310.46	12h 5min 13.5h 12h 2.5h	1month 1min 10min 3weeks 10min	10-15h 5min 10h 15h 15min	Ru Rh Pd Ir Pt	76.6 31.6 169 10 287	1 3 4 6 7
Platinum ore SARM 7	1107.45	4d 4d	3d 3d	24h 24h	Os Pt	0.063 3.74	5 8

6.3 Results - general

The four samples were irradiated under the different conditions shown in Table 11 and twelve spectra were collected. In addition a platinum crucible was irradiated to examine in detail the gamma -ray spectrum from platinum.

Figures 6.2 to 6.5 are shown as typical of the gamma-ray spectra obtained. Table 12 gives a detailed analysis of the peaks observed in the spectrum obtained from the platinum concentrate 26/78 after an irradiation time of 12 h, a long decay time (3 weeks) and a counting time of 15 h. Table 13 gives a detailed analysis of the peaks observed

in the platinum ore SARM 7 after an irradiation time of 4 days, a decay time of 3 days and a counting time of 10 hours.

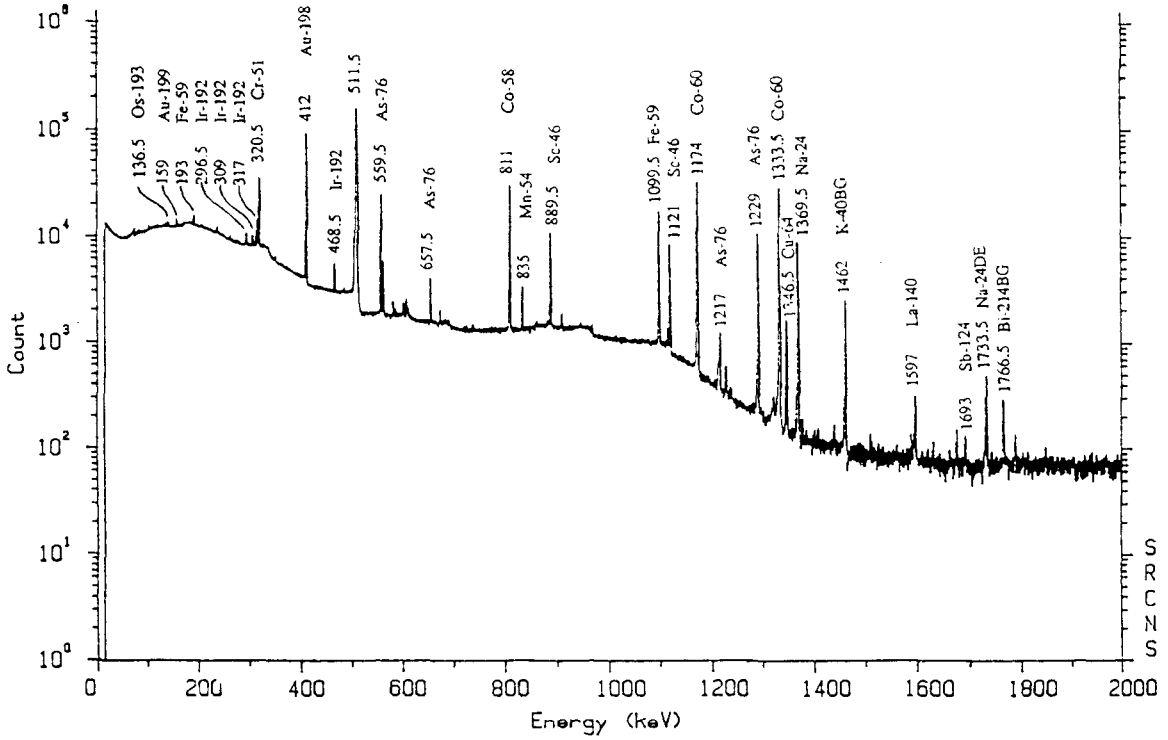


Figure 6.2 Spectrum from platinum concentrate sample 26/78 after Ti=12 h, Td=3 weeks, Tc=15 h.

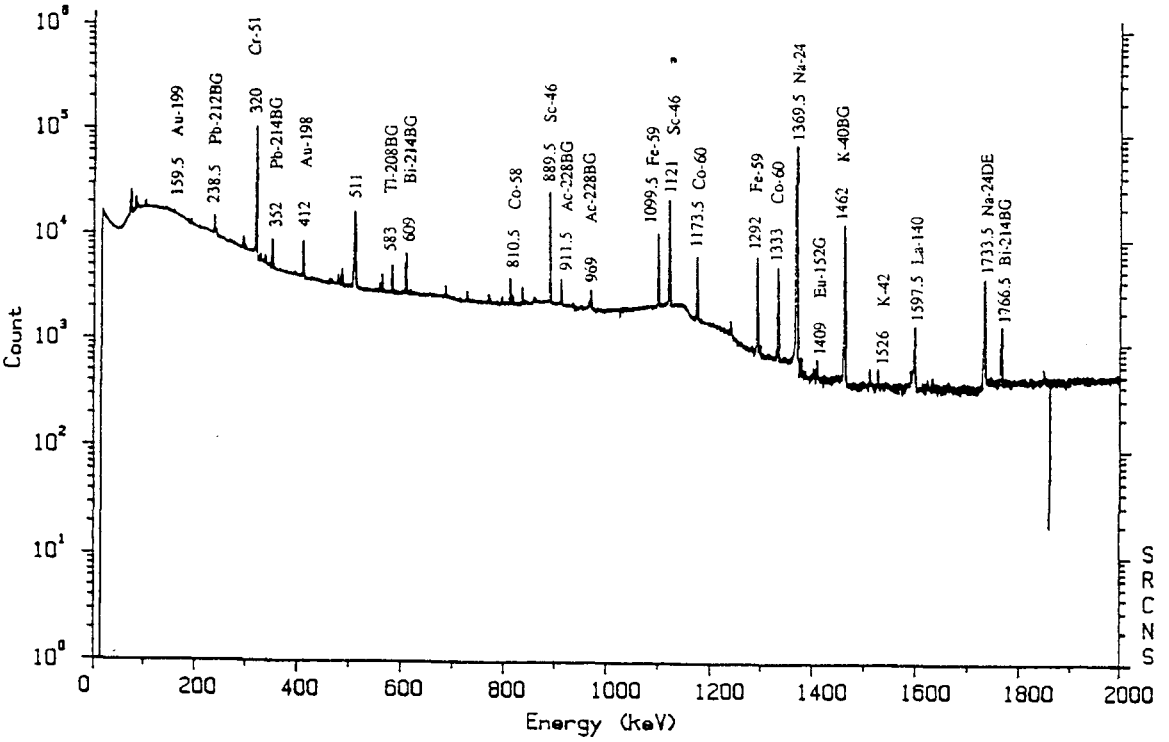


Figure 6.3 Spectrum from platinum ore SARM 7 (for Pt) after Ti=94.5h, Td=3d, Tc=10h.

TABLE 12

γ-RAY PEAKS IDENTIFIED IN SPECTRA FROM PLATINUM CONCENTRATE 26/78
Ti=12h, Td=3 weeks, Tc=15h

Peak Energy keV	Counting Statistics %	Isotope	Reaction	Element
75.5	18		Background	
85.5	27.71		Background	
103.5	18.26	Sm-153	$^{152}Sm(n,\gamma)^{153}Sm$	Sm
136.5	19.66	Os-193	$^{192}Os(n,\gamma)^{193}Os$	Os
159	13.32	Au-199	$^{198}Pt(n,\gamma)^{199}Pt$-$^{199}Au$	Pt
193	8.59	Fe-59	$^{58}Fe(n,\gamma)^{59}Fe$	Fe
209.5	38.23	Au-199	$^{198}Pt(n,\gamma)^{199}Pt$-$^{199}Au$	Pt
239	17.5	Pb-212BG	Background	
296.5	8.73	Ir-192	$^{191}Ir(n,\gamma)^{192}Ir$	Ir
309	8.72	Ir-192	$^{191}Ir(n,\gamma)^{192}Ir$	Ir
317	2.98	Ir-192	$^{191}Ir(n,\gamma)^{192}Ir$	Ir
320.5	0.86	Cr-51	$^{50}Cr(n,\gamma)^{51}Cr$	Cr
329	28.77	La-140	$^{139}La(n,\gamma)^{140}La$	La
412	0.28	Au-198	$^{197}Au(n,\gamma)^{198}Au$	Au
468.5	4.51	Ir-192	$^{191}Ir(n,\gamma)^{192}Ir$	Ir
487.5	32.93	La-140	$^{139}La(n,\gamma)^{140}La$	La
511.5	0.15		Background + others	
559.5	0.58	As-76	$^{75}As(n,\gamma)^{76}As$	As
564	2.47	Sb-122	$^{121}Sb(n,\gamma)^{122}Sb$	Sb
583.5	16.92	Tl-208BG	Background	
604.5	12.38	Sb-124	$^{123}Sb(n,\gamma)^{124}Sb$	Sb
609.5	10.34	Bi-214BG	Background	
657.5	3.9	As-76	$^{75}As(n,\gamma)^{76}As$	As
676	17.73	Au-198	$^{197}Au(n,\gamma)^{198}Au$	Au
811	0.5	Co-58	$^{58}Ni(n,p)^{58}Co$	Ni
835	4.11	Mn-54	$^{53}Mn(n,\gamma)^{54}Mn$	Mn
889.5	1.04	Sc-46	$^{45}Sc(n,\gamma)^{46}Sc$	Sc
1099.5	0.69	Fe-59	$^{58}Fe(n,\gamma)^{59}Fe$	Fe
1116	12.8	Zn-65	$^{64}Zn(n,\gamma)^{65}Zn$	Zn
1121	1.06	Sc-46	$^{45}Sc(n,\gamma)^{46}Sc$	Sc
1174	0.37	Co-60	$^{59}Co(n,\gamma)^{60}Co$	Co
1217	6.07	As-76	$^{75}As(n,\gamma)^{76}As$	As
1229	15.25	As-76	$^{75}As(n,\gamma)^{76}As$	As
1333.5	0.34	Co-60	$^{59}Co(n,\gamma)^{60}Co$	Co
1346.5	3.11	Cu-64	$^{63}Cu(n,\gamma)^{64}Cu$	Cu
1369.5	0.62	Na-24	$^{23}Na(n,\gamma)^{24}Na$	Na
1462	1.39	K-40BG	Background	
1597	12.10	La-140	$^{139}La(n,\gamma)^{140}La$	La
1693	19.78	Sb-124	$^{123}Sb(n,\gamma)^{124}Sb$	Sb
1733.5	5.82	Na-24DE		
1766.5	8.88	Bi-214BG	Background	

TABLE 13

GAMMA-RAY PEAKS IDENTIFIED IN SPECTRA FROM PLATINUM ORE SARM 7
$T_i = 4d$, $T_d = 3d$, $T_c = 10h$

Peak Energy keV	Counting Statistics %	Isotope	Reaction	Element
75	2.82	U-239	Background	
85	5.89	Tm-170	Background	
103.5	11.98	Sm-153	$^{152}Sm(n,\gamma)^{153}Sm$	Sm
159.5	22.49	Au-199	$^{198}Pt(n,\gamma)^{199}Pt$-$^{199}Au$	Pt
192.5	11.94	Fe-59	$^{58}Fe(n,\gamma)^{59}Fe$	Fe
208.5	32.74	Au-199	$^{198}Pt(n,\gamma)^{199}Pt$-$^{199}Au$	Pt
238.5	5.65	Pb-212BG	Background	
242	20.69	Pb-214BG	Background	
295.5	7.93	Pb-214BG	Background	
320	0.36	Cr-51	$^{50}Cr(n,\gamma)^{51}Cr$	Cr
328.5	18.61	La-140	$^{139}La(n,\gamma)^{140}La$	La
352	4.18	Pb-214BG	Background	
412	3.92	Au-198	$^{197}Au(n,\gamma)^{198}Au$	Au
487	10.62	La-140	$^{139}La(n,\gamma)^{140}La$	La
511	1.26		Background + others	
559	13.51	As-76	$^{75}As(n,\gamma)^{76}As$	As
564	8.05	Sb-122	$^{121}Sb(n,\gamma)^{122}Sb$	Sb
583	4.2	Tl-208BG	Background	
609	3.21	Bi-214BG	Background	
768.5	16.83	Bi-214BG	Background	
810.5	5.41	Co-58	$^{57}Ni(n,p)^{58}Co$	Ni
815.5	17.04	La-140	$^{139}La(n,\gamma)^{140}La$	La
834.5	9.73	Mn-54	$^{53}Mn(n,\gamma)^{54}Mn$	Mn
889.5	0.81	Sc-46	$^{45}Sc(n,\gamma)^{46}Sc$	Sc
911.5	5.51	Ac-228BG	Background	
965	23.21	Eu-152G	$^{151}Eu(n,\gamma)^{152}Eu$	Eu
969	8.81	Ac-228BG	Background	
1099.5	1.9	Fe-59	$^{58}Fe(n,\gamma)^{59}Fe$	Fe
1121	0.63	Sc-46	$^{45}Sc(n,\gamma)^{46}Sc$	Sc
1173.5	2.11	Co-60	$^{59}Co(n,\gamma)^{60}Co$	Co
1238.5	15.47	Bi-214BG	Background	
1292	1.24	Fe-59	$^{58}Fe(n,\gamma)^{59}Fe$	Fe
1333	1.75	Co-60	$^{59}Co(n,\gamma)^{60}Co$	Co
1369.5	0.21	Na-24	$^{23}Na(n,\gamma)^{24}Na$	Na
1378.5	12.84	Bi-214BG	Background	
1409	18.9	Eu-152G	$^{151}Eu(n,\gamma)^{152}Eu$	Eu
1462	0.63	K-40BG	Background	
1526	22.5	K-42	$^{41}K(n,\gamma)^{42}K$	K
1597.5	5.47	La-140	$^{139}La(n,\gamma)^{140}La$	La
1733.5	1.61	Na-24DE		Na
1766.5	4.01	Bi-214BG	Background	

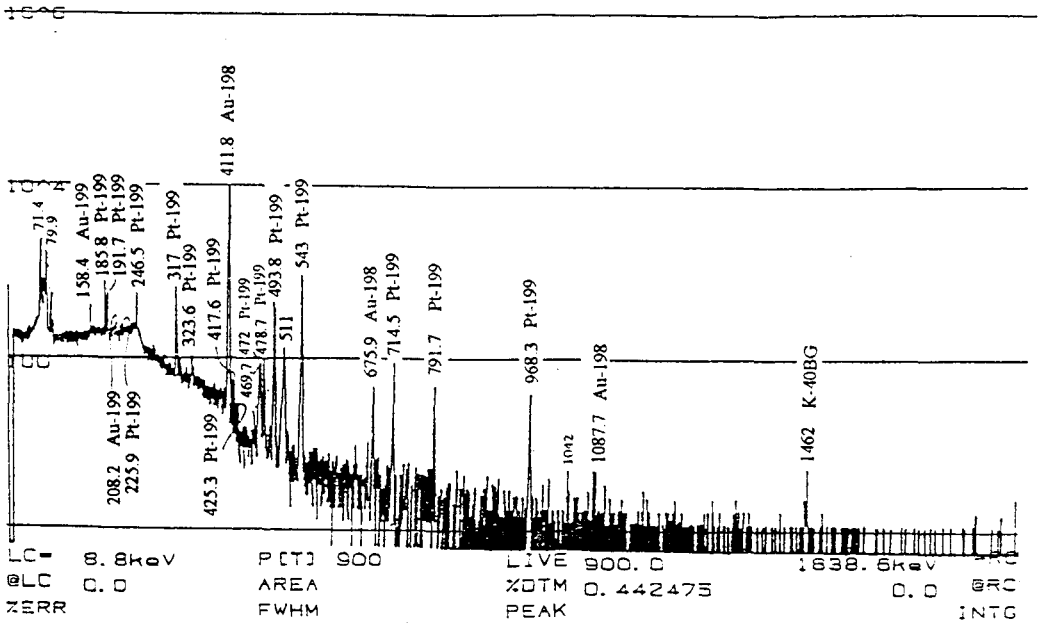


Figure 6.4 Spectrum of platinum cup

after Ti=2.5h, Td=10m, Tc=15m

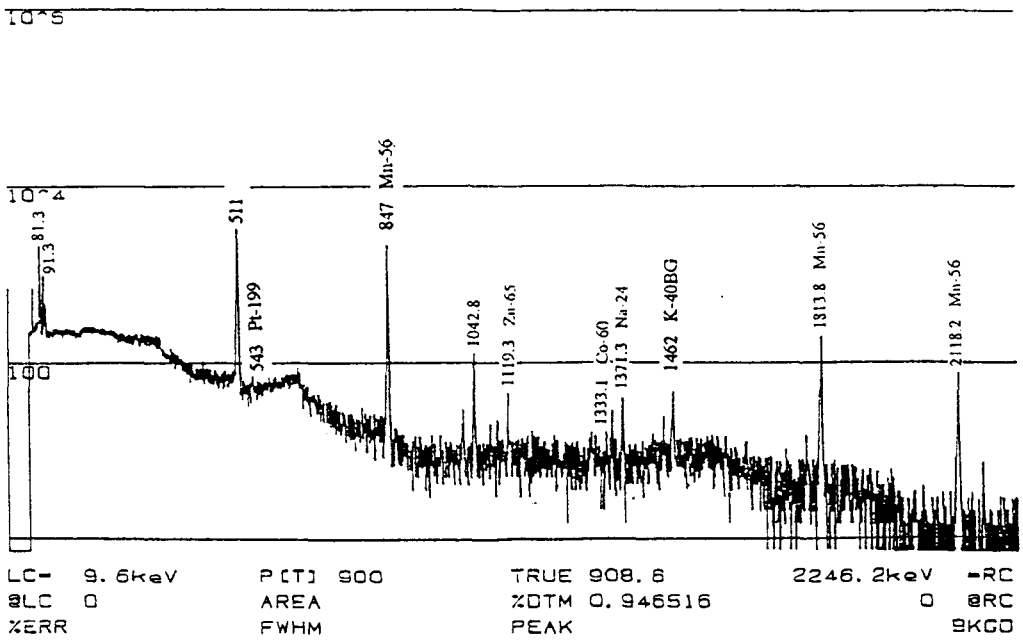


Figure 6.5 Spectrum from platinum concentrate 16/76 (for Pt)

after Ti=2.5h, Td=10m, Tc=15m

6.4 Results - individual elements

Ruthenium

The cross - section for the reaction $^{102}Ru(n,\gamma)^{103}Ru$ is low σ = 2.56 barns. In order to detect the line at 497.1 keV, characteristic for ruthenium, the platinum concentrate 16/76 and the platinum mattes 5/76 were irradiated for 19h and 12h respectively. These two samples had the highest concentrations of Ru. The samples were allowed to decay for one week and counted for periods of 10-15h were repeated for several times during the following month, but the peak at 497 keV could not be detected, because of the low cross - section of the above reaction and the long half-life of the product. The isotopic abundunce of Ru-102, is also comparatively low.

Rhodium

Natural rhodium is found as ^{103}Rh. Its isotopic abundance is 100%. The cross - section for the reaction $^{103}Rh(n,\gamma)^{104}Rh$ is high (σ = 150 barns), but the half-life of Rh-104 is only 42 sec. In this case, as we had to transfer the samples manually, it was not convenient to study this reaction. Instead, there is another reaction taking place with a cross - section of 11 barns, $^{103}Rh(n,\gamma)^{104m}Rh$. The half-life of the isomer Rh-104m is 4.34 min and the main gamma - ray peak is at 51.4 keV, with intensity 48.2%. The same two samples as above were irradiated, for 5min each and after 1min decay time they were counted for 5min. Figure 6.6.a, shows the region around the 51 keV, of the spectrum from the platinum mattes 5/76 sample (concentration of Rh : 31.6 ppm). The peak at 52.3 keV, originates from the Rh-104m isotope. After 16min decay time, a 5min counting was repeated and the peak at the same region disappeared (Figure 6.6.b) as was expected. Under the above conditions, the L.O.D. for Rh is 11.9 ppm and the statistical error of the peak, was 9.6% at a concentration of 31.6ppm.

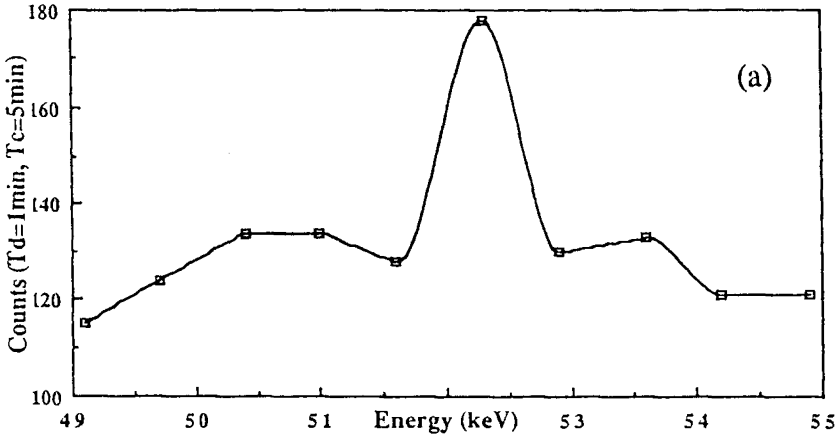


Figure 6.6.a Spectrum from platinum mattes sample5/76 (for Rh)
Ti=5m, Tc=5m, Td=1m

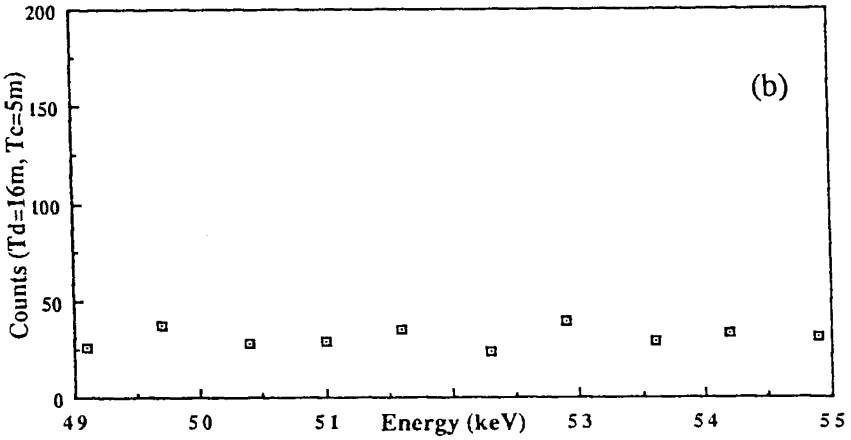


Figure 6.6.b Spectrum from platinum mattes sample5/76 (for Rh)
Ti=5m, Tc=5m, Td=22m

Palladium

The isotope ^{108}Pd has an isotopic abundance of 26.7% and the cross - section of the reaction $^{108}Pd(n,\gamma)^{109}Pd$, is 12 barns. The half-life of the isotope Pd-109 is 13.46h and the main gamma-ray peak is at 88.0 keV with intensity 3.61%. In this spectral region,

there are many interferences from X-rays, from the background and from the natural decay of uranium in the sample, making the detection of palladium complicated. Figure 6.7 shows a representative spectrum from the platinum mattes (concentration of Pd : 169 ppm), with an irradiation time of 13.5h, a decay time of 10m and a counting time of 10h.

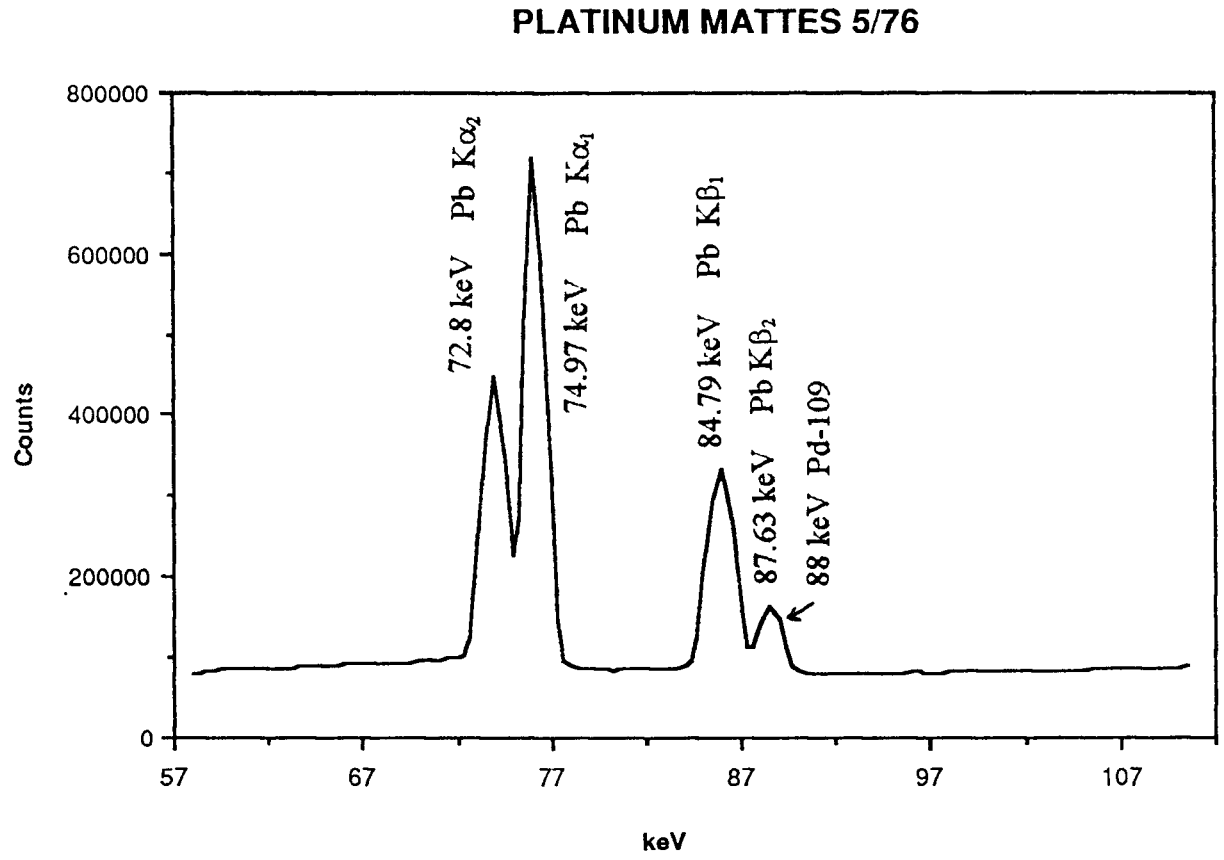


Figure 6.7 Spectrum from platinum mattes sample 5/76 (for Pd) after Ti=13.5h, Td=10m, Tc=10h.

Osmium

There was one sample with a known concentration of Os, the platinum ore SARM 7 with 0.063 ppm Os. Due to the low concentration of the sample, the osmium was not detected. However, osmium was detected in the sample platinum concentrate 26/78 (of unknown concentration in osmium) after an irradiation time of 12 hours, a decay time of 3 weeks and a count time of 15 hours (see Figure 6.2, Table 12).

Iridium

The reaction studied was $^{191}Ir(n,\gamma)^{192}Ir$. The cross - section for this reaction is very high, i.e. 300 b and the half-life of Ir-192 is 73.83 days. The isotopic abundance of Ir-191 is 37.3%. Due to the long half-life of the product, long irradiations and decay times were used, as well as long counting times. The long decay time (one week or more), permitted the background to decay sufficiently, so interferences were greatly reduced. Figure 6.8, shows the energy region where the main peaks from iridium were identified in the platinum matte sample. The spectrum was measured after 12h irradiation, three weeks decay time and 15h counting. The lower level of detection (L.O.D.) under these circumstances, was 2.56 ppm. Figure 6.2 shows the full spectrum from the platinum concentrate 26/78 and in Table 12, there is a description of the peaks. The peaks at 296, 308, 317, 468.5 and possibly a portion from the 604.5 keV, come definitely from Ir-192. These are the most intense lines of this isotope. The spectrum was taken after 3 days irradiation, 4 days decay and 10 hours counting time.

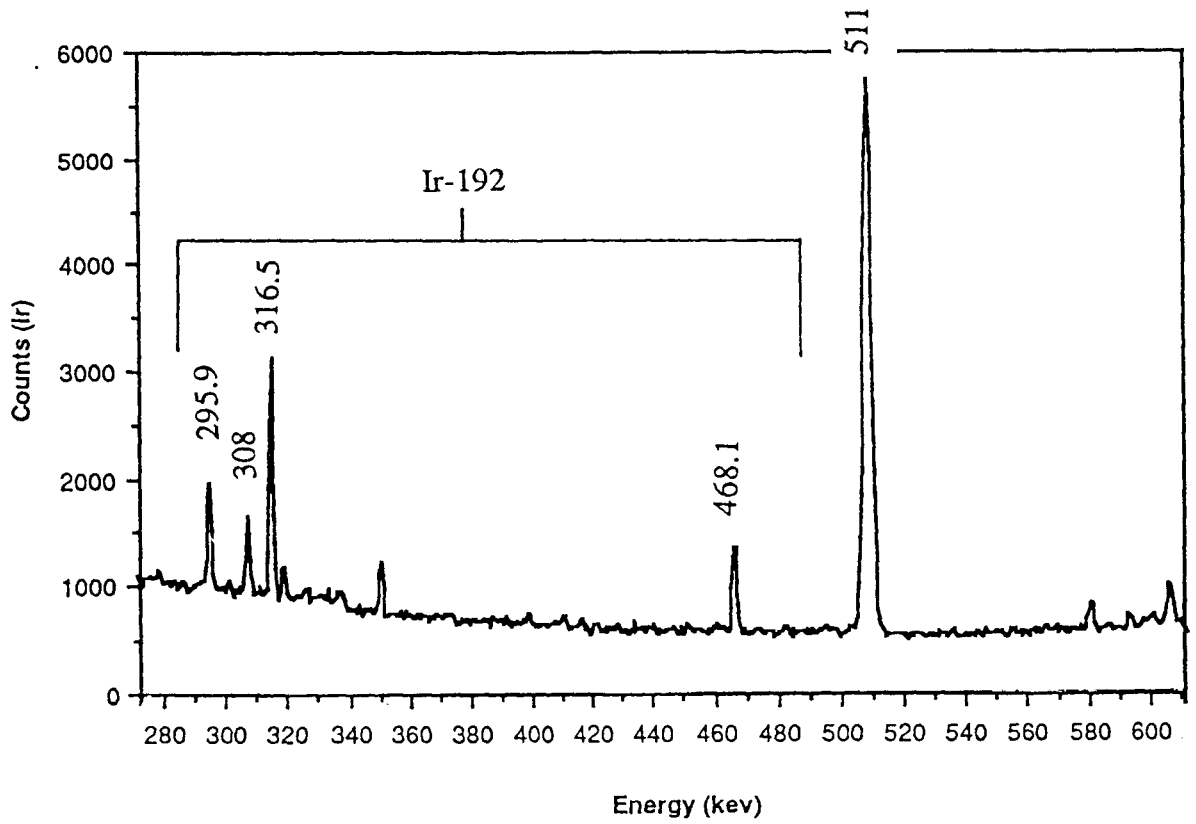


Figure 6.8 Spectrum from platinum mattes sample 5/76 (for Ir) after Ti=12h, Td=3 weeks, Tc=15h.

Platinum

The thermal neutron capture reaction, is $^{198}Pt(n,\gamma)^{199}Pt$. This reaction has a cross - section of 4.0 barns. The natural isotopic abundance of Pt-198 is 7.2% and the half-life of Pt-199 is 30.8 min.

The isotope Pt-199, undergoes β - decay to Au-199, which is also radioactive. Au-199, decays with a half-life of 3.14 days by emitting γ - rays mainly at 158.4 and 208.2 keV, with intensities 36.9% and 8.38% respectively.

Initially, the peaks of Au-199 were studied for the detection of Pt-198. Because of the long half-life of the isotope, long irradiations, decay and count times were used. In Figure 6.2 and from Table 12, the lines at 158.4 keV and 208.2 keV originate from the beta - decay of Pt-199, with statistical errors 13.32% and 38.23% respectively. These peaks were traced in all the samples containing platinum. Figure 6.3, shows the spectrum from the sample platinum ore SARM 7, after 94.5h irradiation time, 3d decay and 10h measurement. Table 13, gives the necessary informations obtained from this spectrum. The peak at 412 keV from the Au-198 can be seen in the same figure. (The sample contains 0.32 ppm of gold). Under these conditions, the L.O.D. for gold in the platinum ore SARM 7 was calculated to be 21 ppb and the L.O.D. for platinum in the same samples using the peak at 158.4 keV, was 1.9 ppm.

In order to identify all the gamma-ray peaks that can be used for the determination of platinum, a platinum crucible (95% Pt and 5% gold), was irradiated for 2.5 h. After 10 min decay time the sample was counted for 15 min. Figure 6.4 shows the spectrum. All the main peaks of platinum are shown clearly, as well as the peaks from Au-198 (from gold) and Au-199 (from the β - decay of Pt-199). After 3h decay time, when the peaks from Pt-199 were decayed, a 15m counting was repeated and the peak from the Au-199 had increased relative to the background as was expected. In the meantime, the background was reduced too, so the statistical error of the peak was improved.

The two samples with the highest concentration in platinum, i.e. platinum concentrate 16/76 (135 ppm Pt) and platinum mattes 5/76 (287 ppm Pt) were irradiated. Irradiation, decay and counting times, were kept the same as for the cup. In the platinum concentrate the peak at 543 keV (Fig. 6.5) can be hardly seen and has a large error. In the platinum mattes (see Fig. 6.9), the peak is slightly better but still has a large error. The statistical error in the latter case is 37%. In both cases, the peak at 158.4 keV from Au-199 was not visible for these decay and counting conditions.

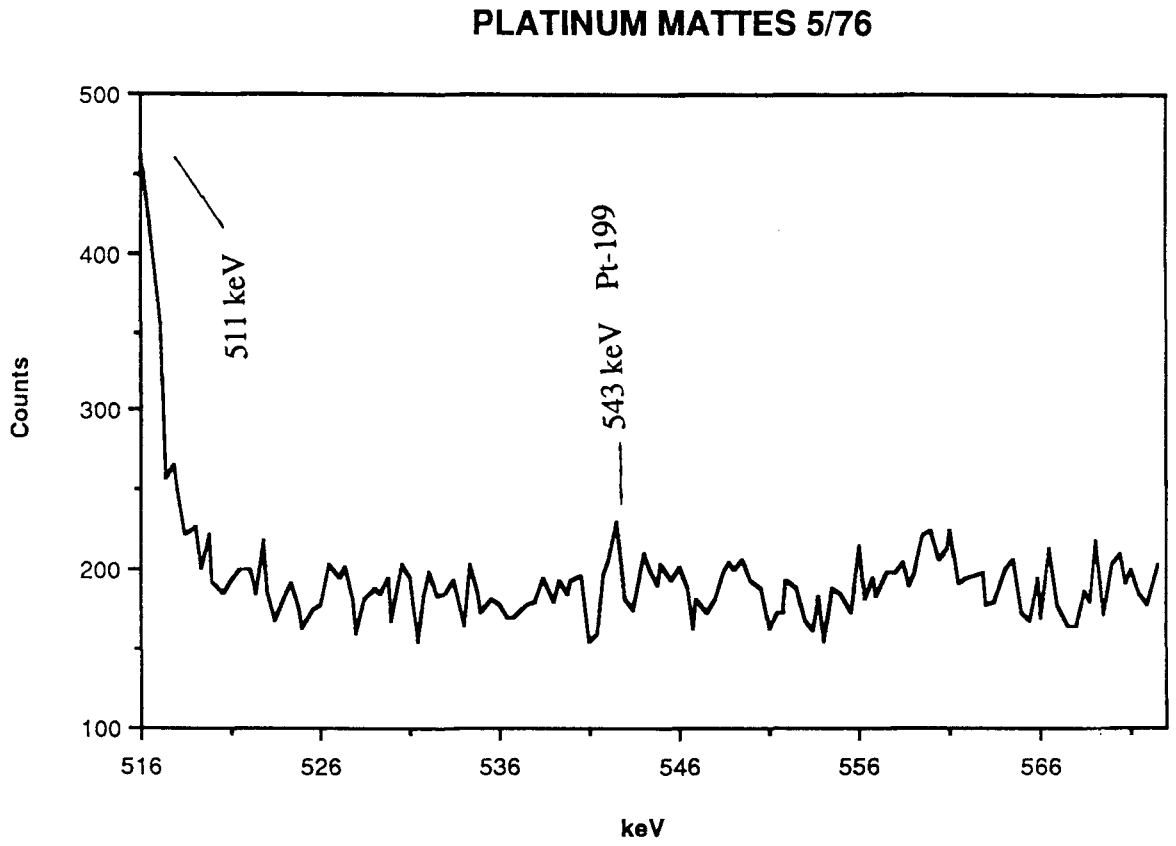


Figure 6.9 Spectrum from platinum mattes 5/76 (forPt) after T_i=2.5h, T_d=10m, T_c=15m

6.5 Discussion

Table 14 gives an overview of the spectra presented, together with the calculated limits of detection (L.O.D.) based on the formula:

$$\text{L.O.D.} = \frac{3\sqrt{B}}{A} \text{ x c}$$

were,

B: the background counts under the peak

A: the area counts of the peak under consideration and

c: the known concentration of the element

The elements of the platinum group are much less active in comparison with gold. Furthermore, the weak neutron flux, which was of the order of 10^6 n.cm^{-2} s^{-1} , was

inadequate in order to measure with a satisfactory sensitivity several elements of the group. However, all elements were detected in different samples, except in the case of ruthenium. Certainly there is need for more work to study each element of the group separately.

The sample mass, was in the range of 300g to 1100g. They were placed in "Marineli" type sample holders. The holders were not filled up to their capacity. In the case of the sample platinum mattes 5/76, 310g were used, which left 3/4 of the holder empty. In the rest of the cases, at least 1/4 of the holders was empty, signifying that even larger masses could have been used, resulting in the same or probably an improved sensitivity. The use of a stronger source (2 or 3 mg of californium-252), would considerably decrease the experimental times and increase the sensitivity of the method.

In conclusion, iridium and platinum were detected after long irradiation, decay and count times, with satisfactory counting statistics down to the level of 2 ppm. Rhodium was detected with very short irradiation and counting times with a level of detection below 12 ppm. Osmium was detected in the sample platinum concentrate 26/78 of unknown concentration of osmium. Palladium needs more study, because the main gamma-ray line at 88 keV interferes with other lines from the room background and the natural activity of the sample.

In addition, gold was detected in all the platinum samples. In the case of the sample SARM 7 (0.32 ppm of gold), after an irradiation time of 4 days, a decay time of 3 days and a count time of 10h, the level of detection for gold was 21 ppb.

TABLE 14

Experimental results for the P.G.E.'s

Element	Sample description	Isotope to be detected	L.O.D. (ppm)	Figure	Table
Ru	Platinum concentrate 16/76	^{103}Ru	N.D.*	-	-
	Platinum mattes 5/76	^{103}Ru	N.D.	-	-
Rh	Platinum concentrate 16/76	^{104m}Rh	** Det.	-	-
Rh	Platinum mattes 5/76	^{104m}Rh	11.9	6.6.a	-
Pd	Platinum mattes 5/76	^{109}Pd	N.D.	6.7	-
Os	Platinum ore SARM 7	^{193}Os	N.D.	-	13
	Platinum concentrate 26/78	^{193}Os	unkn. conc.	6.2	12
Ir	Platinum mattes 5/76	^{192}Ir	2.6	6.8	-
	Platinum concentrate 26/78	^{192}Ir	unkn. conc.	6.2	12
Pt	Platinum concentrate 16/76	^{199}Pt	N.D.	6.5	-
	Platinum mattes 5/76	^{199}Pt	337.3	6.9	-
	Platinum ore SARM 7	^{199}Au	1.9	6.3	13

* N.D.= Not Detected

**Det. = Detected

7. QUANTITATIVE DETERMINATION OF GOLD IN ORES AND ACTIVATED CHARCOAL

7.1 Introduction

The aim of this chapter was to establish a relationship between the specific activity and the concentration of gold in the case of the gold ore and activated charcoal samples.

Four samples of gold ore with concentrations ranging from 0.5 to 12 ppm of gold and seven charcoal samples with concentrations ranging from 33 to 5059 ppm of gold were used and they are described in Appendix A.

7.2 Experimental

7.2.a Experimental for the ores

Two series of experiments have been performed, namely series A and series B.

For the series A, annular sample holders like the one shown in Figure 5.1 were used. The holders were rotating beside the source, with a frequency of three cycles per minute as is shown in Figure 5.2. The distance between the source and the axis of rotation was 10 cm. The masses of the samples, ranged from 400g to 600g. The irradiation time was 17.5h and after 6.5h decay time, they were counted for 10h with the first Ge(Li) detector (described in Chapter 3). During counting, the samples were rotated in front of the detector. As far as possible the same conditions were applied as regards irradiation and counting times. The irradiation and counting geometry is illustrated in Figure 5.2.

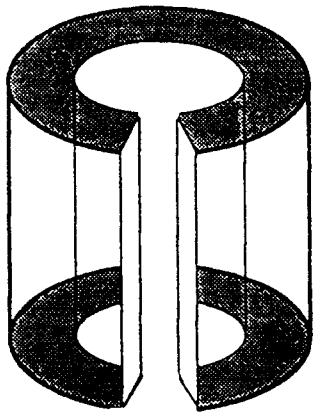


Figure 7.1 Sample holder for the experiments in series B

For the experiments in series B, the typical sample holder is illustrated in Figure 7.1. This time the sample was not rotating, but it surrounded the source. The sample masses were between 300g and 400g. They were irradiated for 14.5h, left 10h to decay and counted for 10h from the n-type Germanium detector. During counting, the samples surrounded the detector. Irradiation and counting geometry is shown in Figure 7.2.

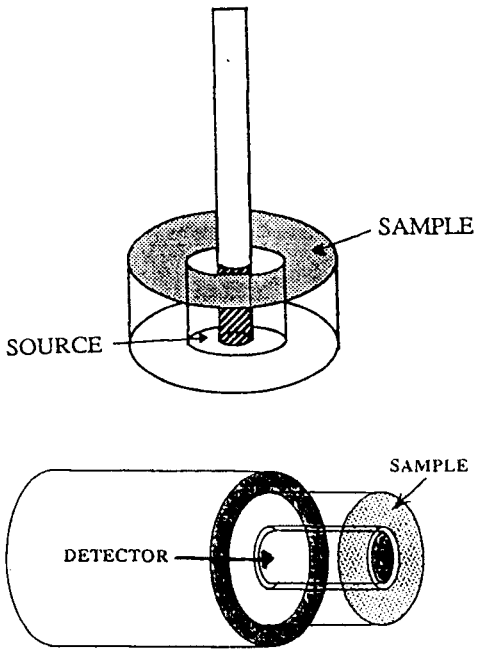


Figure 7.2 Irradiation and counting geometry for series B

In both experiments the samples were irradiated one at a time. The experiment A was performed in order to obtain an even irradiation and the experiment B in order to obtain greater sensitivity.

7.2.b Experimental for the activated charcoal

The sample suite for this experiment consisted of samples with high concentrations of gold. Their masses were between 95g and 100g. The carbon as received and without any treatment was placed in ordinary screw cap polyethylene bottles. They were irradiated for 2h, at the same time, placed symmetrically at the edge of a round base, which rotated around its axis beside the source. After irradiation, they were counted separately for 15m each, with a Ge(Li) detector. During counting, they were also rotated in front of the detector. Figure 7.3 illustrates the irradiation and counting geometry. The experiment lasted less than four hours.

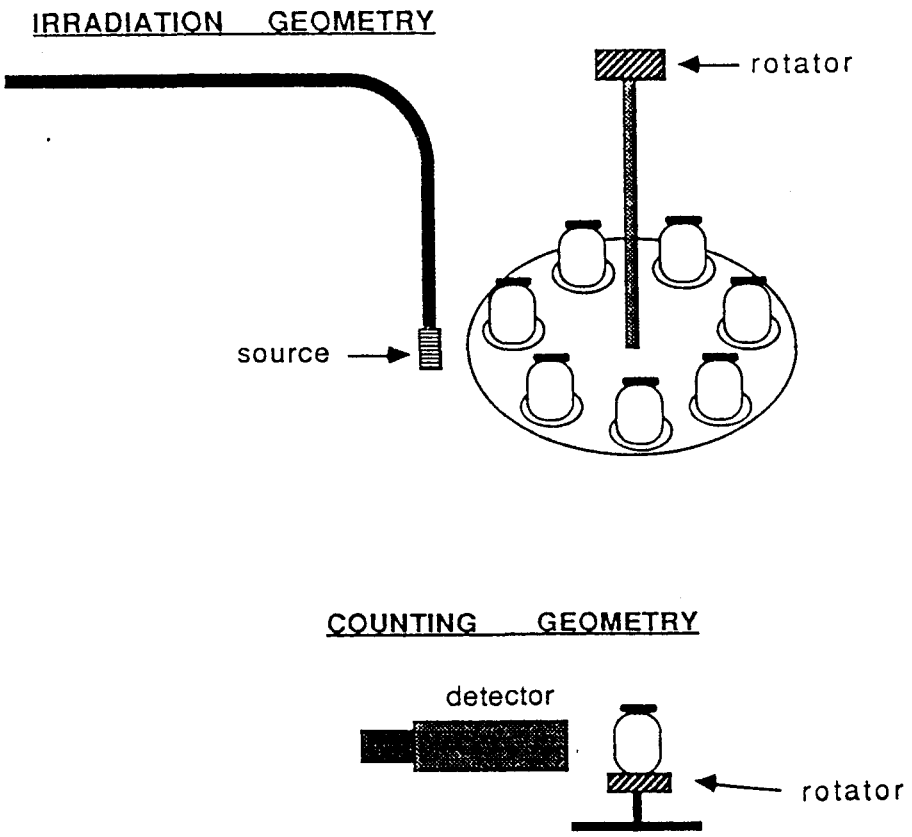


Figure 7.3 Irradiation and counting geometry for the calibration of the activated carbon samples

7.3 Results

7.3.a Results for the ores

The counts per mass of the 412 keV peak were plotted versus the gold concentration. The results are shown in Figure 7.4. The lower curve corresponds to the experiment of the series A and the upper curve to the experiment of the series B. In both cases, the relationship is linear. In the case of the series B, the specific activity is considerably greater.

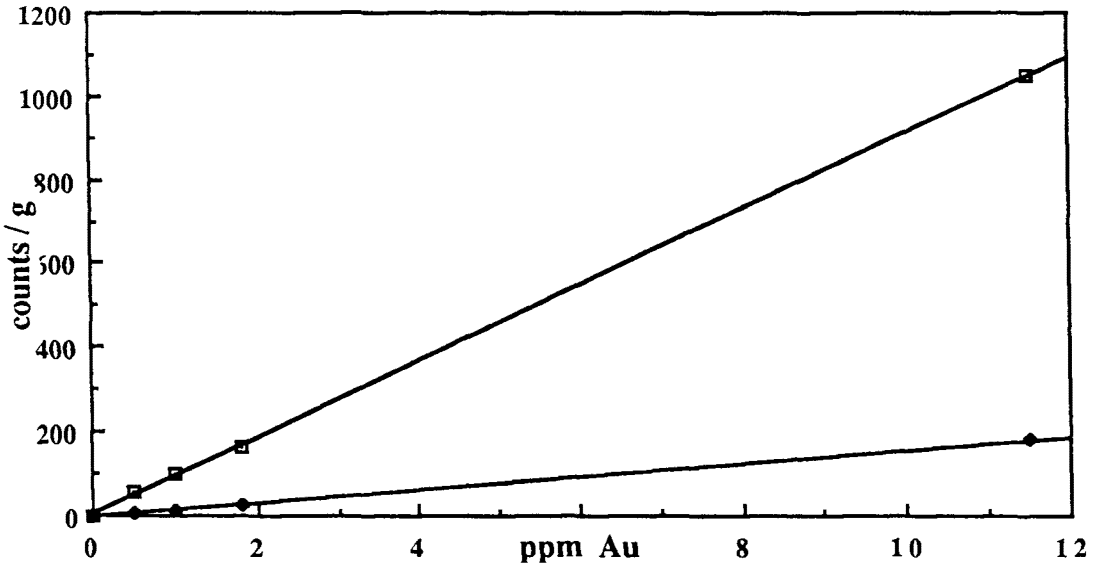


Figure 7.4 Calibration curves for the gold ores

7.3.b Results for the activated charcoal

The results are illustrated in Figure 7.5, where the very satisfactory linear relationship can be used as a calibration curve.

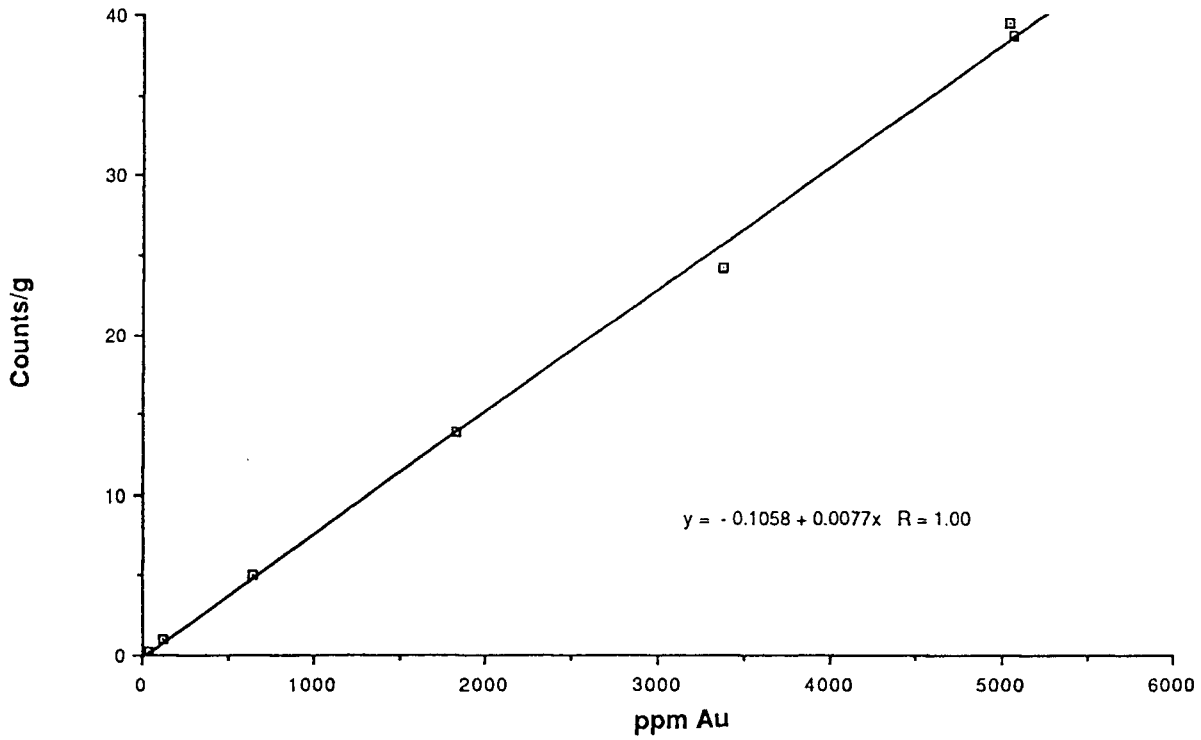


Figure 7.5 Calibration curve for the activated carbon samples

7.4 Discussion

In the case of the calibration curves of the gold ore samples as shown in Figure 7.4, it is evident that although in the series A the masses of the samples were approximately two times larger, the specific counts from the series B were approximately seven times greater. Therefore, the total counts from the series B were approximately three times greater dispite the lower mass of the samples. This observation could be attributed to the following factors:

i) The distance from the source was smaller in the series B, hence the flux was greater.

ii) The irradiation time in the series A was 3h more than the one in the series B, however, the sample was rotating, so the far surface of the sample was receiving little irradiation in comparison with the surface facing the source, because of its additional distance from the source and because of the neutron absorption inside the sample.

iii) The counting geometry also influenced the results, as in the series A the detector's efficiency was different for the surface facing the detector (0.5 cm) and for the surface at the far end of the sample (11.5 cm). The gamma - ray absorption inside the sample must be also taken into consideration. Instead, in the series B, the sample holder was surrounding the detector.

From the above, it is evident that the geometrical efficiency of the experimental arrangements of the series B was clearly much greater.

In the case of the activated charcoal the calibration curve in Figure 7.5 indicates that there is no measurable absorption by the gold itself in these experiments. The gold must be dispersed in a very fine form in these samples.

8. OPTIMISATION OF THE IRRADIATION, DECAY AND COUNTING TIMES

8.1 Introduction

The background activity is of great importance in the determination of the statistical error of a particular photopeak. The optimum decay time depends on the flux level, the sample size, the irradiation and counting times and the relative concentrations of gold and the other elements. It is time consuming to investigate all of these parameters experimentally but a straightforward model can be developed, to show how the optimum decay time and the L.O.D. will depend on these factors[30-33]. The model was also applied to study the effect of irradiation and counting times on sensitivity, as well as the variation of the statistical error with different source sizes.

The development of the model involved a comparison procedure, where the general activation equation was written and solved simultaneously for a known and unknown conditions of a sample.

8.2 Theory - development of a model

The index that determines if the result from a measurement is reliable or not, is the statistical (%) error. Typically, an error should be less than 20%, for a reliable determination to be made. The statistical error of a line, is given by a relationship between the counts of the area and the counts of the background under that area, i.e.

$$\text{Error } \% = \frac{\sqrt{N + kB}}{N} \times 100 \qquad (8 - 1)$$

where,

N = Peak area counts

B = Background counts under the peak

k = a constant dependent on the method used to determine the background

The counts varies with every change in the parameters of an experiment. Each time there is a change in one of the above factors, the statistical error will change [34-35]. It is essential to determine the way that the statistical error varies with these factors, in order to determine the total time that an experiment requires, and thus to obtain reliable results.

8.2.a Formula for peak area and statistical error

The relative error in the peak is given by :

$$Error = \frac{\sqrt{\sigma^2(A)}}{A} \qquad (8 - 2)$$

with $$\sigma^2(A) = T + \frac{(L-R-1)^2}{4}(n_L + n_R) - (n_L + n_R) \qquad (8 - 3)$$

where,

A : is the number of counts of the peak area, ($A = T - B$)

$$A = \sum_{i=L+1}^{R-1} n_i - (L-R-1)\frac{(n_L + n_R)}{2} \qquad (8 - 4)$$

T : is the total number of counts between the left and right bounds L+R,

$$T = \sum_{i=L}^{R} n_i \qquad (8 - 5)$$

n_i : is the number of counts in the i-th channel of the peak area respectively,

B : is the number of counts of the background under the peak. For k channels it is given by :

$$B = \frac{(L-R-1)}{2k}\left(\sum_{L-k+1}^{L} n_i + \sum_{R}^{R+k-1} n_i\right) \qquad (8-6)$$

and $$\sigma^2(B) = \frac{(L-R-1)^2}{4k^2}\left(\sum_{L-k+1}^{L} n_i + \sum_{R}^{R+k-1} n_i\right) = \frac{(L-R-1)^2}{2k}\bar{n} \qquad (8-7)$$

8.2.b Variation of standard deviation with the irradiation, decay and counting time

The background under the peak of interest (in this case the 411.8 keV peak from ^{198}Au), is due to interferences from the other prominent elements in the ore, as well as the room background and the count rate from the natural activity of the ore. Therefore, the total background is :

$$B(T_i, T_d, T_c) = B_r(T_c) + B_s(T_c) + \sum_{j=1}^{n} B_j(T_i, T_d, T_c) \qquad (8-8)$$

where

B_r is the count rate from the room background,
B_s is the count rate from the sample natural radioactivity ($B_s = b_u m c_u$ for example, with b_u the specific count rate from U(+Th) in the sample in the 411.8 keV portion) and
B_j is the background contribution from the j-th isotope i.e.:

$$B_j(T_i, T_d, T_c) = \frac{N_o m f_j c_j r_j \Phi \sigma_j \varepsilon_j \gamma_j}{A_j \lambda_j}(1-e^{-\lambda_j T_i})(1-e^{-\lambda_j T_c})e^{-\lambda_j T_d} \qquad (8-9)$$

Here,
f_j is the corresponding isotopic abundance,
σ_j the cross-section,
c_j the concentration of the relevant element,
γ_j the γ-ray intensity of the analytical peak,
A_j the atomic mass of the isotope,
λ_j the decay constant,

ε_j the total efficiency of the detector for the analytical peak and
r_j the ratio between the analytical peak area for isotope j and the background from that isotope under the peak of interest.

8.3 Experimental results

The optimum decay time was determined experimentally in the case of the sample NIM 38/81 gold ore, with 1.82 ppm of gold.

An amount of 500g of the sample was irradiated for 22h rotating beside the source. The container was as in Fig. 5.1. It was counted at several decay times, for one hour. The experiment lasted more than one week. A Ge(Li) detector and the Tracor Northern MCA were used. The sample was also rotated during counting, using the geometry of series A. Irradiation and counting geometry are as in Figure 5.2.

The counting errors in the peak area were determined as a function of decay time using the formulas (8 - 2) up to (8 - 7) and the experimental results.

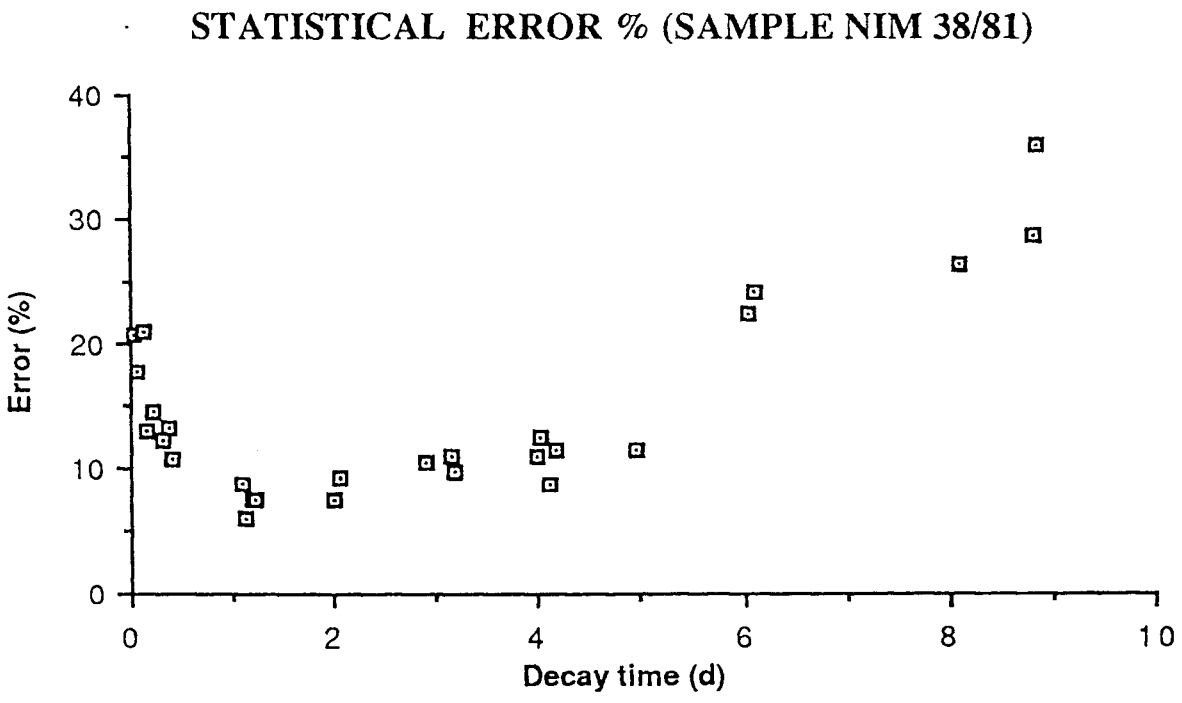


Figure 8.1 Measured statistical error vs decay time

The results are shown in Figure 8.1 for the sample NIM 38/81 containing 1.8 ppm of gold. The error decreases with the decay time, up to approximately 23h, indicating that the background under the peak decays faster than the peak area, then it starts increasing as the gold peak decays. In the case of this gold ore sample, the optimum decay time is approximately 23h.

8.4 Measured components of the background

8.4.a General

The results from section 8.3 indicate that the knowledge of the optimum decay time is essential in order to improve the sensitivity of detection of a particular element.

In previous chapters, several spectra are shown, with most of the peaks originating from the natural radioactivity of the sample and the room background. There are also peaks, mainly from sodium and potassium, characteristic of the composition of the samples. In order to study which would be the optimum decay time for a specific peak, that is when we expect the minimum statistical error, it is essential to take into consideration the contribution to the background under that peak, from all the other peaks in the spectrum plus the contribution of the room background and the natural activity of the ore.

8.4.b Room background and natural activity of the ore

Figure 8.2, shows the spectrum obtained from a 10h measurement of the room background, i.e. the Ge(Li) detector was counting under the same shielding conditions which were used to count the samples, but with no sample in front of it. Figure 8.3, refers to a 10h measurement of the gold ore sample NIM 62/69 which was not irradiated. The difference between the two spectra corresponds to the background coming from the natural activity of the sample. Figure 8.4 refers to a 10h measurement of the same gold ore sample after an irradiation time of 14.5 hours and a decay time of 10 hours.

The difference of the spectra in Figures 8.2, 8.3 and 8.4, indicate that under the given conditions, the room activity contributed 1.5% and the background due to the natural activity of the ore, contributed 22.1% to the total background under the 411.8 keV peak

in Figure 8.4. Hence, for a decay time of 10 hours, after an irradiation time of 14.5 hours under the given conditions, a total of 23.6% of the background is from these constant sources.

8.4.c Background contributions from other elements

The remaining 76.4% portion of the background of the 411.8 keV peak ,under these conditions is due to the interferences from the other elements characteristic of the composition of the ore. These elements are mainly (see Table 15) : sodium, potassium, lanthanum, manganese and arsenic. Each one of them contributes a different percentage to the background, depending on the sensitivity and the half-life of the element.

In order to calculate these contributions, a set of experiments was perfomed. For each case, a spectrum from the irradiation of a pure element, (i.e. an oxide of the specific element), was needed, in order to calculate the ratio between the counts of its peak area and the area of the 411.8 keV line on the same spectrum (peak to Compton ratio). When this ratio was known, the contribution to the gold background in the spectrum from the ore sample could be calculated. In Table 15, the peak to Compton ratios and the contributions from each element are tabulated.

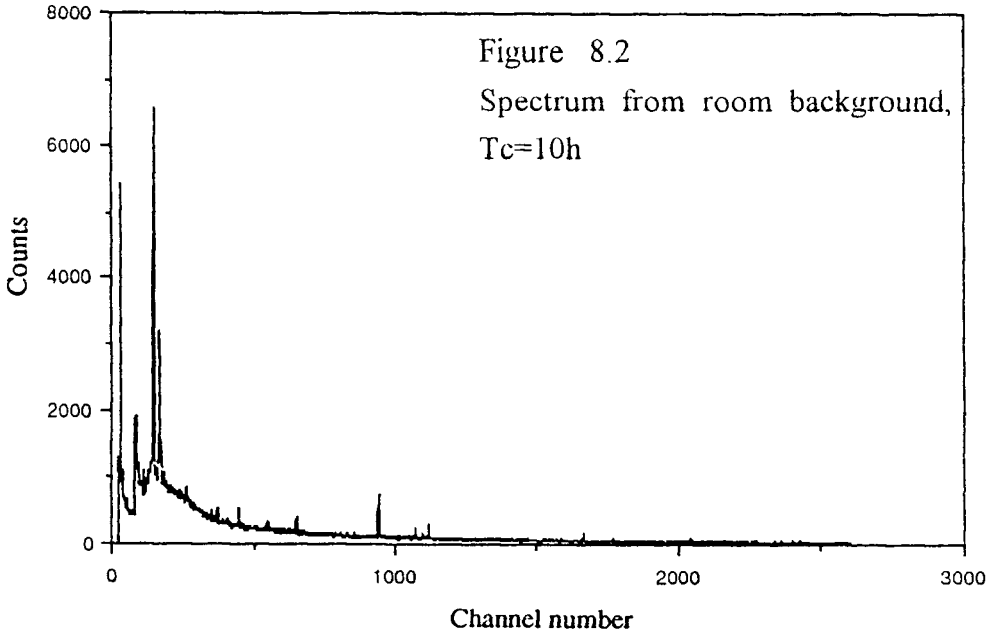


Figure 8.2
Spectrum from room background,
Tc=10h

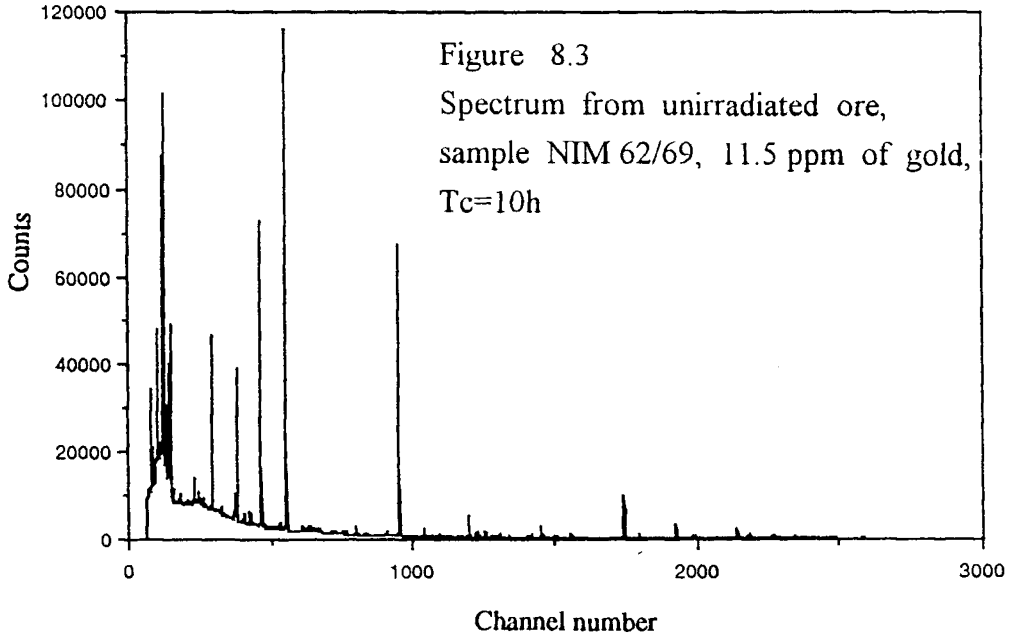


Figure 8.3
Spectrum from unirradiated ore,
sample NIM 62/69, 11.5 ppm of gold,
Tc=10h

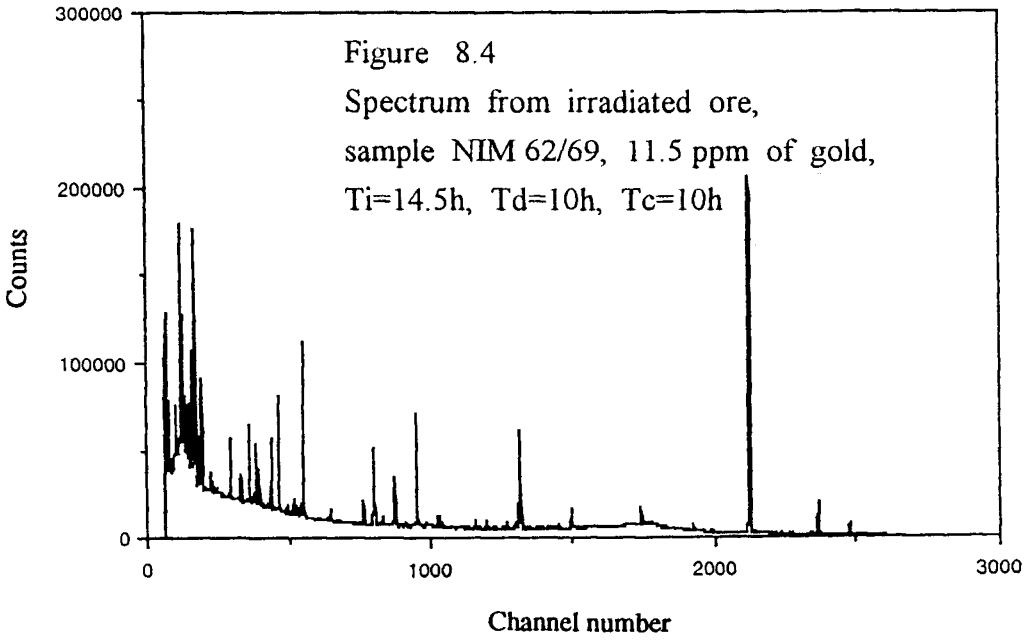


Figure 8.4
Spectrum from irradiated ore,
sample NIM 62/69, 11.5 ppm of gold,
Ti=14.5h, Td=10h, Tc=10h

TABLE 15

Contributions to the background under the 411 keV peak in gold ore

	$T_{1/2}$ (h)	Peak (keV)	Peak to Compton ratio	Contribution (%)
Room Background	-	-	-	1.5
Natural Activity	-	-	-	22.1
Na	15	1369	20.4	37.1
Mn	2.576	847	27.8	6
La	40	487	13.11	3
As	26.5	559	25.82	4
K	12.4	1524	2.73	13.5

From the above Table, it can be seen that the contribution of the sodium is the greatest 37.1%, then the potassium follows with 13.5%. The contribution from the natural activity of the ore, is also high at 22.1%.

The components of the background from these sources decay with different decay constants depending on the element that they originate from. The behavior of the total background at different times, is a combination of the way these components decay.

8.5 Application of the model

8.5.a Optimum decay time for the determination of the 411.8 keV photopeak

Consider the case of the sample NIM 62/69 (11.5 ppm Au) and the experimental results for this sample from experiment B in section 7.2.a. In that experiment 343.17 g of this sample were irradiated for 14.5h, left for 10h to decay and counted for another 10h, under specific conditions of irradiation and counting geometry.

If N_1 is the number of counts in the 411.8 keV peak area and B_1 is the number of counts in the background under that peak, then N_1 should be given by the general equation of activation analysis (2-1), with $T_i = 14.5$ h, $T_c = 10$ h, $T_d = 10$ h and $T_{1/2} = 2.7$ days for the gold.

For a new Td_2, with the rest of the variables the same, the new number of the peak area counts N_2 is :

$$N_2 = N_1 e^{\lambda(Td_1 - Td_2)} \qquad (8\text{-}10)$$

which in the case of gold can be calculated with $\lambda = \frac{0.693}{2.7 \text{ days}}$

If the results from (8-10) and (8-8) are replaced to (8-1), the statistical error for the new decay time Td2 can be calculated. With the aid of a computer program, results for several different decay times are obtained.

In Figure 8.5, the values of the statistical error from these calculations are plotted versus the decay time. The curve has a minimum at approx. 22 - 23 h, which agrees with the experiment.

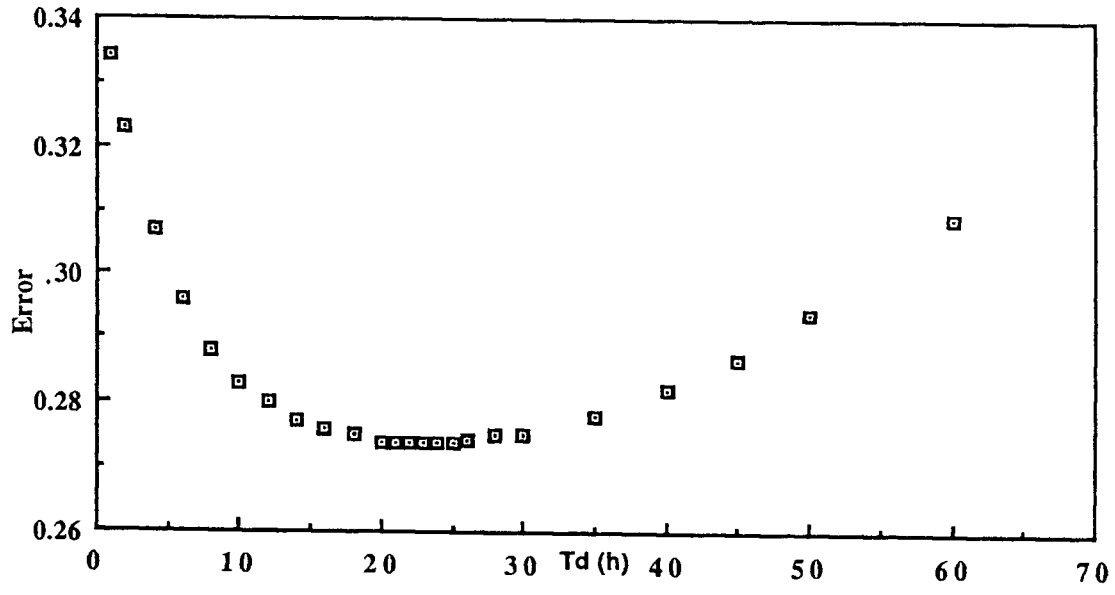


Figure 8.5 Calculated statistical error vs decay time

8.5.b Variation of the statistical error with the irradiation and counting times

The model described above can be used to investigate the way in which the statistical error depends on the irradiation and counting times.

Considering 343.17 g of the same sample as previously and using a counting time of 10h and a decay time of 23h (the optimum decay time) and based on the formulas (2-1) and (8-1), the statistical (%) error can be calculated for different irradiation times. The number of counts of the 411.8 keV area and its background are calculated separately, taking into consideration all the interferences in the background. This time, the irradiation time is varied and the other parameters are kept constant.

In Figure 8.6, the statistical error of the 411.8 keV is plotted against the irradiation time. It is a logarithmic curve and it can be noticed that in the first 8 hours approximately, the error decreases very sharply.

The same calculations are repeated, this time taking values for the error using an irradiation time of 10h, decay time 23h and varying the counting time. A similar curve is obtained (see Figure 8.7). Again the error decreases sharply in the first eight hours.

The way that these two curves vary with time, leads to the question what would the result be if long irradiations and short count times were considered and the opposite. How the statistical error would be influenced as a function of the way the available time for irradiation and counting is divided.

In order to calculate all this, the optimum decay time for gold (Td=23h) was taken and a total time for irradiation and counting of T = 50 hours was considered. All the other parameters were kept constant and T_i and T_c were varied so that $T_i + T_c = T$. The counts in the 411.8 keV peak area and the background were calculated as well as the statistical error. Figure 8.8, shows the relationship between the statistical error and T_i/T. The curve has a minimum when $T_i/T = 0.54$, or in the specific case, $T_i = 27h$ and $T_c = 23h$, which is the best way to share the available time T.

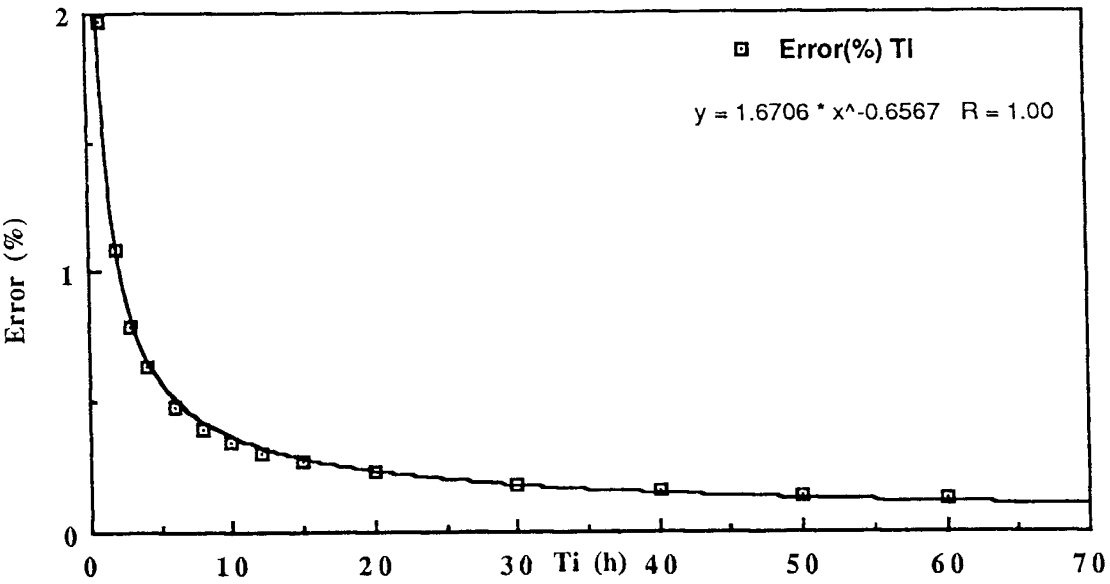


Figure 8.6 Statistical error vs irradiation time

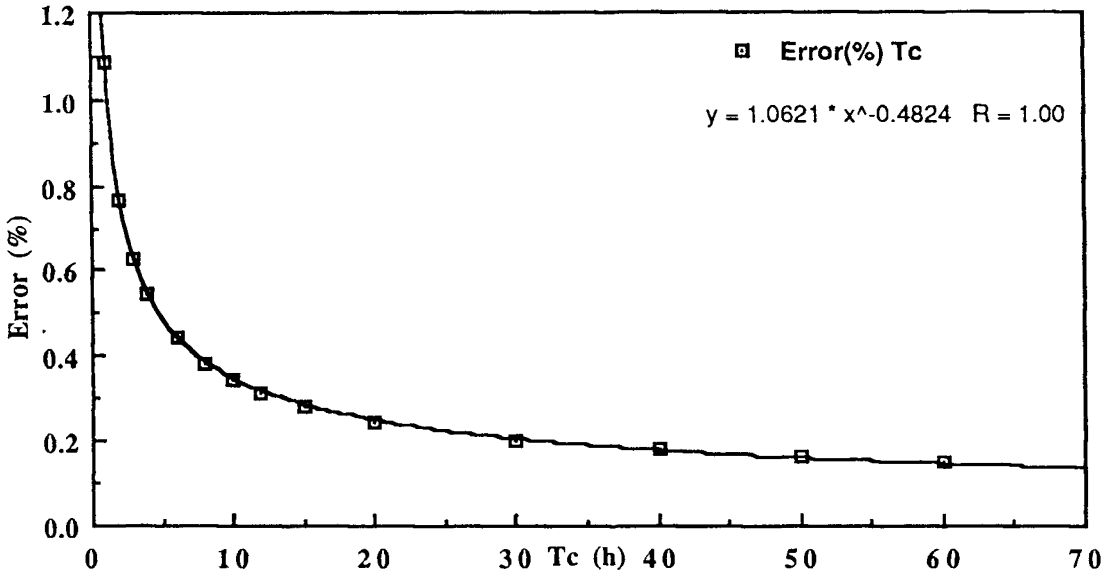


Figure 8.7 Statistical error vs counting time

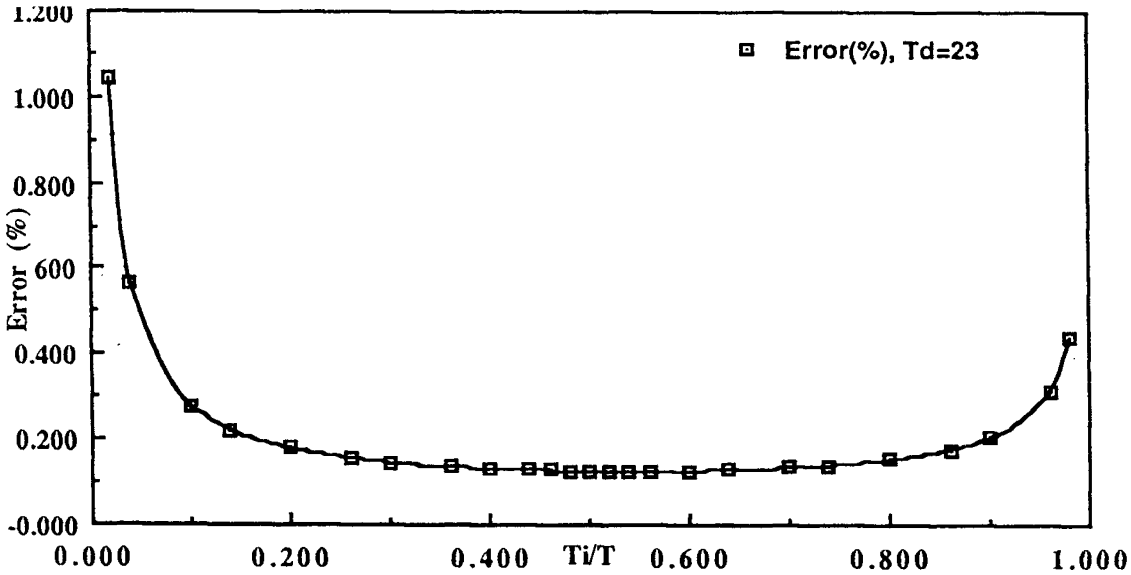


Figure 8.8 Statistical error vs Ti/T, considering the constant background

8.5.c Variation of the statistical error with source strength

Using the same sample and keeping all the variables the same as previously, the counts of the gold peak area and background, were calculated as a function of the strength of the source. The count-rate is directly proportional to the strength of the Cf - 252 neutron source.

The source, was considered to be equivalent to 0.5 mg of Cf-252 at the time of the experiment and that gave $N_1 = 359968$ counts for the area and $B_1 = 97054$ counts for the background. Substituting in formula (8-1), shows that the statistical error varies as $\frac{1}{\sqrt{s}}$, where s is the source strength. The results are illustrated in Figure 8.9, again for 343g of sample NIM 62/69 (11.5 ppm gold).

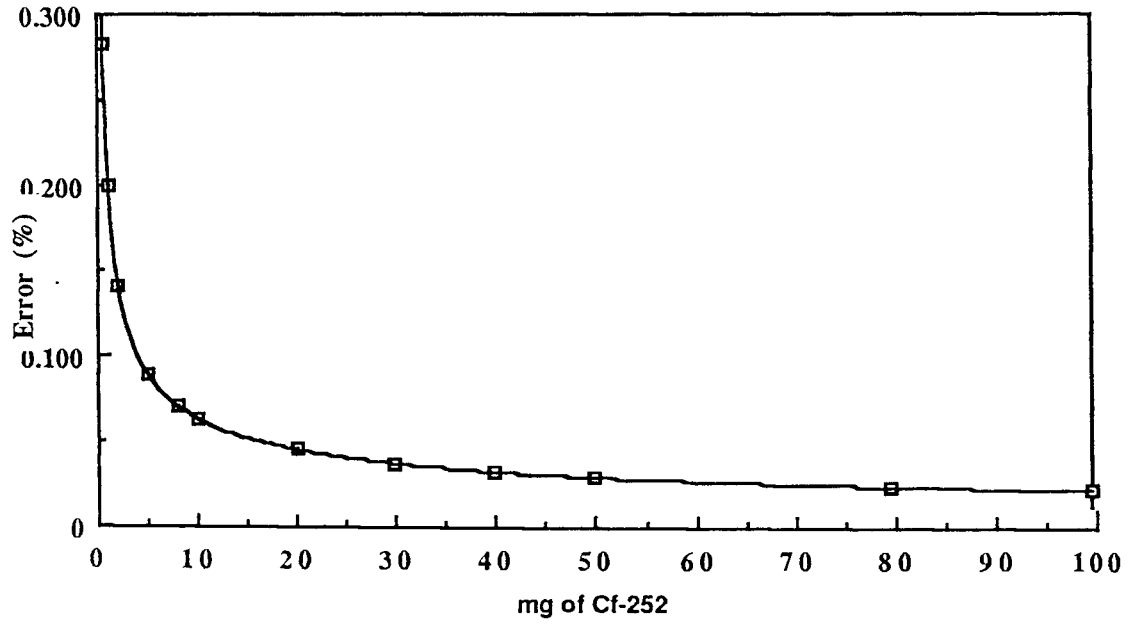


Figure 8.9 Statistical error vs source strength

9. NEUTRON AND GAMMA-RAY ABSORPTION

9.1 Introduction

As the sample size increases, the total number of counts increases, but as the sample size increases, self-absorption should produce non-linearities in the calibration. As a result of these conflicting factors, there will be an optimum sample thickness.

Large samples have not been widely used, undoubtedly because of the difficulty arising from neutron and γ-ray absorption in the sample, as well as the decrease of the neutron flux with the distance from the source.

Gamma-ray absorption is exponential and in a first order approximation, so is neutron absorption. The effects of gamma-ray and neutron absorption were determined experimentally.

The aim of this part of the work is to investigate the limitations on the sample size and the effects of neutron and γ-ray absorption in determining this limitation. This was examined in the specific case of gold in samples of activated carbon, produced in the "carbon in pulp" method for the extraction of gold. The samples used are described in detail in Appendix A.

9.2 Theory - Neutron and γ-ray absorption coefficients

Neutrons and γ-rays can travel a long distance within a sample in comparison with a charged particle, but after a certain distance (or time) they do get absorbed.

In section 2.4 (Chapter 2), there is a brief description of the interactions of neutrons with matter. An assumption as a first approximation is that when a

beam of neutrons or gamma-rays enters a target, its intensity decreases in accordance with the formula:

$$I = I_0 e^{-\mu\rho t} \qquad (9\text{-}1)$$

where,

I = the intensity of the beam after travelling a distance t,
I_0 = the initial intensity,
ρ = the density of the target,
μ = the neutron or γ-ray mass absorption coefficient,
ρt = (mass of the target) / (target area perpendicular to the beam) = m/unit area.

9.3 Experimental

In this section two series of simple experiments were performed in order to establish the mass absorption coefficient for both radiations, as they are essential in the study for the optimum thickness of a sample. In the experiment, the intensity is represented by the number of counts.

For the experiments, the carbon sample 1/78 (1015 - 1081 ppm gold), was used.

The experiments were performed using ten identical boxes made from thin (1mm) aluminium sheet. All had the same thickness (thickness of sample inside each box = 1 cm).

Because of the high concentration in gold of the above sample, a NaI(Tl) detector was used, which gave higher efficiency during counting. Irradiation and counting times were also short, in comparison with the times needed for the gold ores.

(a) Experimental investigation of γ-ray absorption

Figure 9.1, shows the irradiation and counting geometry. One of the aluminium boxes was irradiated for two hours and after a certain decay time, it was placed at a fixed distance in front of the NaI detector. A 15 min count was taken and after that, the other (non irradiated) boxes were placed one after the other beside

the first one, facing the detector and taking counts for 15 min each time. When the last box was placed, there was a sample of thickness 9 cm in front of the irradiated box.

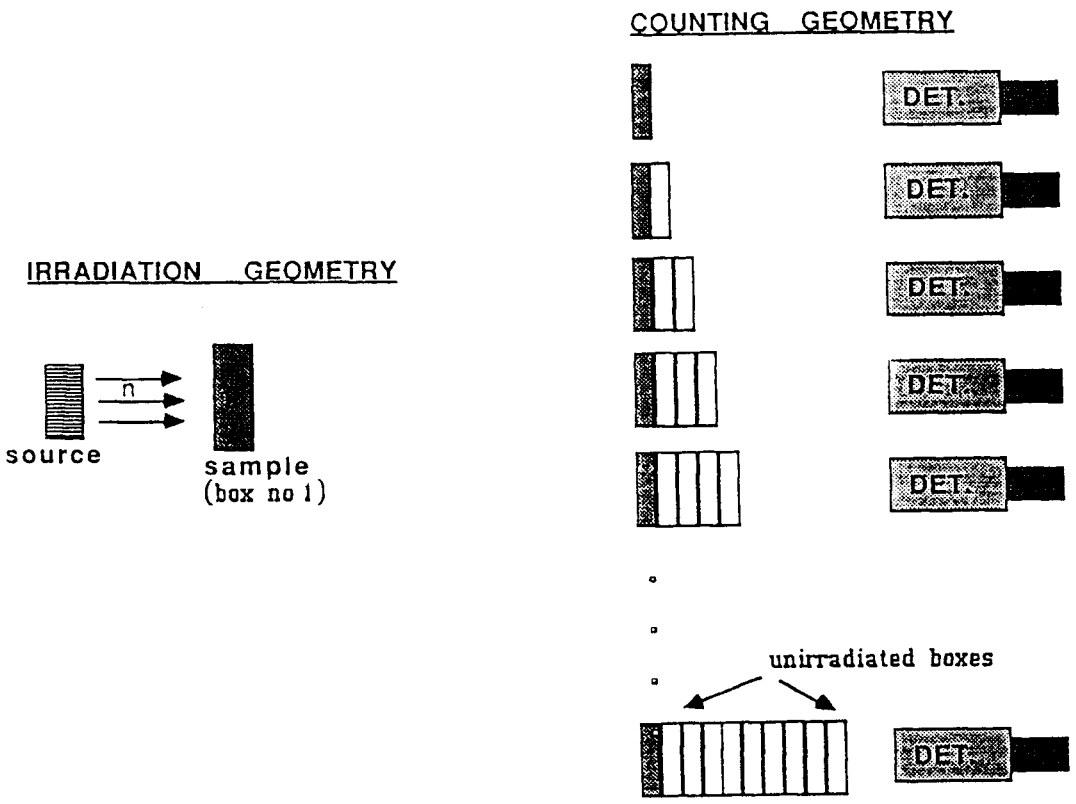


Figure 9.1 Irradiation and counting geometry for the gamma-ray mass absorption coefficient of activated carbon

(b) Experimental investigation of neutron absorption

Figure 9.2, represents schematically the irradiation and counting geometry. Nine boxes were placed one beside the other, at a fixed distance from the neutron source, so that the neutrons entered from the front surface of the first box and traversed a 9 cm thick sample.

Two separate experiments were conducted to investigate the absorption of thermal and epithermal neutrons

An irradiation time of two hours was used. After a decay time of few hours, the boxes were counted for 15 min each, with the back surface facing the NaI detector.

After three weeks, (in order to allow sufficient time for the gold peak to decay), the experiment was repeated, this time using epi-cadmium neutrons. The irradiation and counting geometries were kept the same as in Fig. 9.2. The nine boxes were placed inside cadmium shielding. The thickness of the cadmium sheet was 1 mm. Cadmium, absorbs the thermal neutrons, hence only neutrons in the epithermal energy region entered the sample in this case. The irradiation time was 20 h, i.e. much longer, because the neutron flux was decreased and the activity was low. The counts were carried out the same way as before, 30 min for each box.

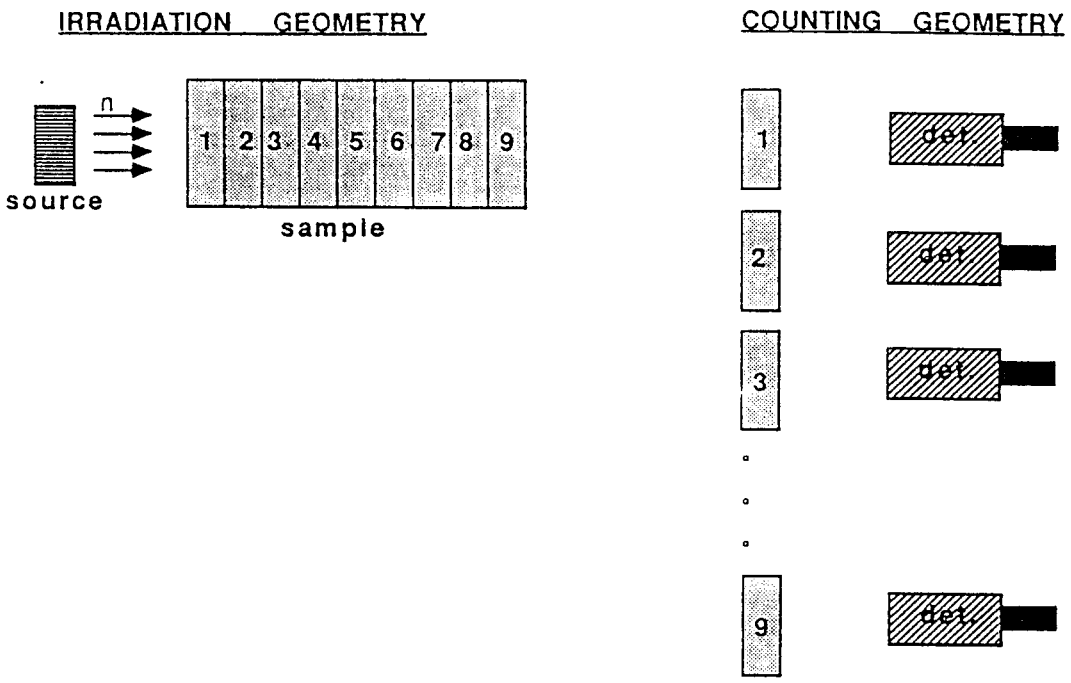


Figure 9.2 Irradiation and counting geometry for the neutron mass absorption measurement for activated carbon

(c) Combined neutron and gamma-ray absorption - optimum thickness

Finally, nine aluminium boxes were irradiated as shown schematically in Fig. 9.3, using thermal neutrons. The irradiation time was 2.25 hours. The sample was left for 5 days to decay. There were two sets of countings. Figures 9.4.a and 9.4.b, indicate the counting geometries. In the figures, each box is represented by a number in order to indicate its position during counting. In the first case, the NaI detector faced the irradiated surface of the sample, in the second case it faced the opposite surface. The count time was 15 min for each row in the figures.

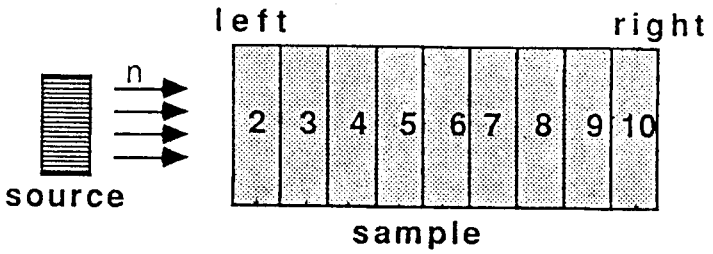


Figure 9.3 Irradiation geometry for the determination of the optimum thickness

a) Detector to the left

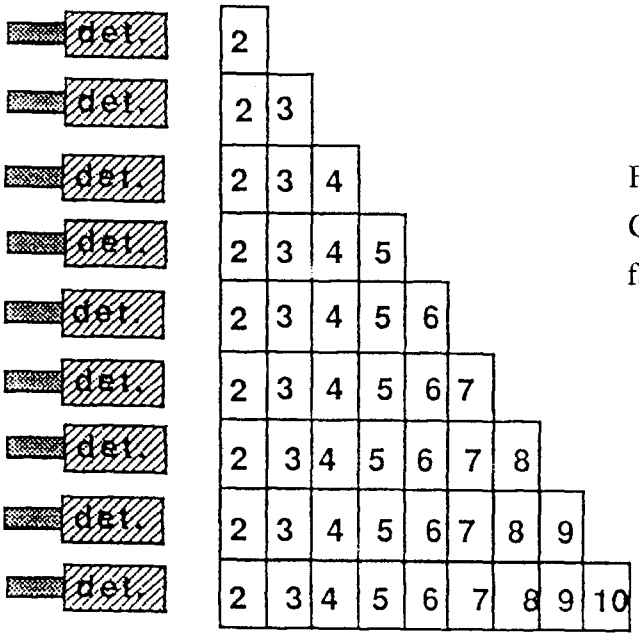


Figure 9.4.a
Counting geometry with the detector facing the irradiated surface of the sample

b) Detector to the right

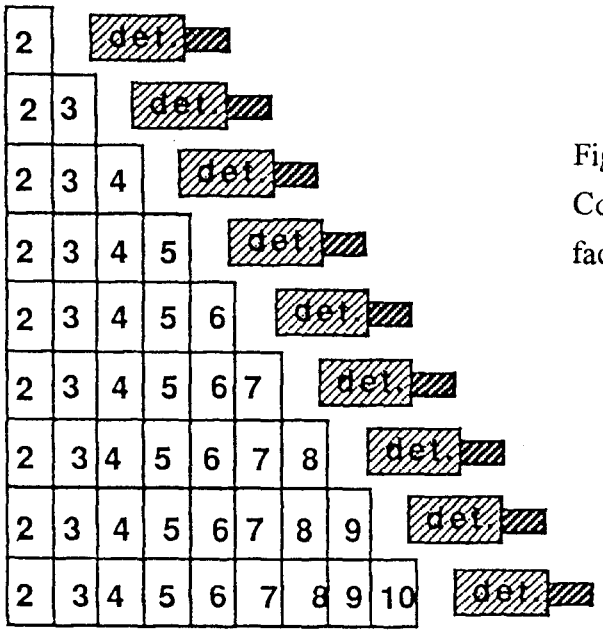


Figure 9.4.b
Counting geometry with the detector facing the opposite surface of the sample

9.4 Results

(a) Results for γ-ray absorption

Figure 9.5 illustrates the results which are plotted on a semilog scale. The results were analysed taking into consideration the effect of the aluminium boxes. Based on equation (9-1) and from the slope of the graph the mass absorption coefficient for the γ-rays μ_γ can be calculated, since the slope = $-\mu_\gamma$. loge, hence μ_γ = -0.167 $cm^2.g^{-1}$.

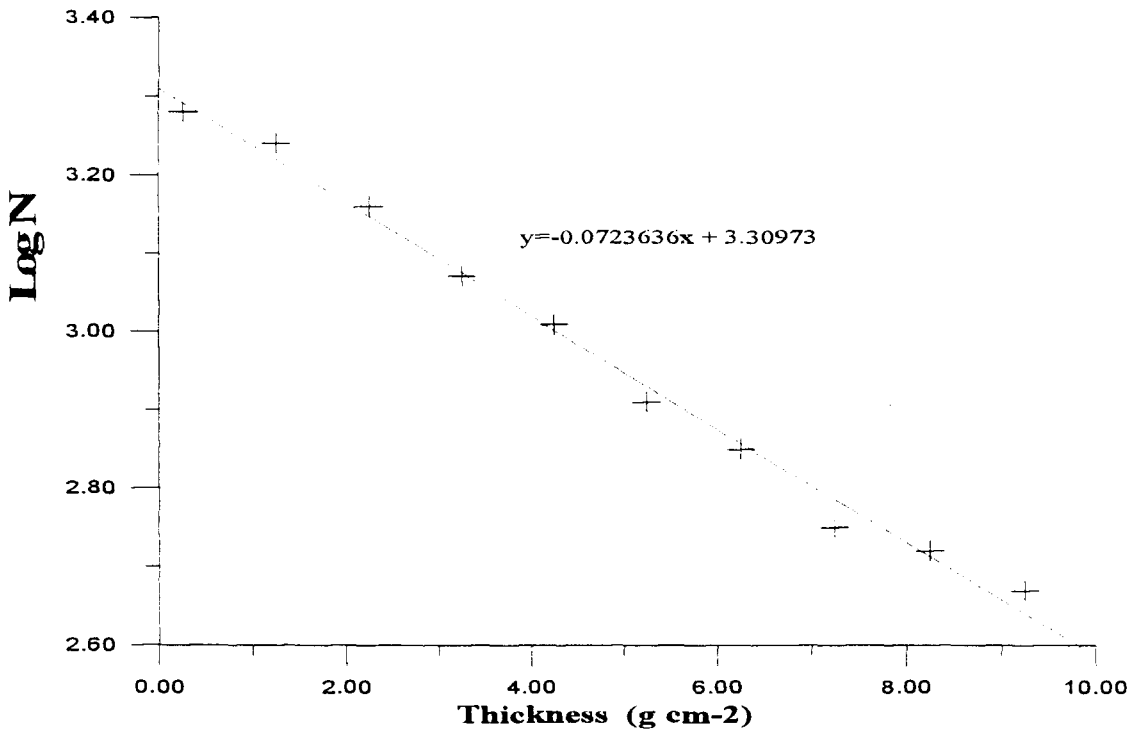


Figure 9.5 Gamma-ray mass absorption for activated carbon

(b) Results for neutron absorption

The graph in Figure 9.6 illustrates the variation of the neutron flux within the sample. The lower curve corresponds to the thermal radiation and the upper curve to the epithermal one. Both curves plotted on a semilog scale are with a good

approximation linear relationships of the counts as a function of the mass per unit area.

It is important to notice that in both cases, the variation of the neutron flux with the distance from the source during irradiation is included in the results. The variation of the flux with the distance from the source for thermal and epithermal irradiation can be seen in the Figures 4.1 and 4.2 respectively. This variation is quite significant within the length of the sample, which covered a distance from 3 cm up to 14 cm including the thickness of the aluminium containers.

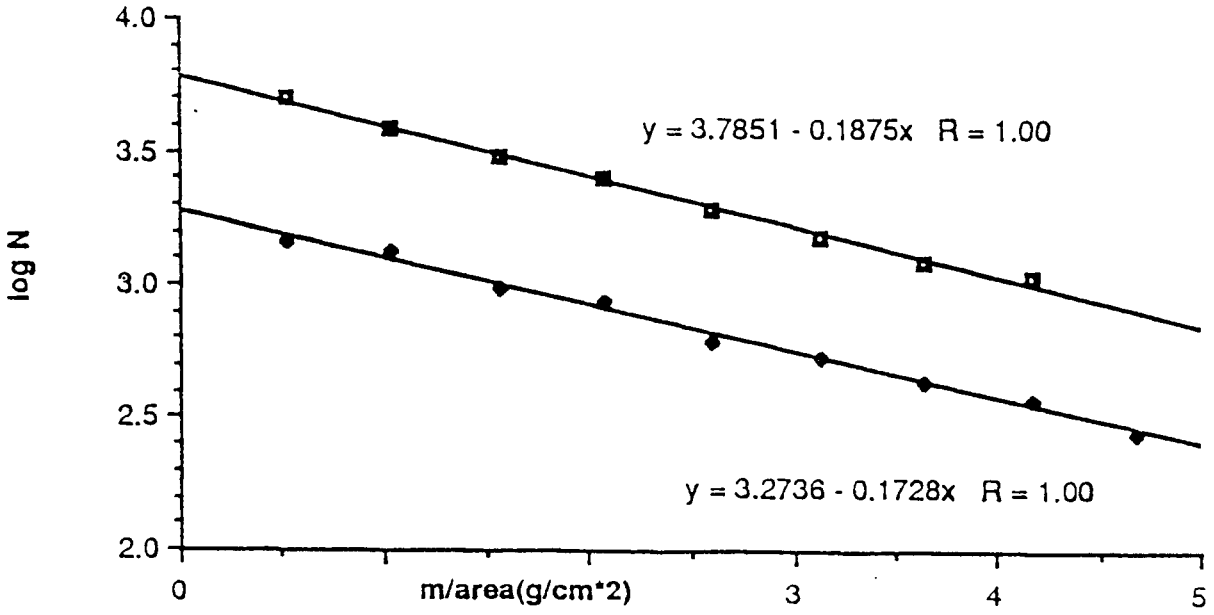


Figure 9.6 Variation of the neutron flux inside the activated carbon sample

(c) Combined neutron and gamma-ray absorption - optimum thickness

Both curves, are shown in Figure 9.7. The graph, represents the counts as a function of the sample thickness. Figure 9.8, shows the variation of the statistical

error in both cases, as a function of the thickness as well. The lower curve refers to the measurements with the configuration of Figure 9.4.a., the upper curve refers to Figure 9.4.b.

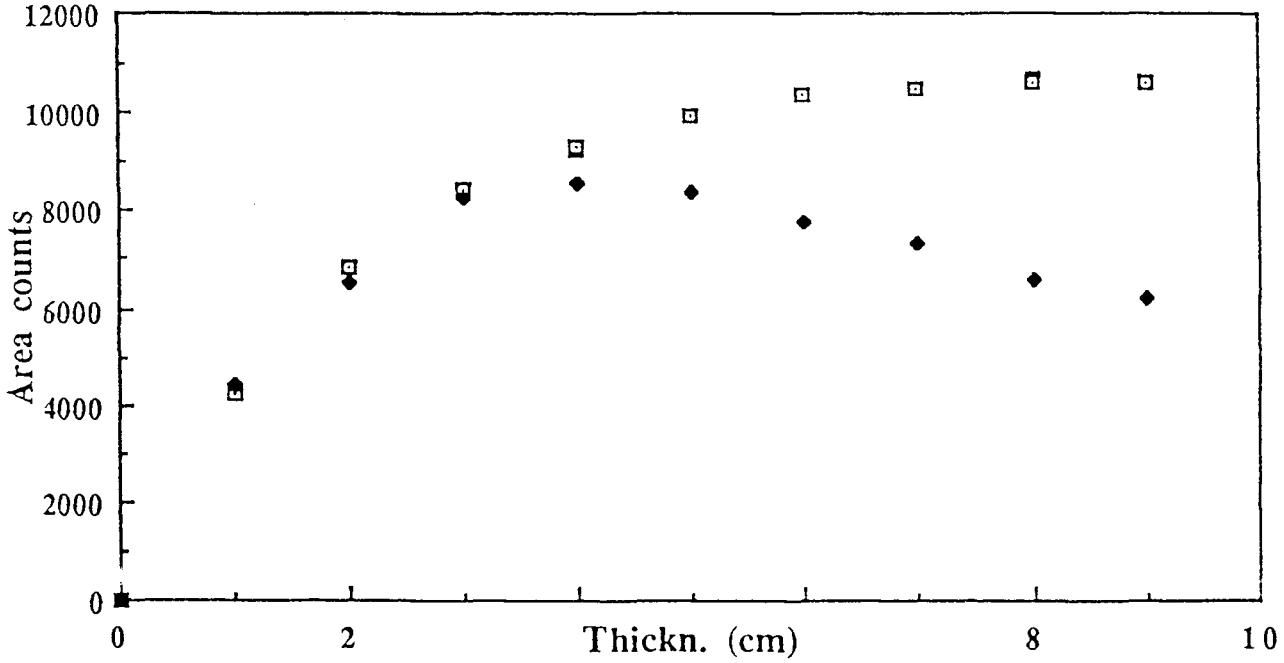


Figure 9.7 Graph of measured counts against sample thickness after Ti=2.25h, Td=5d, Tc=15m

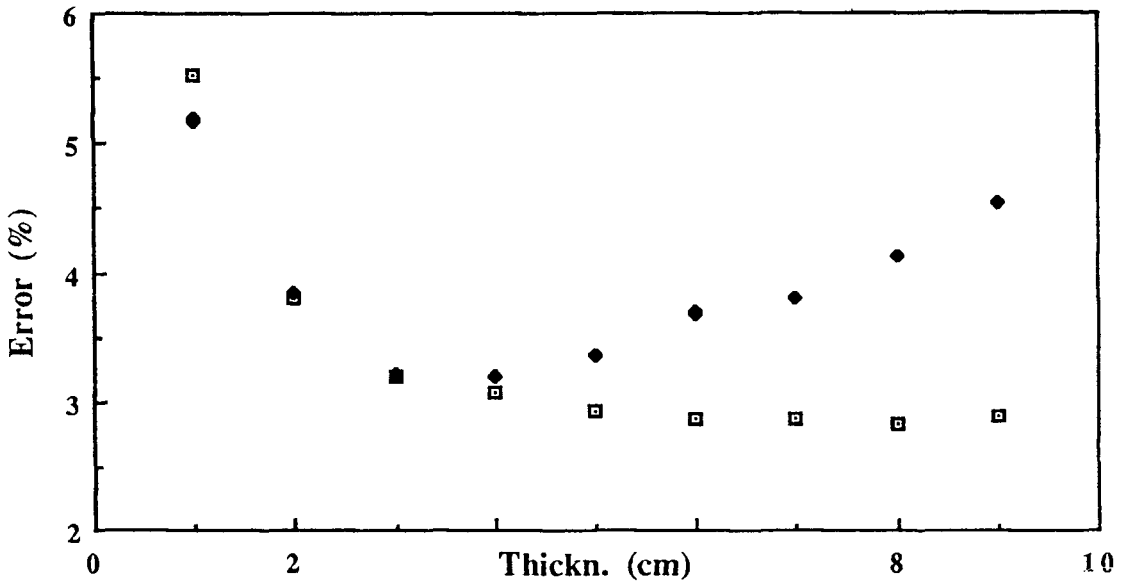


Figure 9.8 Graph of measured statistical error against sample thickness after Ti=2.25h, Td=5d, Tc=15m

9.5 Discussion

The reason for the small difference between thermal and epithermal flux (Figure 9.6), is probably due to the fact that the epithermal flux is being thermalised inside the carbon. Hence, the upper curve in Figure 9.6 represents the group that entered the graphite boxes as epithermal neutrons and have subsequently been thermalised.

The epithermal flux decreases more dramatically with the distance from the source, as can be seen in Figure 4.2 in comparison with the flux in Figure 4.1. The level of activity depends directly on the neutron flux in the sample and this should be related to the neutron flux in the medium (water) in the absence of the sample. Figure 9.9 shows the variation of the activity (directly related to the flux in the sample) and compared to the flux in the water at the same distance in the absence of a sample. Figure 9.10, illustrates the same variations in the case of epithermal neutron flux.

It is interesting to note that the average flux in the carbon sample is higher than in the water. This effect appears stronger in the case of epithermal neutrons (Figure 9.10), as the upper and lower curve differ more. Overall however, the slope of the thermal flux inside the sample is slightly less.

The concentration of gold in the sample is high (of the order of 1000 ppm Au). The macroscopic cross-section Σ of the sample is (see section 2.4.a):

$$\Sigma = \sigma_C N_C + \sigma_{Au} N_{Au}$$

Where $\sigma_C = 0.0034$ b the absorption cross-section for carbon and $\sigma_{Au}=93$ b is the absorption cross-section for gold. N_C and N_{Au} are the number of atoms per unit volume for carbon and gold respectively. The result for the macroscopic cross-section of the sample, indicates that similar absorption is expected from both carbon and gold nuclei.

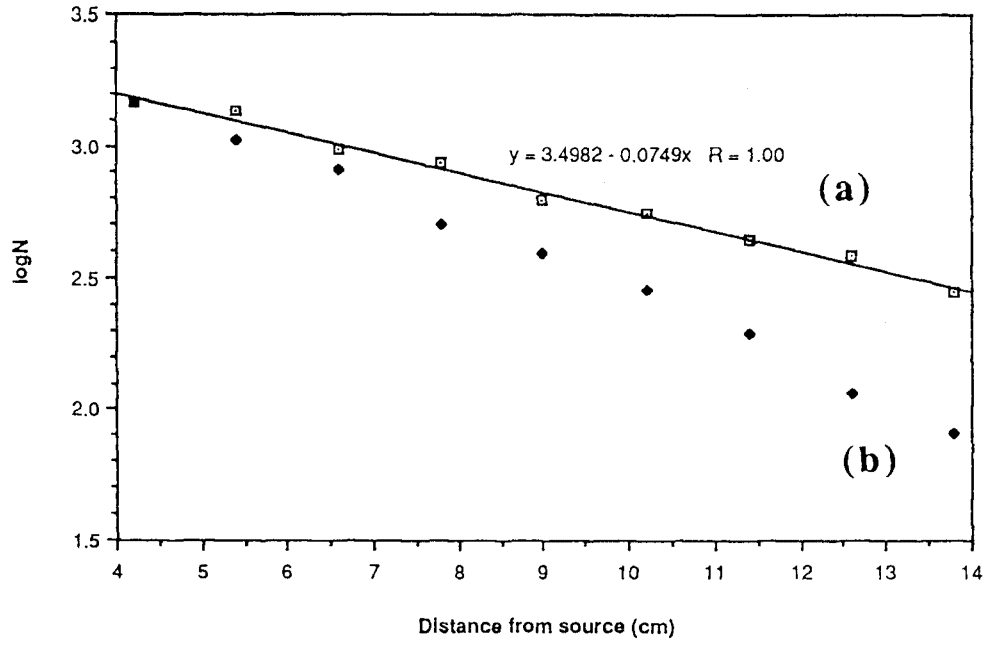


Figure 9.9 (a) Variation of the activity inside the sample after thermal irradiation.
(b) Variation of the thermal neutron flux

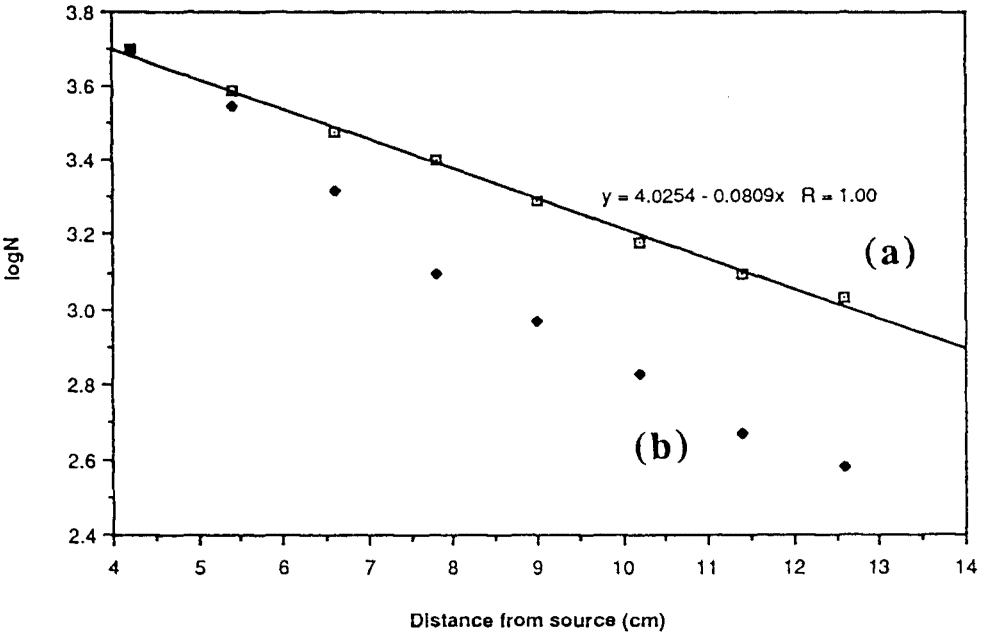


Figure 9.10 (a) Variation of the activity inside the sample after epithermal irradiation.
(b) Variation of the epithermal neutron flux

The upper curve in Fig. 9.7, represents the counts with the detector facing the irradiated side (Figure 9.4.a). The detector is not sensitive to the gold activity at thicknesses greater than 7 cm. This is in effect an infinite thickness as far as this type of sample is concerned in this irradiation and counting geometry.

The lower curve in Fig. 9.7, is the result obtained from the counting geometry in Figure 9.4.b, i.e. with the detector facing the back of the samples. The counts increase as the mass increases up to a thickness of 4 cm and then they decrease. For the first 3.5 cm of sample thickness, the two curves nearly coincide, indicating that for such thickness there is little neutron absorption. The upper curve in Figure 9.8 has a minimum at 4 cm, while the lower one decreases slowly after about 6 cm.

In conclusion, the maximum depth of sample that can produce some additional activity is at approximately 7 centimeters of sample thickness. There is essentially no additional activity for the counting geometry of Figure 9.4.a for thicknesses greater than this. For the counting geometry of Figure 9.4.b the optimum thickness for the optimum error and hence the minimum L.O.D. is 4 cm.

It is also worth noting, that the best counting geometry is with the detector counting from the right (Fig. 9.4.b), since for this geometry the sensitivity distribution along the sample is more even (similar activity from each centimeter). Both of the results in Figure 9.7 represent the convolution of the neutron flux distribution in the series of samples and the variation of the detector sensitivity with distance. In the case of the counting geometry in Fig. 9.4.a, if the sample is thicker than 4 cm, most of the activity comes from the first centimeters of sample and very little from the last.

The results of this section, cannot be extrapolated to the case of the ores, as the neutron and gamma-ray absorption coefficients are completely different. In addition carbon thermalises neutrons and consequently the optimum thickness is greater in this case.

10. CONCLUSIONS

The sensitivity of reactor neutron activation analysis has made it a highly desirable technique for many applications. However, isotopic sources may offer a simple and economical way to use neutron activation analysis in potential industrial applications particularly in the mining industry.

In reactor neutron activation analysis, a typical neutron flux is from 10^{12} to 10^{13} n $cm^{-2}s^{-1}$ With a typical reactor sample of the order of 300 mg of gold ore for example, the lower level of detection would then be below 1 ppm for gold. The question is what would the sensitivity be using a 1000 g sample, which is greater by a factor of 3000, with the use of an isotopic source of neutrons, like the Cf-252 with a typical flux of 10^{8} n cm^{-2} s^{-1}. There are some specific analytical problems related with the use of large samples, which have to be investigated in order to establish what can be measured in practice and the way this can be optimised. The aim of this work is to examine whether large samples (of the order of 1 kg) can be used to determine gold and the P.G.E. in useful concentrations in real samples (mineral samples) and to assess the effects of sample size on sensitivity and accuracy, using a 0.5 mg ^{252}Cf neutron source.

Neutrons and gamma-rays have no charge, therefore they are both highly penetrating radiations. Their ability to penetrate deeply in to the matter allows the analysis of larger samples in comparison with other radiations. However, they also get absorbed after some time and it is essential to determine the upper limit of a practical sample size. The absorption effects of both neutron and gamma-rays become important in the study of bulky samples, as they result in non-linearities in the calibration curves.

In the case of gold in samples of activated carbon, produced in the "carbon in pulp" method for the extraction of gold, the gold content could be easily determined at the

relatively high concentrations that are of interest in gold extraction. The accuracy achieved in terms of calibration was very satisfactory. Using seven samples with masses ranging from 95 to 100g and a total time for irradiation, decay and counting of less than four hours, a very satisfactory linear relationship between counts per gram and gold concentration in ppm was obtained (Figure 7.5), indicating that under the specific conditions of the experiment, the effect of gamma-ray and neutron absorption was negligible.

The effects of neutron and gamma-ray absorption were investigated in the specific case of gold in activated charcoal, using the sample carbon 1/78 (1015-1081 ppm gold). Thermal and epithermal neutron radiation was used for the study of the variation of the neutron flux inside the sample. There was only a slight difference in the absorption coefficients (see Figure 9.6), indicating that the bulky carbon sample thermalises the epithermal neutrons. The optimum sample thickness for the specific sample, for the counting geometry of Figure 9.4, was determined using thermal neutron radiation and it was found to be 4 centimeters. The maximum depth of sample that can produce some additional activity was found to be approximately 7 centimeters (see Figure 9.7). Furthermore, the best counting geometry that ensures a more even sensitivity distribution along the bulk of the sample, is with the detector facing the side of the sample that was furthest away from the neutron source during irradiation.

In the case of gold in ore, samples of Witwatersrand gold ore were used, with concentrations in the range of 0-100 ppm. The mass of the samples was between 150g and 1200g. The samples were placed inside annular sample holders in the form of "Marinelli beakers" in order to achieve an optimum use of the neutrons during irradiation and to allow a good geometrical efficiency during counting. In this range of concentrations, longer irradiation and count times were needed. Gold was detected in all the samples with good counting statistics, using a total time of irradiation and count from one to four days. In the case of the sample NIM 23/81 (0.5 ppm of gold), after an irradiation time of 69h, a decay time of 1 day and a counting time of 10h, the L.O.D. for gold was 0.017ppm. With a neutron source of 10^8 n s^{-1}, it would be possible to determine gold in the range of few ppm within a total time of 3 days.

The accuracy achieved in the study of gold in ores in terms of calibration was satisfactory. Using samples with masses in the range of 300g to 600g and a total time of irradiation and count of approximately one day per sample, linear calibration curves

were obtained, indicating that the effect of absorption in this range of masses and under the specific irradiation and counting geometries (as described in chapter 7), was negligible.

An important analytical problem arises from the complexity of the gamma-ray spectra. The background under the Au-198 photopeak is due to interferences from the other prominent elements in the ore, as well as the room background and the counts from the natural activity of the ore. As a result, the total background decays with a different decay constant than that of Au-198, therefore there is an optimum decay time. The determination of the optimum decay time is essential in order to improve the sensitivity of detection. In the case of the ores, the optimum decay time was established using the sample NIM 38/81 containing 1.8 ppm of gold, to be approximately 23 h (Figure 8.1). By allowing 23 hours for the background to decay sufficiently, the statistical error decreases by half in comparison with statistical errors measured after decay times of the order of one hour. A mathematical model was developed in order to calculate errors for ranges of other conditions of the same sample.

The same model was also applied to investigate the way in which the statistical error depends on the irradiation and count times. These variations follow logarithmic curves, indicating that there is a sharp decrease of the error for irradiation or count times in the first 8 hours and that there is practically very little improvement in the counting statistics using much longer irradiation or count times (Figures 8.6, 8.7). Furthermore, it was found that for a given span of time, equal portions assigned for irradiation and counting would give the smallest statistical error (Figure 8.8).

The variation of the error with source strength was determined using the same mathematical model. Figure 8.9 shows that the statistical error varies with the source strength following the inverse square law. It can be calculated that 300 g of the sample NIM 62/69 (11.5 ppm of gold), under the irradiation and counting geometries as shown in Figure 7.2, after a decay time of 23 h, a total time for irradiation and counting of 1.3 h, using a 0.5 mg Cf-252 source would produce a statistical error of 5%. The same sample under the same conditions, using a 10 mg Cf-252 source, would produce the same error in less than 0.3 h total time for irradiation and counting. Sources of the order of 50 mg or more would be very impractical and very expensive. A maximum of 3 mg californium-252 neutron source would probably be feasible and the sensitivity improvement would be great.

Gold was also detected in all the platinum samples. In the case of the platinum ore SARM7 (0.31 ppm of gold), after an irradiation time of 3d, a decay time of 3d and a counting time of 1d, the L.O.D. was 21 ppb (Figure 6.3).

In the case of the P.G.E.'s, three different types of sample were used, namely ores, concentrates and mattes. Sample masses ranged approximately from 300 g to 1100 g. The sample holders were of the "Marinelli" type. The estimated neutron flux during the experiments was of the order of 10^6 n cm^{-2} s^{-1}. Irradiation and counting geometries are shown in Figure 6.1. Rhodium, iridium, platinum and osmium were detected (Table 12). After long irradiation and count times, iridium and platinum were detected with good counting statistics down to the level of approximately 2 ppm. In the case of 310.5 g of the sample platinum mattes 5/76, after an irradiation time of 12 h, a decay time of 3 weeks and a counting time of 15 h, the L.O.D. for iridium was calculated to be 2.6 ppm. In the case of 1107 g of the sample platinum ore SARM 7, after an irradiation time of 4 days, a decay time of 3 days and a counting time of 1 day, the L.O.D. for platinum was 1.9 ppm. Rhodium was detected with very short irradiation and count times (of the order of less than 5 min) in the platinum concentrate 16/76 (9ppm of Rh) and in the platinum mattes 5/76 (31.6 ppm of Rh), with a L.O.D. below 12 ppm. Osmium was detected in the sample platinum concentrate 26/78 (of unknown concentration in Os), with a sample mass of 817 g, after an irradiation time of 3 days, a decay time of 4 days and a counting time of 10 hours. Palladium interferes with peaks from the background, making its detection complicated. Ruthenium was not detected due to the low cross-section of the reaction $^{102}Ru\ (n,\gamma)^{103}Ru$ and the long half-life of the product.

In the case of the platinum group elements, further work is necessary to study each element separately. The method applies with satisfactory results in the case of platinum and iridium, using long irradiation and count times. Rhodium can be detected with good counting statistics, using a total time for irradiation and count of the order of 10 minutes. Under different laboratory facilities, enabling quick transfer of the samples from the irradiation to the counting site, rhodium could be detected through the reaction $^{103}Rh\ (n,\gamma)^{104}Rh$, thus resulting in great improvement of the sensitivity in much shorter times.

Using thermal neutron activation analysis and the delayed gamma - ray technique, all indications are that it can provide an accurate, cost-effective, time saving method for

the determination of gold, even in low - content ores. For example, it is envisaged that this method could analyse a 500 g crushed sample of gold ore, without any further preparation. It could also be used to assay a borehole core for gold non - destructively, or to determine the gold in a large sample of carbon in less time than one hour.

APPENDIX A

TABLE

DESCRIPTION OF SAMPLES

Sample Identification	Description	Elements	Recommended Value (ppm)
SARM 7	Platinum Ore (Merensky Reef)	Pt	3,74
		Pd	1,53
		Au	0,31
		Ag	0,42
		Rh	0,24
		Ru	0,43
		Ir	0,074
		Os	0,063
NIM 16/76	Platinum Concentrate	Au	9,0
		Pd	67,8
		Pt	135
		Rh	9,0
		Ru	18,6
NIM 26/78	Platinum Concentrate	Au	6,9
		Pd	35,2
		Pt	62,9
		Rh	3,5
		Ru	7,8
NIM 5/76	Platinum Mattes	Au	14,8
		Ir	10
		Pd	169
		Pt	287
		Rh	31,6
		Ru	76,6
NIM 14/75	Platinum Ore	Ir	(0,38)
		Pd	(1,3)
		Pt	(2,8)
		Rh	(0,47)
		Ru	(0,96)

TABLE (continued)

Sample Identification	Description	Elements	Recommended Value (ppm)
NIM 62/69	Gold Ore	Au	11,5
NIM 23/81	Gold Ore	Au	0,50
NIM 27/81	Gold Ore	Au	0,99
NIM 38/81	Gold Ore	Au	1,82

TABLE (continued)

CARBON (ACTIVATED) SAMPLES

SAMPLE	Ag ppm	Au ppm	Ca ppm	Fe ppm	Ni ppm	Si ppm
2/86	16	121	0.254	0.625	667	0.73
3/86	65	33	0.164	0.276	160	0.87
4/86	92	640	2.76	0.161	2064	0.87
5/86	330	1828	1.60	0.154	2221	1.35
6/86	207	3374	1.88	0.154	1437	2.46
7/86	522	5034	3.27	911	4477	0.352
8/86	735	5059	3.01	1.37	2017	1.13
1/78	630	1015-1081	1.78%	522	4427-4816	3610
2/78	195-200	63-71	1.37%	1818-1830	3863-3957	1.32%

APPENDIX B

TABLE

NUCLEAR DATA AND REACTIONS FOR THE DETERMINATION OF GOLD AND THE PGE[19-22]

Element	Reaction	f · %	σ barn	T 1/2	Peak (keV)	Intensity %
Au	$^{197}Au(n,\gamma)^{198}Au$	100	98.8	2.7 d	68.9 Hg Kα2 X-Ray	0.81
					70.8 Hg Kα1 X-Ray	1.38
					80.2 Au Kβ2 X-Ray	0.47
					82.5 Hg Kβ2 X-Ray	0.13
					411.8	95.5
					675.9	1.06
					1087.7	0.23
Pt	$^{198}Pt(n,\gamma)^{199}Pt$	7.2	4.0	30.8 m	67.0 Au Kα2 X-Ray	1.17
					68.8 Au Kα1 X-Ray	2
					77.2	1.5
					77.9 Pt Kβ2 X-Ray	0.69
					80.2 Au Kβ2 X-Ray	0.19
					185.8	3.26
					191.7	2.38
					219.4	0.39
					225.9	0.17
					240	0.18
					246.5	2.16
					317	4.87
					323.6	0.25
					417.6	0.39
					425.3	0.17
					465.8	0.93
					468.1	1.0
					474.7	1.15
					493.8	5.73
					543	14.8
					714.5	1.86
					791.7	1.07
					968.3	1.10
	$^{199}Pt\ (\beta^-)^{199}Au$			3.14 d	49.8	0.33
					68.9 Hg Kα2 X-Ray	4.47
					70.8 Hg Kα1 X-Ray	7.59
					80.2 Au Kβ2 X-Ray	2.62
					82.5 Hg Kβ2 X-Ray	0.72
					158.4	36.9
					208.2	8.38

TABLE CONT.

Element	Reaction	f %	σ barn	T 1/2	Peak (keV)	Intensity %
Ir	$^{191}Ir(n,\gamma)^{192}Ir$	37.3	300	73.83 d	61.5 Os $K\alpha_2$ X-Ray	1.26
					63.0 Os $K\alpha_1$ X-Ray	2.17
					65.1 Pt $K\alpha_2$ X-Ray	2.71
					66.8 Pt $K\alpha^1$ X-Ray	4.65
					71.3 Os $K\beta_1$ X-Ray	0.75
					73.4 Os $K\beta_2$ X-Ray	0.19
					75.7 Pt $K\beta_1$ X-Ray	1.59
					77.9 Pt $K\beta_2$ X-Ray	0.42
					136.3	0.18
					201.3	0.46
					205.8	3.20
					283.3	0.26
					295.9	28.7
					308.4	29.7
					316.5	82.9
					374.4	0.73
					416.5	0.67
					468.1	48.1
					484.6	3.16
					489.1	0.40
					588.6	4.58
					604.4	8.33
					612.4	5.43
					884.5	0.30
Pd	$^{108}Pd(n,\gamma)^{109}Pd$	26.7	12	13.46 h	22.1 Ag $K\alpha_1$ X-Ray	28.5
					25.0 Ag $K\beta_1$ X-Ray	6.02
					88.0 D	3.61
					311.4	0.032
					647.3	0.024

TABLE CONT.

Element	Reaction	f %	σ barn	T 1/2	Peak (keV)	Intensity %
Os	$^{192}Os(n,\gamma)^{193}Os$	41	1.6	30.5 h	63.3 Ir Kα2 X-Ray	3.74
					64.9 Ir Kα1 X-Ray	6.46
					73.0	3.2
					73.5 Ir Kβ2 X-Ray	2.22
					75.6 Ir Kβ2 X-Ray	0.57
					96.8	0.10
					107.0	0.64
					138.9	4.27
					180.0	0.18
					181.8	0.19
					219.1	0.28
					251.6	0.22
					280.4	1.24
					288.8	0.14
					298.8	0.19
					321.6	1.28
					361.8	0.30
					387.5	1.26
					420.3	0.17
					460.5	3.95
					484.2	0.17
					557.4	1.30
					559.3	0.49
Ru	$^{102}Ru(n,\gamma)^{103}Ru$	31.6	2.56	39.25 d	20.1 Rh Kα2 X-Ray	7.11
					22.8 Rh Kβ1 X-Ray	1.47
					53.3	0.38
					295.0	0.25
					443.8	0.32
					497.1	89.5
					557.0	0.832
					610.3	5.64
Rh	$^{103}Rh(n,\gamma)^{104}Rh$	100	139	42.3 s	19.2 Ru Kα2 X-Ray	0.24
					21.7 Ru Kβ1 X-Ray	0.050
					358.1 2	0.016
					555.8	1.99
					1237.0	0.066
	^{104m}Rh		11	4.34 m	19.2 Ru Kα2 X-Ray	0.28
					20.2 Rh Kα1 X-Ray	55.1
					22.8 Rh Kβ1 X-Ray	11.4
					51.4	48.2
					77.5	2.07
					97.1	3.00
					555.8 D	2.38
					767.8	0.10

LIST OF REFERRENCES

1. J.N. Barrandon, J.P. Callu, C. Brenot,
"The Analysis of Constantinian Coins (A.D. 313-40), by Non-Destructive Californium-252 Activation Analysis",
Archaeometry (GB), Vol. 19, Pt. 2, pp 173-86, July 1977

2. Lu Huijuan, Zhou Yunlu,
"Determination of Gold and Silver in Geological Standard Samples MGI by Instument Neutron Activation Analysis",
Nucl. Tech. (China), Vol. 10, No 7 pp 24-6, July 1987

3. Y. Maruyama, J.L. Beach, J. Hazle, M. Ashtari, C.B. Schroy, M.H. Olson,
"Therapeutic Dosimetry for Cf-252 Neutron Brachytherapy of Pelvic Cancer",
Int. J. Radiat. Oncol. Biol. Phys. (GB), Vol.11, No 5, pp 927-35, May 1985

4. J. Kuusi,
"The Application of Isotopic Neutron Sources to Chemical Analysis for Process Control in the Metallurgical Industry",
Proc. 1968 Conf. Modern Trends in Activ. Anal.,
NBS Spec. Publ. 312, Vol. 1 (1968), p.540

5. J.R. Rhodes,
"Applications of Neutron Activation to On-Stream Analysis",
Isotopes and Radiation Technology, Vol. 6 (1969), pp 359-368

6. D. Duffey, P.F. Wiggins, F.E. Senftle,
"Ore Process Analysis with Neutron Capture Gamma Rays Using ^{252}Cf",
Society of Mining Engineers - TRANSACTIONS - Vol. 254, June 1973

7. J.I.W. Watterson, A.H. Andeweg, J. Ramahlo,
"Isotope Source Neutron Activation for the Accurate Analysis of Kilogram Samples of Ores and Rocks",
J. of Radioanal. Chem. Vol. 71 No 1-2 (1982), pp 365-375

8. L. Alaerts, J.P. Op De Beeck, J. Hoste,
"An ^{227}Ac-Be Isotopic Neutron Source for Application in High - Accuracy Neutron Activation Analysis",
Anal. Chim., Acta 69 (1974), pp 1-9

9. A. Cardosa, F.W. Lima,
J. Radioanal. Chem., 36 (1977) 577

10. F.A. Iddings, W.R. Mack, R.G. Shaw,
"Large Volume Samples for Calcium Determination",
International Advances in Nondestructive Testing, Vol. 5 (1977), pp 361-5

11. K.W. Mac Murdo, W.W. Bowman
"Automated Absolute Activation Analysis with Californium-252 Sources"
Savannah River Laboratory, AIKEN, S. Carolina

12. C.L. Lewis et al.
"The On-Stream X-Ray Analysis Installation at the Lake Dufault Mine",
CIM Bulletin Vol. 61 (1968), pp 513-518

13. A.I. Aliev, V.I. Drynkin, D.I. Leipunskaya, V.A. Kasatkin,
Handbock of Nuclear Data for Neutron Activation Analysis,
Israel Programme for Scientific Translations, 1970

14. Nuclear Chemustry - Theory and Applications,
Gregory R. Choppin, Jan Rydberg,
PERGAMON PRESS

15. Andeweg A. H.,
Neutron Source Transfer System,
University of the Witwatersrand,
Schonland Research Centre,
Report No. SRCNS 83/16 (1983)

16. Neutron Sources for Basic Physics and Applications
Barschall H.H. Cierjacks,
Second Edition

17. Activation Foils,
Reactor experiments, Inc.,
San Carlos, California

18. Takashi Suzuki, Yukio Inokoshi, Haruo Chisaka, Takashi Nakamura,
"Optimum Geometry of Large Marinelli - Type
Vessels for In - situ Environmental Sample
Measurements with Ge(Li) Detectors",
Appl. Radiat. Isot. Vol. 39, No. 3, pp. 253 - 256, 1988
Int: J. Radiat. Appl. Instrum. Part A

19. C.M. Lederer, J.M. Hollander, I. Perlman,

Table of Isotopes

20. Handbook of Chemistry and Physics,
63 Edition 1982-1983

21. D.I. Garber, R.R. Kinsey,
Neutron Cross Sections, Vol. II, Curves, January 1976

22. U. Reus, W. Westmeier,
Atomic Data and Nuclear Data Tables,
Catalog of Gamma Rays from Radioactive Decay,
Part I, Vol. 29 No 1, July 1983
Part II, Vol. 29 No 2, September 1983

23. J.C. Miller, J.N. Miller,
Statistics for Analytical Chemistry (1984),
Ellis Horwood, Chichester

24. C.B. Ward,
"Assay of Gold Ores by Neutron Activation",
Nucl. Geophys. Vol. 5, No 3, pp 291-296, 1991

25. D.I. Leipunskaya, S.I. Savosin, V.I. Drynkin, A.I. Aliev, Y.B. Finkelstein, N.N. Popova, E.S. Zemchikhin,
"Cupel Assay of Gold by an Activation Method",
J. of Radioanal. Chem. Vol. 7 (1971), pp 299-308

26. A.A. EL Cady, D. Duffey, P.F. Wiggins,
"Neutron Capture γ - Ray Techniques for Iron and Gold in Mixtures",
Anal. Chim. Acta, 54 (1971), pp 97-104

27. S.J. Parry,
"Detection Limits in Epithermal Neutron Activation Analysis of Geological Materials",
J. of Radioanal. Chem., Vol. 59, No 2 (1980), pp 423-427

28. H. Blok, R.D. Morse, B.L.Twaites,
"Comparison of Analysis Techniques for Gold",
J. Geochem. Explor. 25 (1/2) May 1986

29. Andeweg A.H., Private Communication

30. The Physics of Experimental Method,
H.J.J. Braddick,
Chapman and Hall Ltd, 1963

31. Instrumental Analysis Manual,
G.G. Guilbault, L.G. Hargis,
Dekker, New York, 1970

32. G. Friedlander, J.W. Kennedy, J.M. Miller,
Nuclear Radiochemistry, 2nd Ed.,
Wiley, New York, 1964

33. Handbook of Nuclear Data for Neutron Activation Analysis,
A.I. Aliev, V.I. Drynkin, V.A. Kasatkin
Israel Program for Scientific Translations, 1970

34. J.R. Rhodes,
Applications of Neutron Activation Analysis to
On-Stream Analysis,
Isotopes and Radiation Technology,
Vol.6 (1969), pp 359-368

35. J.I.W. Watterson, A. Pillay, Private communication,
Schonland Research Centre for Nuclear Sciences
University of the Witwatersrand,

3010033018
LYCOUDI, M.
Neutron activation analysis for the determination of gold and the platinum group elements in large samples.

THESIS
QC
7[illegible]
LYC

University of the Witwatersrand, Johannesburg

The Library

This book may *not* be retained after the last date stamped below. A renewal for a further period of seven days may be granted unless the book is in demand. *Fines, as scheduled in the Rules and Regulations, are incurred on overdue books.*

13 FEB 1996		
20 MAR 1996		
29 APR 1996		

This book is *not transferable*. It will remain your charge until returned by you in person.